# SMIP94

## SMIP94 SEMINAR ON SEISMOLOGICAL AND ENGINEERING IMPLICATIONS OF RECENT STRONG-MOTION DATA

Los Angeles, California
May 26, 1994

## PROCEEDINGS

Sponsored by

Strong Motion Instrumentation Program
Division of Mines and Geology
California Department of Conservation

Supported in Part by

California Seismic Safety Commission

The California Strong Motion Instrumentation Program (SMIP) is a program within the Division of Mines and Geology of the California Department of Conservation and is advised by the Strong Motion Instrumentation Advisory Committee (SMIAC), a committee of the California Seismic Safety Commission. Current program funding is provided by an assessment on construction costs for building permits issued by cities and counties in California, with additional funding from the California Department of Transportation, the Office of Statewide Health Planning and Development, and the California Department of Water Resources.

## DISCLAIMER

Neither the sponsoring nor supporting agencies assume responsibility for the accuracy of the information presented in this report or for the opinions expressed herein. The material presented in this publication should not be used or relied upon for any specific application without competent examination and verification of its accuracy, suitability, and applicability by qualified professionals. Users of information from this publication assume all liability arising from such use.

# SMIP94

## SMIP94 SEMINAR ON SEISMOLOGICAL AND ENGINEERING IMPLICATIONS OF RECENT STRONG-MOTION DATA

Los Angeles, California
May 26, 1994

## PROCEEDINGS

Edited by

M.J. Huang

Sponsored by

Strong Motion Instrumentation Program
Division of Mines and Geology
California Department of Conservation

Supported in Part by

California Seismic Safety Commission

## PREFACE

The California Strong Motion Instrumentation Program (SMIP) in the Division of Mines and Geology of the California Department of Conservation promotes and facilitates the improvement of seismic codes through the Data Interpretation Project. The objective of this project is to increase the understanding of earthquake strong ground shaking and its effects on structures through interpretation and analysis studies of SMIP and other applicable strong-motion data. The ultimate goal is to accelerate the process by which lessons learned from earthquake data are incorporated into seismic code provisions and seismic design practices.

Since the establishment of SMIP in early 1970s, over 550 stations, including 135 buildings, 20 dams and 25 bridges, have been installed. Significant strong-motion records have been obtained from many of these stations. One of the most important sets of strong-motion records is from the 1994 Northridge earthquake during which strong-motion records were obtained from 116 ground-response stations and 77 extensively-instrumented structures. Other important sets include those from the Loma Prieta earthquake of October 17, 1989, the Cape Mendocino (Petrolia) earthquake of April 25, 1992, the Landers and Big Bear earthquakes of June 28, 1992. These records have been and will be the subject of SMIP data interpretation projects.

The SMIP94 Seminar is the sixth in a series of annual events designed to transfer recent interpretation findings on strong-motion data to practicing seismic design professionals and earth scientists. In both oral presentations and poster sessions, six investigators will provide state-of-the-art data and analysis results from recent interpretation studies of SMIP data during the past year. In addition, two papers are presented by SMIP staff on the topics of special interest.

The papers in this Proceedings volume represent interim results obtained by the investigators. Following this seminar the investigators will be preparing final reports with their final conclusions. These reports will be more detailed and will update the results presented here. SMIP will make these reports available after the completion of the studies.

## TABLE OF CONTENTS

SEMINAR PROGRAM

SOME IMPLICATIONS OF STRONG-MOTION DATA FROM THE 1994 NORTHRIDGE EARTHQUAKE . . . . . 1
A.F. Shakal, M.J. Huang and R.B. Darragh

SITE RESPONSE STUDIES FOR PURPOSE OF REVISING NEHRP SEISMIC PROVISIONS . . . . . 21
C.B. Crouse, J.W. McGuire

ANALYSIS OF STRONG MOTION RECORDS FROM NON-DUCTILE CONCRETE MOMENT FRAME BUILDINGS . . . . . 35
D. Bleiman, S. Kim and M.-C. Chen

INTERACTION AT SEPARATION JOINTS OF THE I10/215 BRIDGE DURING EARTHQUAKES . . . . . 49
P.K. Malhotra, M.J. Huang and A.F. Shakal

RESPONSE OF THE NORTHWEST CONNECTOR IN THE LANDERS AND BIG BEAR EARTHQUAKES . . . . . 61
G.L. Fenves and R. DesRoches

SEISMIC RESPONSE STUDY OF THE US 101/PAINTER STREET OVERPASS USING STRONG MOTION RECORDS . . . . . 75
R.K. Goel and A.K. Chopra

UTILIZATION OF CSMIP STRONG-MOTION RECORDS TO RATIONALIZE HORIZONTAL FORCE FACTORS (Cp) . . . . . 89
R.M. Czarnecki, D.N. Rentzis, M.A. Bello and D.M. Bergman

EVALUATION OF OVERTURNING FORCES ON SHEAR WALL BUILDINGS . . . . . 105
W.E. Gates, G.S. Hart, S. Gupta and M. Srinivasan

# SMIP94 Seminar Proceedings

## SMIP94 SEMINAR ON

## SEISMOLOGICAL AND ENGINEERING IMPLICATIONS

## OF RECENT STRONG MOTION DATA

Los Angeles Airport Marriott, California
May 26, 1994

**PROGRAM**

| | |
|---|---|
| 8:30-9:30 | **Registration** |
| 9:30-9:40 | **Welcoming Remarks**<br>*James F. Davis*, State Geologist, Division of Mines and Geology and<br>*LeRoy Crandall*, Seismic Safety Commission, and Chair, Strong Motion Instrumentation Advisory Committee (SMIAC) |
| 9:40-9:45 | **Introductory Remarks**<br>*Anthony Shakal*, Manager, Strong Motion Instrumentation Program |
| **SESSION I** | **Ground Response**<br>**Moderator:** *Bruce Bolt*, UC Berkeley/Seismic Safety Commission Chair, SMIAC Ground-Response Subcommittee |
| 9:45-10:10 | **Some Implications of Strong-Motion Data from the 1994 Northridge Earthquake**<br>*A. Shakal, M. Huang and R. Darragh*, SMIP |
| 10:10-10:35 | **Site Response Studies for Purpose of Revising NEHRP Seismic Provisions**<br>*C.B. Crouse, J. McGuire*, Dames & Moore, Seattle |
| 10:35-11:00 | Break |
| **SESSION II** | **Building Response and Lifeline Structure Response**<br>**Moderator:** *Wilferd Peak*, Consulting Engineering Geologist Chair, SMIAC Data Interpretation Subcommittee |
| 11:00-11:25 | **Analysis of Strong Motion Records from Non-ductile Concrete Moment Frame Buildings**<br>*D. Bleiman, S. Kim and M. Chen*, Cygna Consulting Engineers, Oakland |
| 11:25-11:50 | **Interaction at Separation Joints of the I10/215 Bridge During Earthquakes**<br>*P. Malhotra, M. Huang and A. Shakal*, SMIP |
| 11:50-12:20 | **Poster Session for Sessions I & II** |

12:20-2:10 **Lunch**
Introduction *LeRoy Crandall*, Chair, SMIAC
Welcome *Michael Byrne*, Director, Department of Conservation
Keynote Speaker *Chris Poland*, President, H.J. Degenkolb Associates

**SESSION III** **Lifeline Structure Response**
**Moderator:** *Vern Persson*, Division of Safety of Dams, DWR
Chair, SMIAC Lifelines Subcommittee

2:10-2:35 **Response of the Northwest Connector in the Landers and Big Bear Earthquakes**
*G. Fenves and R. DesRoches*, University of California, Berkeley

2:35-3:00 **Seismic Response Study of the US 101/Painter Street Overpass Using Strong Motion Records**
*R. Goel and A. Chopra*, University of California, Berkeley

3:00-3:20 Break

**SESSION IV** **Building Response**
**Moderator:** *Chris Poland*, H.J. Degenkolb Associates
Chair, SMIAC Buildings Subcommittee

3:20-3:45 **Utilization of CSMIP Strong-Motion Records to Rationalize Horizontal Force Factors (Cp)**
*R. Czarnecki, D. Rentzis, M. Bello and D. Bergman*, URS Consultants, San Francisco

3:45-4:10 **Evaluation of Overturning Forces on Shear Wall Buildings**
*W. Gates, G. Hart, S. Gupta and M. Srinivasan*, Dames & Moore, Los Angeles

4:10-4:45 **Poster Session for Sessions III and IV**

# SOME IMPLICATIONS OF STRONG-MOTION RECORDS FROM THE 1994 NORTHRIDGE EARTHQUAKE

A.F. Shakal, M.J. Huang and R.B. Darragh

California Department of Conservation
Division of Mines and Geology
Strong Motion Instrumentation Program

## ABSTRACT

Some of the highest acceleration ever recorded at structural and ground response sites occurred in the Northridge earthquake. These accelerations are greater than most existing attenuation models would have predicted. The thrust mechanism of this event as well as its location under a metropolitan area may have contributed to the number of high acceleration recordings. Although the accelerations are high, the correspondence between measured acceleration and damage requires further study, since some sites with high acceleration experienced only moderate damage. Some vertical accelerations were larger than the horizontal, but in general this event fits the pattern observed in previous earthquakes. Strong-motion records processed to date show significant differences in acceleration and velocity waveforms and amplitudes across the San Fernando Valley.

Analysis of processed data from four buildings in the San Fernando Valley indicate that the stiff, short-period building experienced large forces and relatively low story drift during the Northridge earthquake. On the other hand, three moment frame buildings (periods between 1 and 3 seconds) experienced large drifts. The two non-ductile concrete moment frame buildings suffered column cracking and other damage. For this earthquake, accelerations did not always amplify from base to roof for flexible structures like these three buildings, but the displacements were always larger at the roof. The records from a base-isolated building indicate that high-frequency motion was reduced significantly by the isolators, which only deflected 3.5 cm. The records from a parking structure show important features of the seismic response of this type of structure.

## INTRODUCTION

The 6.7M (moment magnitude) earthquake that occurred near Northridge, California on January 17, 1994 produced an important set of strong-motion recordings. The epicenter is located about 32 km northwest of Los Angeles in the densely populated San Fernando Valley. Although the Northridge earthquake had nearly the same magnitude as the 1971 San Fernando earthquake, it was much more damaging.

Strong-motion records were recovered from nearly 200 stations of the California Strong Motion Instrumentation Program (CSMIP) after the Northridge earthquake. Highlights and copies of the recorded accelerograms are presented in a CSMIP data report (Shakal and others, 1994). The results of the digitization and processing of the 27 ground-response records completed to

date are presented in four CSMIP processed data reports (Darragh and others, 1994a-d). This paper presents some initial interpretation results from the recorded accelerograms and the processed data.

## GROUND RESPONSE

Strong-motion records were obtained at 116 CSMIP ground-response stations during the Northridge earthquake. Several conclusions can be drawn from an analysis of the general features of the accelerograms recorded at CSMIP and USGS stations (Porcella and others, 1994) during the Northridge earthquake:

1) Maximum Accelerations The maximum horizontal accelerations from this earthquake are compared to a standard attenuation relationship (Joyner and Boore, 1988) in Fig. 1. The Northridge accelerations are greater than would have been predicted by this relationship and are also greater than those in the 1971 San Fernando earthquake. The tendency for observed strong-motion data to exceed values predicted by attenuation relationships was also documented for the 1987 Whittier earthquake (Shakal and others, 1988) and the Landers and Big Bear earthquakes (Cramer and Darragh, 1994).

2) Vertical Acceleration The maximum vertical acceleration is often, on average, about two-thirds of the peak horizontal acceleration. However, as occasionally occurs for other earthquakes at close-in distances, vertical accelerations were equal to or greater than the maximum horizontal acceleration at a few stations for this earthquake, as shown in Fig. 2. In general, the Northridge earthquake fits the pattern of most other earthquakes with regard to vertical accelerations.

3) Spectral Acceleration The spectral acceleration for three recent California earthquakes at ground-response stations near the fault is shown in Fig. 3. For reference, the spectral shape from the Uniform Building Code (UBC) is also shown. The spectral acceleration for the 6.7M Northridge earthquake at the Sylmar and Newhall stations is significantly greater than both the 7.1M Loma Prieta earthquake at the Santa Cruz station and the 7.3M Landers earthquake at the Joshua Tree station.

4) Duration The duration of strong shaking for three recent California earthquakes is shown in Fig. 4 for the same stations as in Fig. 3. The duration of strong shaking for the 6.7M Northridge earthquake is about 10 seconds at Sylmar and Newhall. This is comparable to the durations for the 6.6M San Fernando and 7.1M Loma Prieta events, but significantly less than the 30-second duration of the 7.3M Landers earthquake.

5) Site Amplification of Strong Motion No clear trend in amplification of ground motion at soil sites is apparent in the strong-motion data for the Northridge earthquake, in contrast to the 1989 Loma Prieta earthquake. Further investigation of the effects of site geology and basin effects will be necessary to determine the role of local site conditions on ground motions and damage during this earthquake.

The recorded accelerograms and processed data at five stations were selected to highlight important features of the ground-response data. The accelerations for these stations are shown in Fig. 5 and the corresponding velocities are shown in Fig. 6.

**Tarzana** The record from the Tarzana station, about 5 km south of the epicenter, shows repeated accelerations over 1 g for 7 to 8 seconds, with a maximum horizontal acceleration of 1.8 g. Only moderate damage was observed in the vicinity, although structural types in the area are limited to 1 and 2 story wood frame homes. Fig. 5 shows the instrument-corrected acceleration at Tarzana, and the velocity is shown in Fig. 6. The peak velocity was over 100 cm/sec at Tarzana; velocities this high have been observed infrequently in California.

The station is located near the crest of a low (20 m) natural hill on the south side of the San Fernando Valley. The site is underlain by a variable thickness of colluvial soil (silty clay) estimated to be about 0.5 to 1.5 m in thickness. The soil is derived by in-place weathering of a soft claystone and siltstone of the Upper Modelo Formation which underlies the soil. During the 1987 Whittier earthquake this site also had an unusually high acceleration, but not during the principal aftershock.

Additional accelerographs were deployed near the station after the Northridge earthquake and numerous aftershock records were obtained, some with peak acceleration as high as 0.25 g. The accelerations and response spectra at Tarzana and a nearby reference station are compared in Fig. 7 for the largest aftershocks. The reference site is located about 120 m from the Tarzana station, off the gentle hill. For the largest aftershock (5.3M) the stations have almost identical peak accelerations of about 0.25 g. In other words, no amplification of peak acceleration is observed in the shaking from the largest aftershock. For that event, the spectra for Tarzana and the reference site (Fig. 7) are similar at short periods and long periods but show an amplification of 2 to 3 times near 0.2 seconds (5 Hz) at Tarzana. For the 4.4M aftershock, the Tarzana peak acceleration was 0.12 g, three times that at the reference site (0.04 g). For this event, the Tarzana spectrum is nearly 4 times that of the reference site in the 3 to 5 Hz range, but now the Tarzana spectrum is also amplified at short periods, reflecting the amplified peak acceleration. Analysis of additional records is underway to investigate the stability of the spectral shape. These two stations document the large variability of strong ground motion possible over a distance of only 120 m and indicate the source of some of the scatter in peak accelerations in Fig. 1.

The causes of the large motions at Tarzana are still under investigation. Darragh and others (1994e) reported that the Tarzana site amplified peak acceleration by a factor near two for many of the aftershocks. Spudich and others (1994) report a predominance of 2 to 6 Hz motion in weak motion recordings at Tarzana. Site characterization work has not established a cause for the large motions and large durations. A borehole was drilled to 30 m and logged by Fumal and others (1981), who report a shear-wave velocity in the claystone of about 400 m/sec. However, this borehole was drilled about 260 m west of the present CSMIP station location so only the deeper portion of the borehole may be extrapolated laterally to beneath the station.

**Arleta** The second closest CSMIP ground response station, approximately 10 km east of the epicenter, recorded a maximum horizontal acceleration of 0.35 g, but a higher vertical acceleration of 0.59 g. In Figs. 5 and 6 the acceleration and velocity at this station are compared with Tarzana. Both stations are located within 10 km of the epicenter in the San Fernando Valley. Arleta recorded significantly lower maximum accelerations, velocities and displacements than at Tarzana; the maximum velocities and displacements are about one-third the values at Tarzana. The reasons for these low values have not yet been determined.

**Newhall** The Newhall station is located about 20 km north of the epicenter, in the direction of rupture propagation. This station recorded a maximum acceleration near 0.6 g on all three components; the north component is shown in Fig. 5. As shown in Fig. 6 the maximum velocity is similar to Tarzana. Maximum velocities near 100 cm/sec were also recorded at Sylmar, which is also shown in Fig. 6.

**Santa Monica** The ground-response station at Santa Monica City Hall recorded a peak horizontal acceleration of 0.93 g (Fig.5). This station is approximately 23 km south of the epicenter and there are many damaged buildings in the area. The velocity record in Fig. 6 shows late-arriving energy near 15 seconds that is also observed at several other stations in the Los Angeles basin.

**Pacoima Dam** The Pacoima Dam was strongly shaken during the Northridge earthquake. During the 1971 San Fernando earthquake a then-unprecedented horizontal acceleration of 1.25 g (0.7 g vertical) was recorded at the upper left abutment of this 365-foot high concrete arch dam constructed in 1929. Since the 1971 earthquake, the dam has been extensively instrumented with additional sensors on the dam structure and at a downstream site. During the Northridge earthquake the instrumentation system recorded high acceleration levels with maximum accelerations exceeding 2 g. The instrument at the upper left abutment, at the same site where the 1971 record was obtained, recorded an acceleration of 1.5 g or greater on the horizontal and 1.4 g on the vertical component. The concrete pier that the instrumented is attached to appears to be well connected to the rock ridge at the left abutment, and there is no evidence of relative motion between the pier and the rock. In contrast to the pier, the gunite and thin concrete on the rock nearby is badly broken up and shifted. The Pacoima Dam downstream site, in the narrow canyon below the dam, recorded peak accelerations of 0.44 and 0.20 g on the horizontal and vertical directions, respectively. This site is approximately 130 m (430 feet) downstream from the base of the dam. Fig. 8 compares the 1994 accelerations recorded at these two Pacoima Dam stations. Fig. 9 compares the response spectra at the two sites, as well as the spectra for the 1971 earthquake at the upper left abutment. The 1994 upper left abutment recording shows amplification at all frequencies compared to the downstream recording. In addition, the 1994 recording shows higher response at short periods than the 1971 recording, but the 1971 recording shows larger response at periods greater than about 1 second.

## STRUCTURAL RESPONSE

Strong-motion records were obtained at 57 CSMIP-instrumented buildings during the Northridge earthquake. Table 1 lists the maximum recorded accelerations

at 27 buildings that recorded accelerations greater than 0.15 g during the Northridge earthquake. Maximum accelerations are given for both the transverse and longitudinal directions in the structure. Some of these buildings also recorded previous earthquakes such as the 1987 Whittier or the 1971 San Fernando earthquakes. Some preliminary interpretation results of the records from several of these buildings are discussed below.

**Sylmar County Hospital** This 6-story hospital replaced the hospital that collapsed in the 1971 San Fernando earthquake. The structure was built with concrete shear walls on the lower two stories and steel shear walls on the upper four stories. Fig. 10 shows a profile of the acceleration records at the roof, 4th, 3rd and ground floors in the north-south direction. The integrated displacements are shown in Fig. 11 and the response spectra in Fig. 12. These figures show that the building is relatively stiff and has a fundamental period of about 0.4 second. In addition, the total drift between the roof and the ground floor is about 5 cm, which is much smaller than the maximum ground displacement (28 cm). The preliminary estimate of the damping ratio for this building is about 10%. The building suffered no apparent structural damage, although there was damage to non-structural components and equipment.

**Van Nuys Hotel** This 7-story building is a non-ductile concrete moment frame structure. Fig. 14 shows a profile of the accelerations recorded in the east-west direction. For reference, the peak acceleration at the base, 0.45 g, is twice that recorded during the 1971 San Fernando earthquake. A profile of the integrated displacements is shown in Fig. 15 and the response spectra are shown in Fig. 13. The total drift between the roof and the base is about 23 cm, which is about 1.1% of the building height. In addition, the records also show that the building experienced significant torsional displacement which contributed about 40% of the total drift. For reference, the San Fernando record showed that the building fundamental period is about 1.5 seconds. Fig. 13 indicates that the building period apparently lengthened from 1.5 to 2 seconds during the Northridge earthquake. The building suffered structural damage and concrete spalling occurred at the columns just below the fifth floor slab on the south side of the building.

**Sherman Oaks Building** This building is a non-ductile concrete moment frame structure with 13 stories above ground and 2 stories below ground. The record shows that the building has a fundamental period of about 2.8 seconds during the Northridge earthquake. The total drift between the roof and the base is about 23 cm in the transverse direction and 29 cm in the longitudinal direction. The building had cracks at many beam-column joints.

**Burbank Steel Building** This 6-story building is a perimeter steel moment frame building. Fig. 16 shows the accelerations recorded in the east-west direction. The integrated displacements are shown in Fig. 17 and the response spectra are shown in Fig. 18. The total drift between the roof and the base is about 9 cm, which is about 0.4% of the building height. The spectra clearly show that the first mode is about 1.4 seconds and the second mode is about 0.5 second. Note that the spectrum at periods less than 0.3 second was smaller than at the ground level.

**Comparisons of Drift and Torsion** Profiles of the drift and torsional displacements at instrumented floors for the above four buildings are plotted in Fig. 19. The drift for the Sylmar hospital is smallest because it has steel shear walls and concrete shear walls. The other three buildings are moment frame buildings and their drifts are relatively large. For the two steel buildings, the torsional displacements are relatively small compared with the drift. The two non-ductile concrete frame buildings suffered structural damage.

**Parking Garage** A 6-story parking structure near downtown Los Angeles is the first parking structure from which significant strong-motion data has been recorded. In this structure, the lateral forces are resisted by six exterior concrete shear walls in the north-south direction and two interior shear walls in the east-west direction. Accelerations recorded at several locations in the north-south and vertical directions are shown in Fig. 20. Four features are observed from these records: 1) the motion of the shear wall was amplified from 0.28 g at the base to 0.58 g at the top with a fundamental period of about 0.5 second; 2) diaphragm motion is apparent as indicated by 0.58 g at the end wall and 0.84 g at center of the roof; 3) large amplifications occurred at the parapet (1.21 g); 4) large vertical amplification with a period of about 0.25 second occurred at the center of the girder that supports the slab (0.52 g). In addition, rocking motion of the shear wall occurred as indicated by the records from a pair of vertical sensors at the base. These features are important in understanding the seismic behavior of parking structures and can not be neglected in modelling their seismic response.

**Base-isolated University Hospital** The University Hospital is a 7-story braced steel frame building with a 1-story basement. The seismic isolation system consists of 149 isolators between the foundation and the lowest level of the superstructure. A profile of the accelerations recorded in the north-south direction is shown in Fig. 21. The peak horizontal acceleration at the free-field site was 0.49 g and the peak acceleration at the foundation below the isolators was 0.37 g. The peak acceleration was 0.13 g above the isolators and 0.21 g at the roof level. The earthquake force was reduced significantly by the isolators. The relative displacement across the isolators and the drifts in the superstructure are shown in Fig. 22. The relative displacement indicates that the isolators deformed about 3.5 cm, which is much less than the design displacement (about 40 cm). In the 1992 Landers earthquake, the recorded motion indicates the isolators deformed about 0.8 cm (Huang and others, 1993). The response spectra in Fig. 23 indicate that the first mode of the building was near 1.3 seconds and the second mode was near 0.5 second. A significant amount of motion at periods less than 0.4 second was filtered out by the isolators. Fig. 22 indicates that the Northridge earthquake ground motion at this site did not have enough energy at periods longer than 1 second to shift the building period to the design period, which is about 2.3 seconds.

## SUMMARY

The strong motion records from the Northridge earthquake provide important information on the ground motions and the response of structures to the strong shaking that occurred in this event. Design criteria, assumptions and

analysis techniques for structures can be verified by analyzing these records in greater detail. The processed data for these records are available from SMIP and other records are currently being processed for distribution.

## REFERENCES

Cramer, C. and R. Darragh (1994). Peak accelerations from the 1992 Landers and Big Bear, California earthquakes, Bull. Seism. Soc. Am., 84, June.

Darragh, R., T. Cao, C. Cramer, V. Graizer, M. Huang and A. Shakal (1994a-d). Processed CSMIP Strong-Motion Records from the Northridge, California Earthquake of January 17, 1994: Release No. 1 through Release No. 4, Calif. Dept. of Conservation, Div. Mines and Geology, Office of Strong Motion Studies, Report No. OSMS 94-06 through 94-10.

Darragh, R., A. Shakal, T. Cao, C. Cramer and V. Graizer (1994e). Outstanding features of the ground motion from the 1994 Northridge, California earthquake (abstract), SSA94 - Program for Northridge Abstracts.

Fumal, T., J. Gibbs and E. Roth (1981). In-situ measurement of seismic velocity at 19 locations in the Los Angeles, California region. U.S. Geological Survey, Report No. OFR 81-399.

Huang, M., P. Malhotra and A. Shakal (1993). Analysis of records from four base-isolated buildings during the 1992 Landers earthquake, Proc. of SMIP93 Seminar on Seismological and Engineering Implications of Recent Strong Motion Data, Calif. Div. Mines and Geology, p. 77-90.

Joyner, W. and D. Boore (1988). Measurement, characterization, and prediction of strong ground motion, Proc. of Earthquake Engineering & Soil Dynamics II GT Div/ASCE, Park City, Utah, June 27-30, 1988, p.1-60.

Porcella, R., E. Etheredge, R. Maley and A. Costa (1994). Accelerograms recorded at USGS national strong-motion network stations during the Ms=6.6 Northridge, California earthquake of January 17, 1994, US Geol. Survey Open File Report 94-141, 100 pp.

Shakal, A., M. Huang, and T. Cao (1988). The Whittier Narrows, California earthquake of October 1, 1987 - CSMIP strong motion data, Earthquake Spectra, 4, p. 75-100.

Shakal, A., M. Huang, R. Darragh, T. Cao, R. Sherburne, P. Malhotra, C. Cramer, R. Sydnor, V. Graizer, G. Maldonado, C. Petersen and J. Wampole (1994). CSMIP Strong-Motion Records from the Northridge, California Earthquake of 17 January 1994, Calif. Dept. of Conservation, Div. Mines and Geology, Office of Strong Motion Studies, Report No. OSMS 94-07, February 18, 1994, 308 pp.

Spudich P., D. Harlow, W. Lee and R. White (1994). Strong site effects observed at the Tarzana accelerograph site using aftershocks of the 1994 Northridge, California earthquake: implications for microzonation (abstract), SSA94 - Program for Northridge Abstracts.

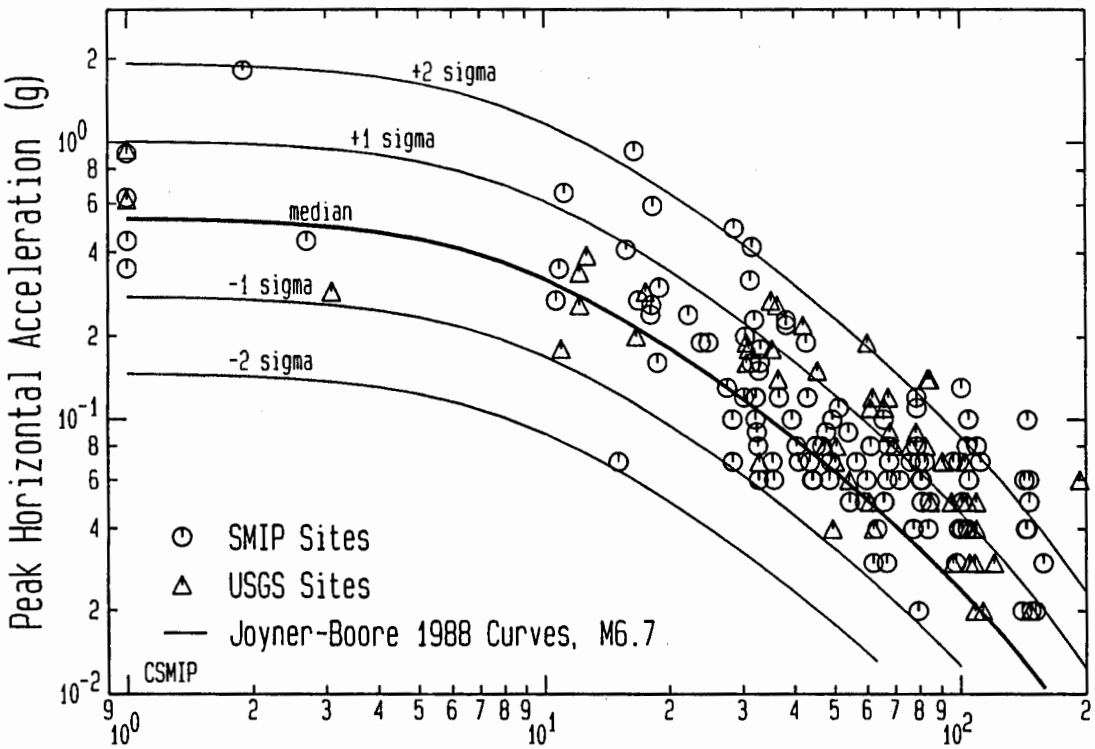


Fig. 1. Maximum horizontal acceleration versus distance for the Northridge earthquake. Distance is from the surface projection of the aftershock zone, as defined by Joyner and Boore (1988). Largest of the two horizontal components is plotted. Bold line is the median curve of Joyner-Boore (1988) for a 6.7M earthquake. Light lines indicate ±1 and ±2 standard deviations. Circles indicate CSMIP stations, triangles indicate USGS stations.

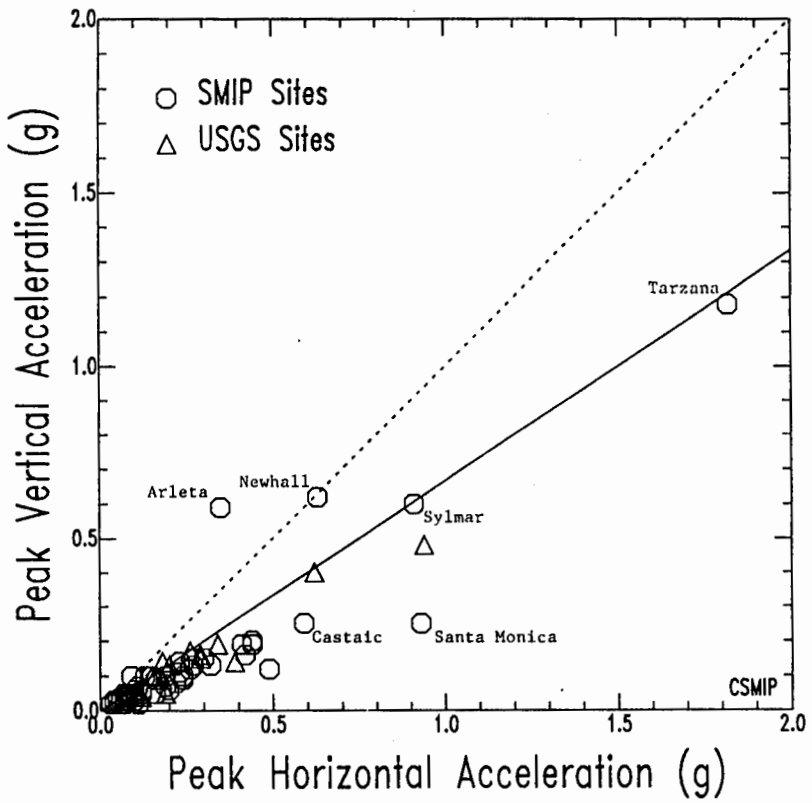


Fig. 2. Maximum horizontal acceleration versus maximum vertical acceleration. The solid line is for vertical acceleration equal to two-thirds of the horizontal acceleration, the dashed line is for vertical acceleration equal to the horizontal acceleration.

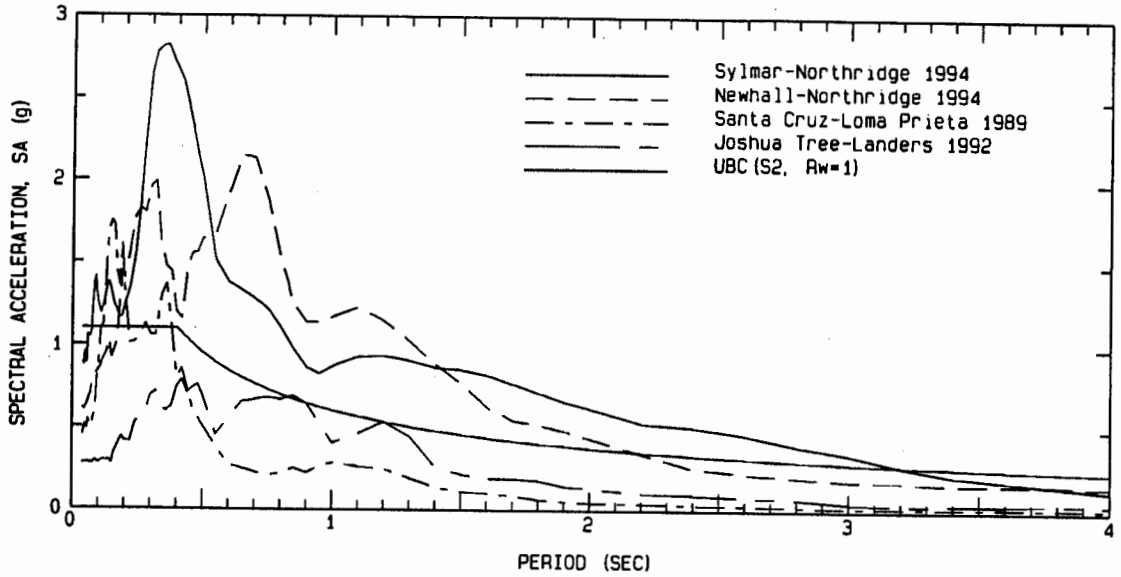


Fig. 3. Spectral acceleration (5% damped) at similar distances (10 - 20 km) from the fault. Stations include Sylmar and Newhall for the 6.7M Northridge earthquake, Santa Cruz for the 7.1M Loma Prieta earthquake, and Joshua Tree for the 7.3M Landers earthquake. The UBC spectrum is included for reference.

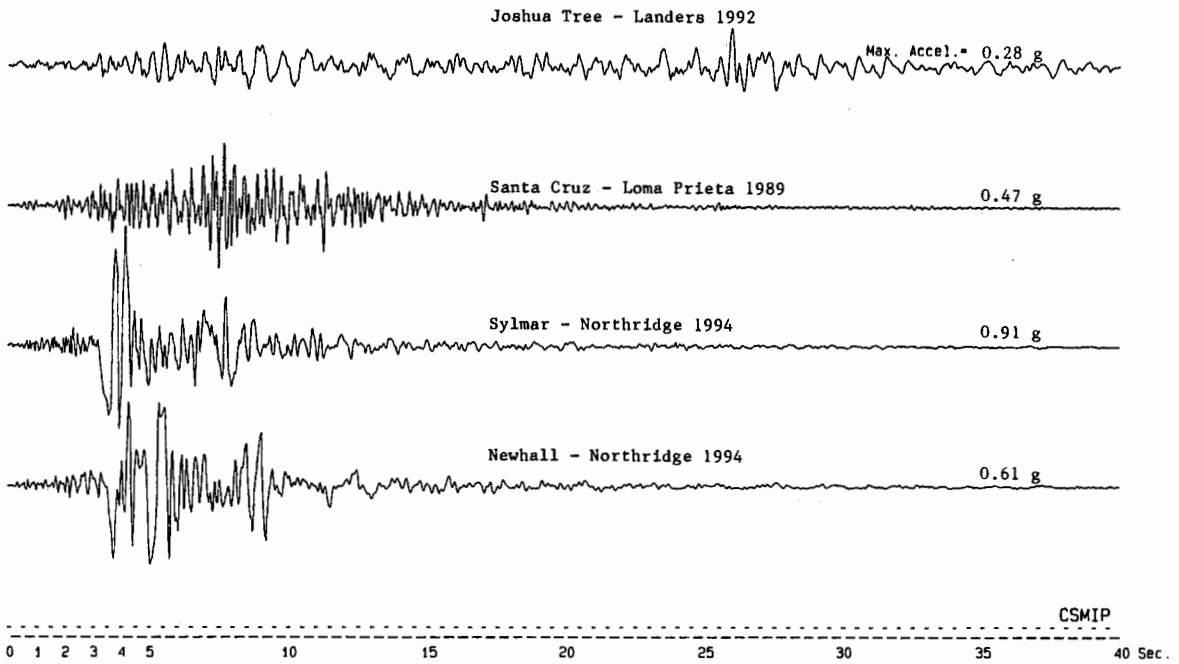


Fig. 4. Duration of strong ground shaking. Accelerograms are from Joshua Tree for the 7.3M Landers earthquake, Santa Cruz for the 7.1M Loma Prieta earthquake, and Sylmar and Newhall for the 6.7M Northridge earthquake. Stations are at similar distances (10 - 20 km) to the fault.

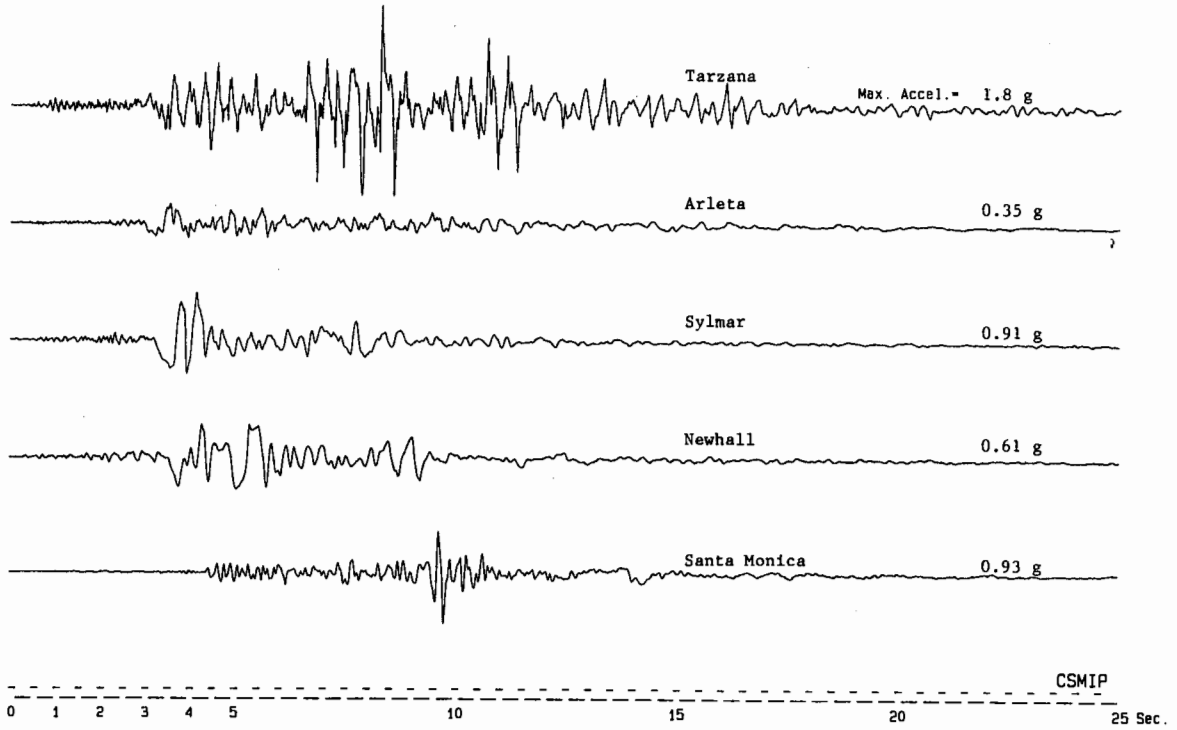


Fig. 5. Comparison of acceleration waveforms at five ground-response stations within 25 km of the epicenter of the Northridge earthquake. Tarzana, Arleta and Sylmar are in the San Fernando Valley. Newhall is north of the valley and Santa Monica is located to the south in the Los Angeles basin.

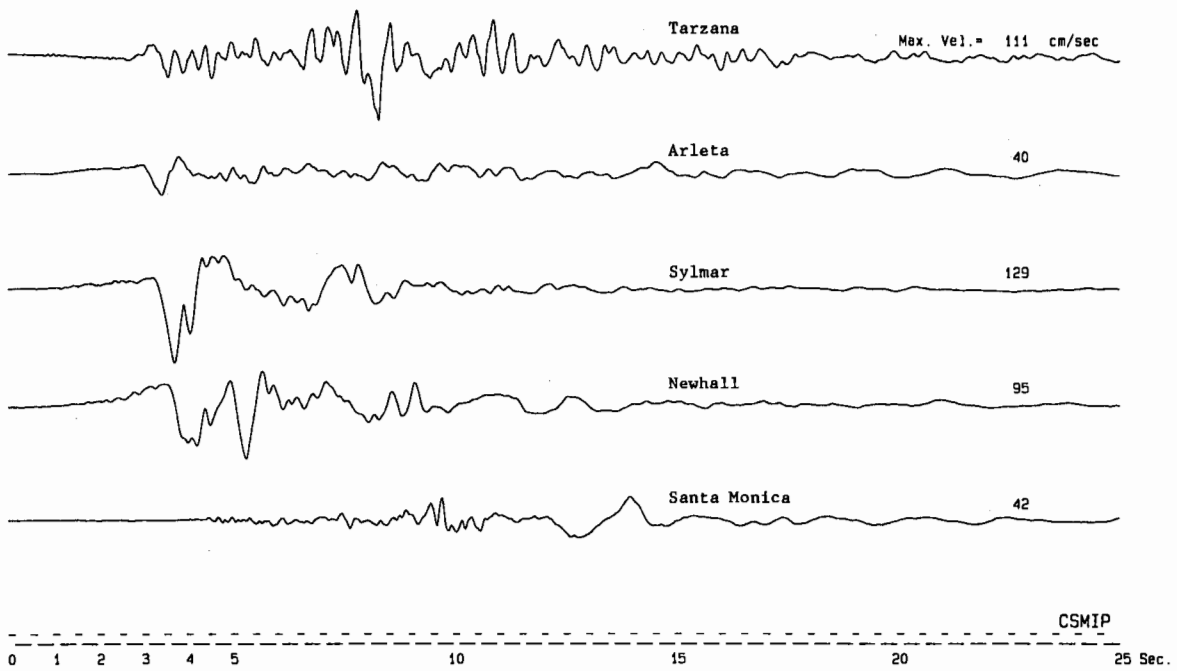


Fig. 6. Comparison of velocity waveforms at the five ground-response stations considered in Fig. 5.

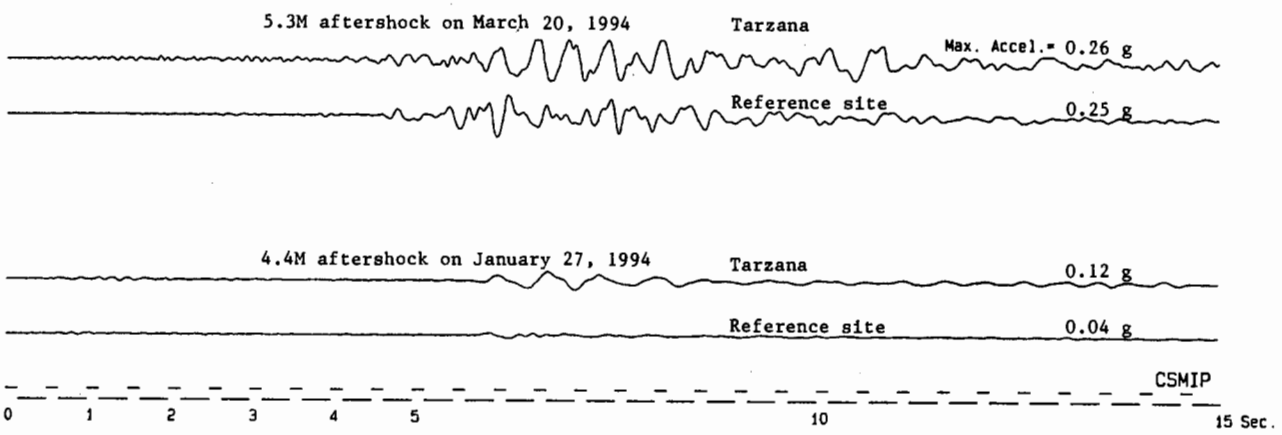


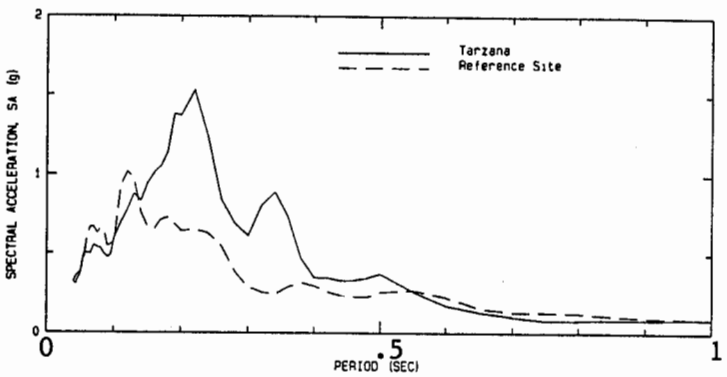


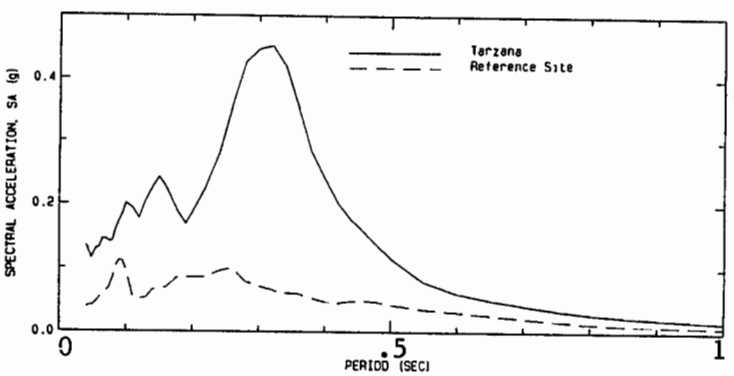


Figure 7: Comparison of accelerograms and spectra (5% damped) for the two largest Northridge aftershock records from the Tarzana CSMIP station and a nearby reference site off the hill and about 120 m from the Tarzana site. Peak accelerations of 0.26 g at Tarzana and 0.25 g at the reference site were recorded during the 5.3M aftershock on March 20, 1994. Peak accelerations of 0.12 g at Tarzana and 0.04 g at the reference site were recorded during the 4.4M aftershock of January 27.

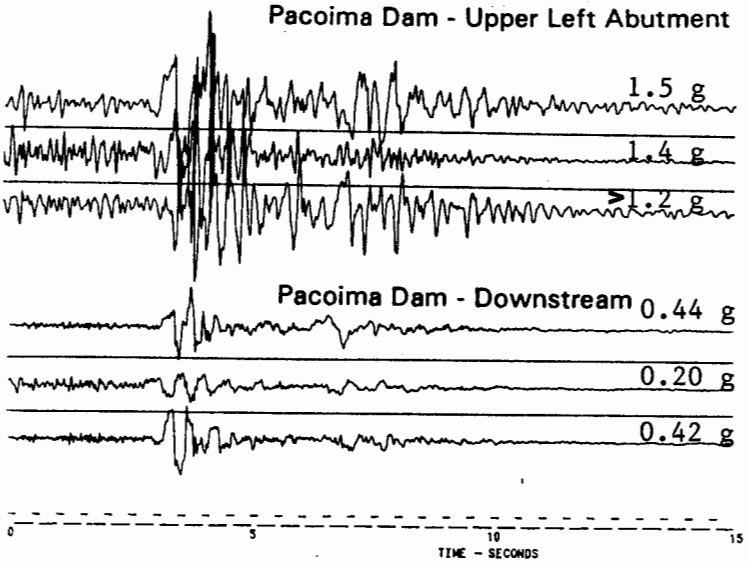


Fig. 8. Acceleration records from the Pacoima Dam upper left abutment site and the downstream site in the narrow canyon below the dam. The records show dramatic differences in accelerations amplitudes and waveforms.

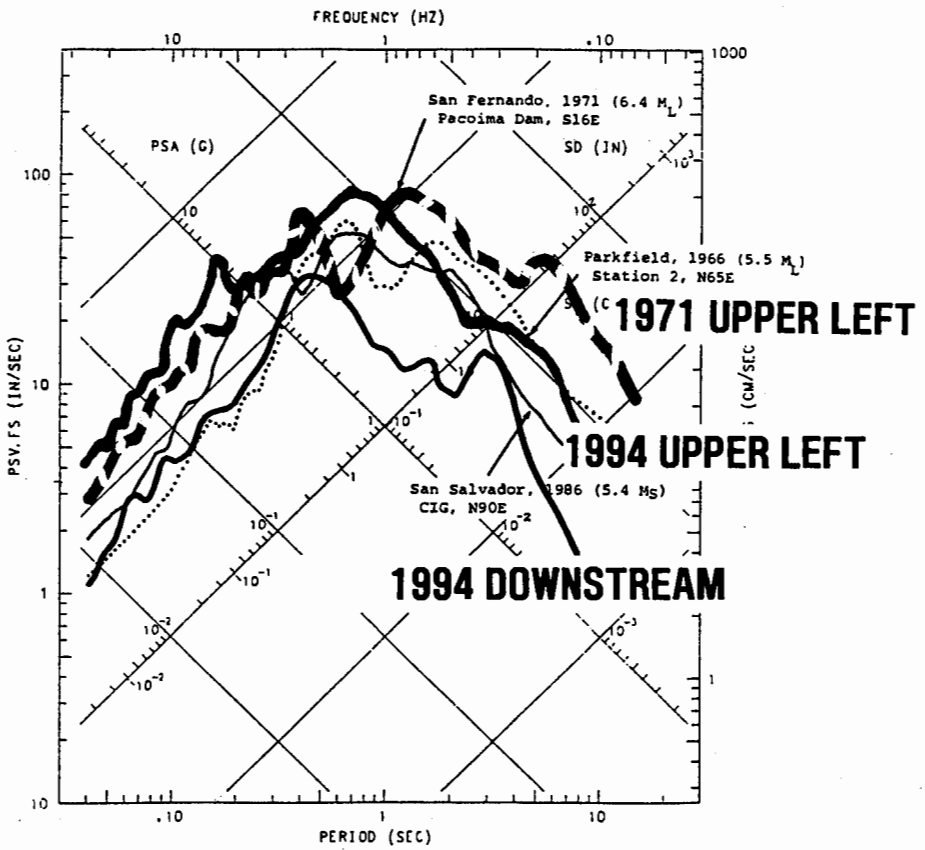


Fig. 9. Comparison of the response spectra (5% damped) from the Pacoima upper left abutment site for the 1971 San Fernando and 1994 Northridge earthquakes. The response spectra at the Pacoima downstream site for the 1994 Northridge earthquake is also shown for comparison.

Table 1. CSMIP Building Records from the Northridge Earthquake with Maximum Acceleration Over 0.15 g

| Building Name | Design Date | Max. Acceleration (g) Transverse Direct. Base | Transverse Direct. Struct. | Longitudinal Direct. Base | Longitudinal Direct. Struct. |
|---|---|---|---|---|---|
| Concrete Moment Frame: | | | | | |
| Los Angeles - 5-story Warehouse | 1970 | 0.26 | 0.29 | 0.20 | 0.25 |
| Van Nuys - 7-story Hotel | 1965 | 0.41 | 0.59 | 0.47 | 0.59 |
| Pasadena - 9-story Commercial Bldg. | 1963 | 0.16 | 0.19 | 0.20 | 0.29 |
| Sherman Oaks - 13-story Commercial Bldg. | 1964 | 0.46 | 0.90 | 0.24 | 0.39 |
| Los Angeles - 14-story Hollywood Storage Bldg. | 1925 | 0.29 | 0.51 | 0.21 | 1.61 |
| North Hollywood - 20-story Hotel | 1967 | 0.33 | 0.66 | 0.13 | 0.34 |
| Concrete or Masonry Shear Wall: | | | | | |
| Los Angeles - 6-story Parking Structure | 1975 | 0.29 | 1.21 | 0.15 | 0.31 |
| Whittier - 8-story Hotel | 1984 | 0.19 | 0.49 | 0.11 | 0.23 |
| Burbank - 10-story Residential Bldg. | 1974 | 0.35 | 0.79 | 0.28 | 0.54 |
| Ventura - 12-story Hotel | 1970 | 0.13 | 0.31 | 0.12 | 0.30 |
| Los Angeles - 17-story Residential Bldg. | 1980 | 0.19 | 0.58 | 0.26 | 0.46 |
| Steel Moment Frame: | | | | | |
| Lancaster - 5-story Hospital | 1986 | 0.06 | 0.15 | 0.07 | 0.28 |
| San Bernardino - 5-story Hospital | 1986 | 0.05 | 0.23 | 0.06 | 0.23 |
| Burbank - 6-story Commercial Bldg. | 1976 | 0.24 | 0.28 | 0.35 | 0.49 |
| Los Angeles - 7-story UCLA Math-Science Bldg. | 1969 | 0.29 | 0.77 | 0.25 | 0.46 |
| Pasadena - 12-story Commercial/Office Bldg. | 1971 | --- | 0.32 | --- | 0.20 |
| Pasadena - 12-story Office Bldg. | 1971 | 0.14 | 0.18 | 0.23 | 0.31 |
| Los Angeles - 15-story Govt. Office Bldg. | 1961 | 0.14 | 0.23 | 0.21 | 0.23 |
| Los Angeles - 19-story Office | 1967 | 0.32 | 0.53 | | |
| Los Angeles - 54-story Office Bldg. | 1988 | 0.13 | 0.19 | 0.09 | 0.14 |
| Steel Braced Frame: | | | | | |
| Los Angeles - 3-story Commercial Bldg. | 1974 | 0.33 | 0.66 | 0.33 | 0.97 |
| Los Angeles - 6-story Office Bldg. | 1988 | 0.20 | 0.29 | 0.24 | 0.59 |
| El Segundo - 14-story Office Bldg. | 1985 | 0.13 | 0.22 | 0.09 | 0.25 |
| Los Angeles - 19-story Office Bldg. | 1967 | | | 0.20 | 0.65 |
| Los Angeles - 54-story Office Bldg. | 1988 | 0.15 | 0.41 | 0.11 | 0.23 |
| Steel Frame and Shear Wall: | | | | | |
| Sylmar - 6-story County Hospital | 1976 | 0.82 | 1.70 | 0.42 | 0.79 |
| Base-isolated: | | | | | |
| Los Angeles - 2-story Fire Command Control Bldg. | 1988 | 0.22 | 0.35 | 0.18 | 0.09 |
| Los Angeles - 7-story University Hospital | 1988 | 0.17 | 0.19 | 0.37 | 0.21 |

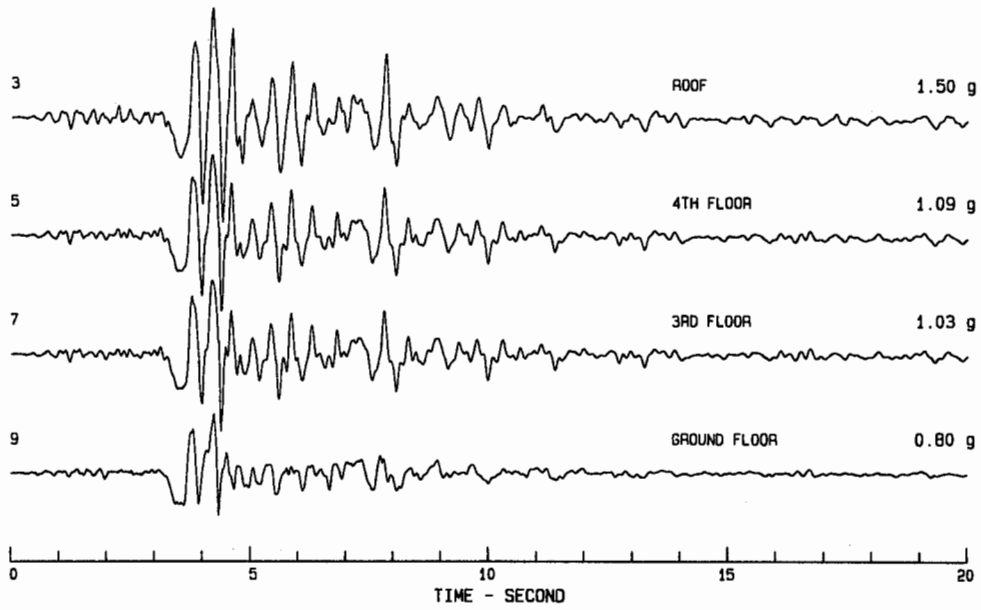


Fig. 10. Accelerations in the north-south direction recorded at the Sylmar 6-story County Hospital during the 1994 Northridge earthquake.

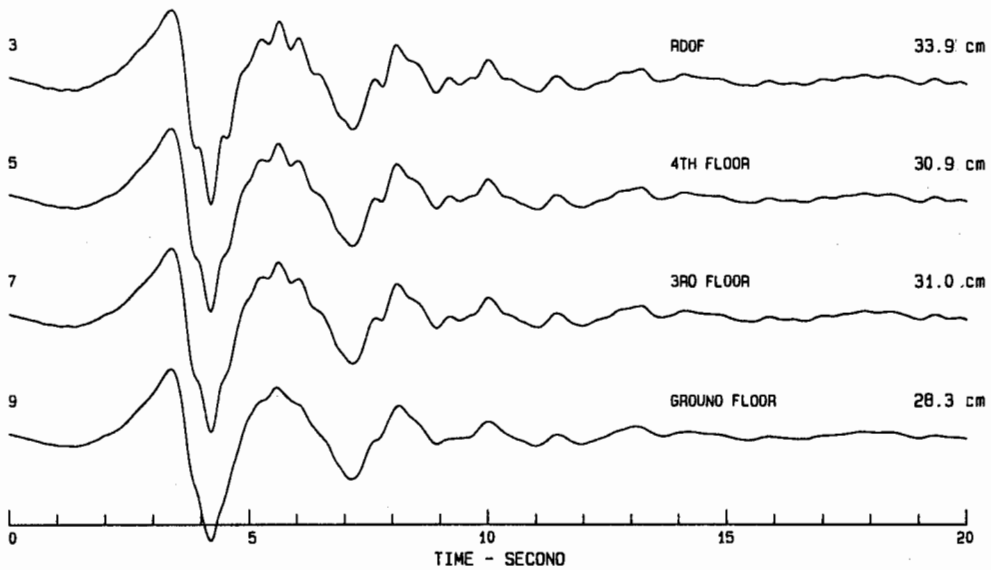


Fig. 11. Displacements corresponding to the accelerations in Fig. 10.

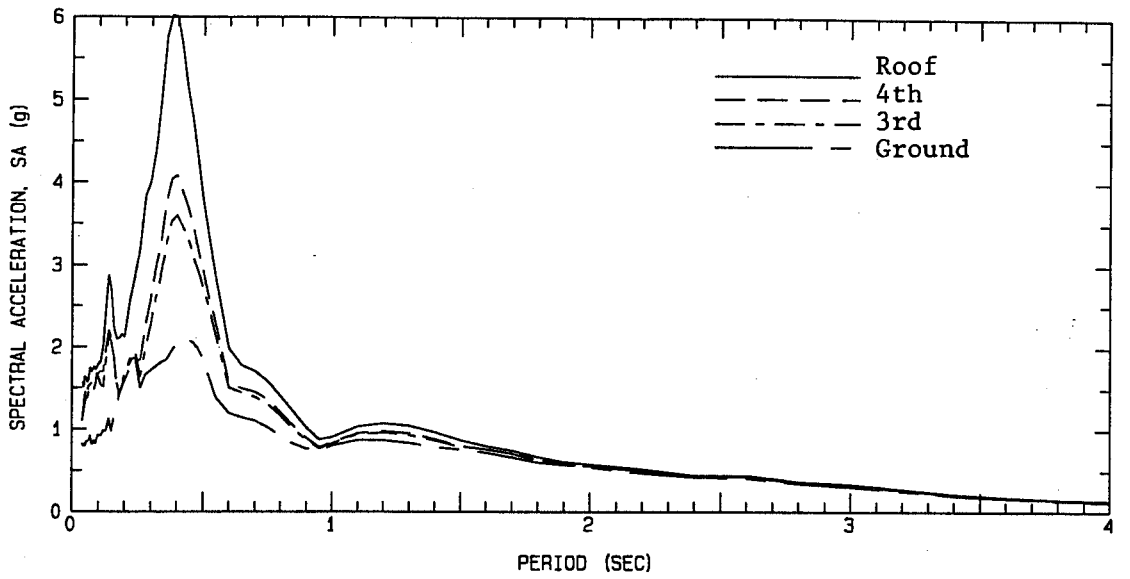


Fig. 12. Response spectra (5% damping) for the roof, 4th, 3rd and ground floors of the Sylmar Hospital corresponding to the accelerations in Fig. 10.

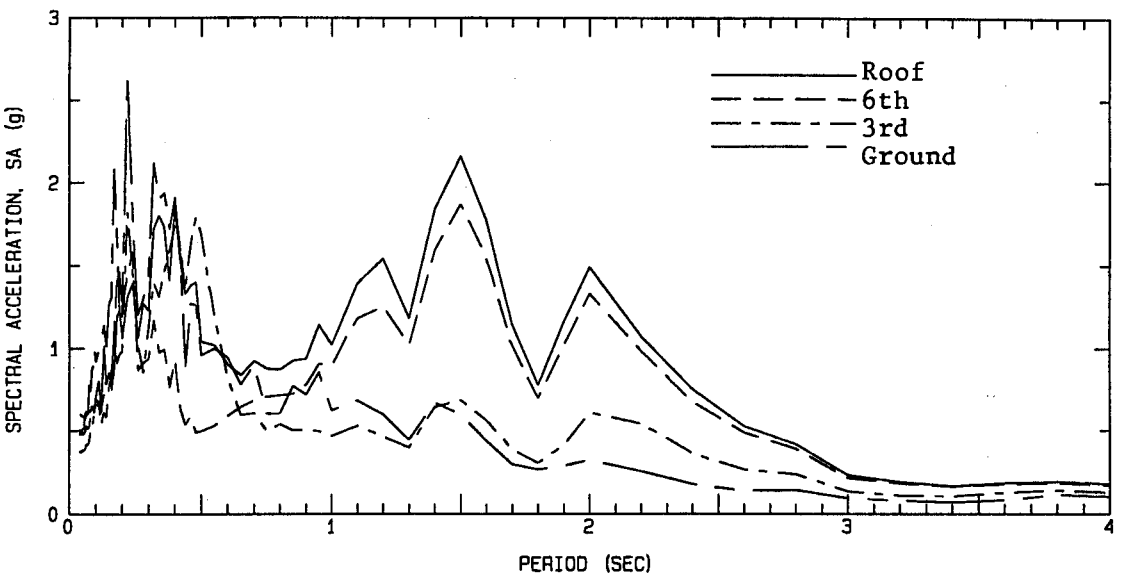


Fig. 13. Response spectra (2% damping) for the roof, 6th, 3rd and ground floors of the Van Nuys Hotel corresponding to the accelerations in Fig. 14.

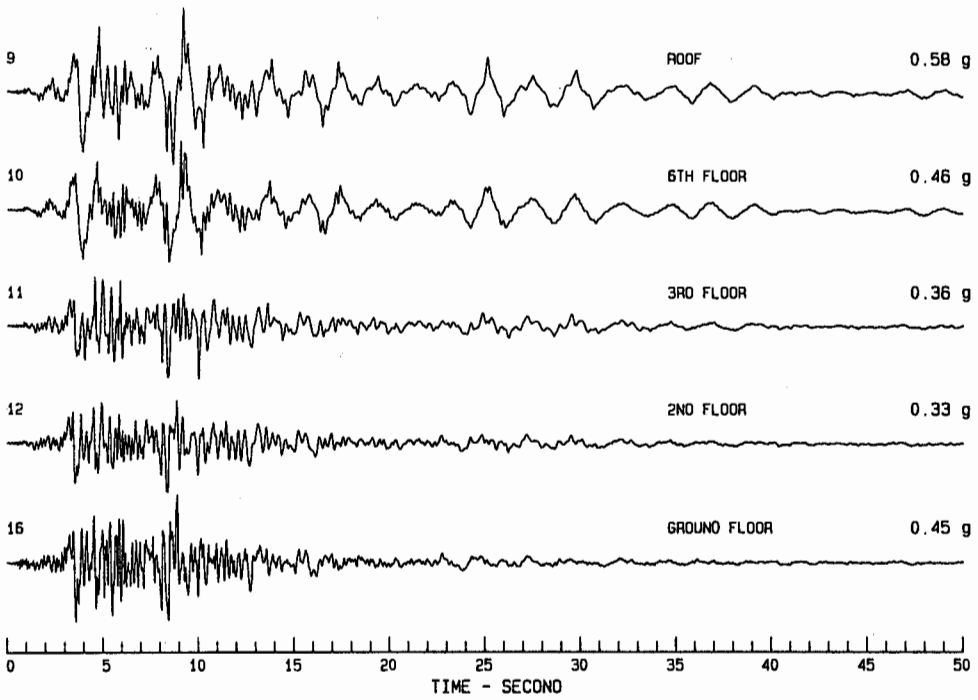


Fig. 14. Accelerations in the east-west (longitudinal) direction recorded at the Van Nuys 7-story concrete hotel during the 1994 Northridge earthquake.

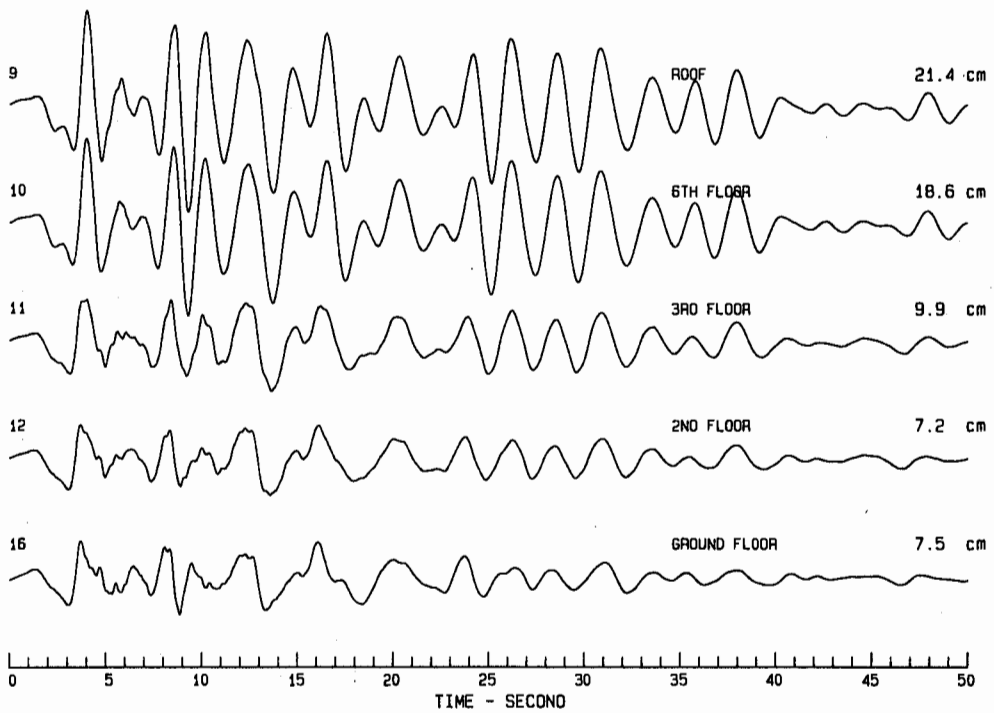


Fig. 15. Displacements corresponding to the accelerations in Fig. 14.

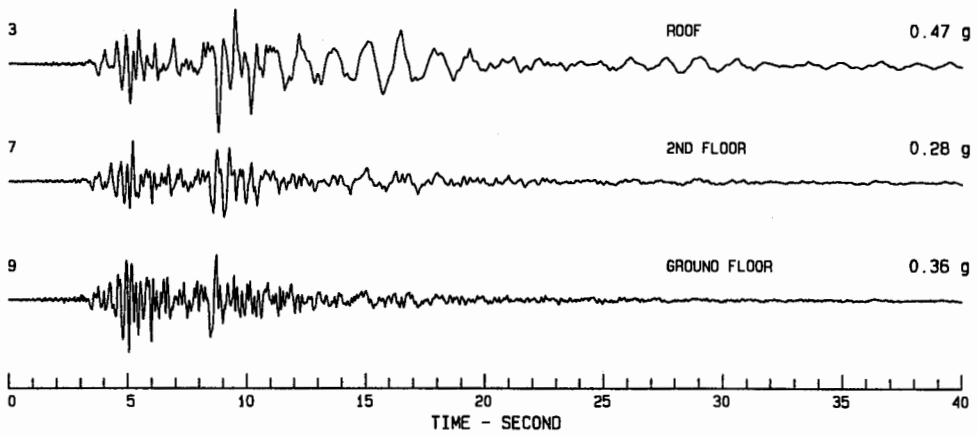


Fig. 16. Accelerations in the east-west direction recorded at the Burbank 6-story steel building during the 1994 Northridge earthquake.

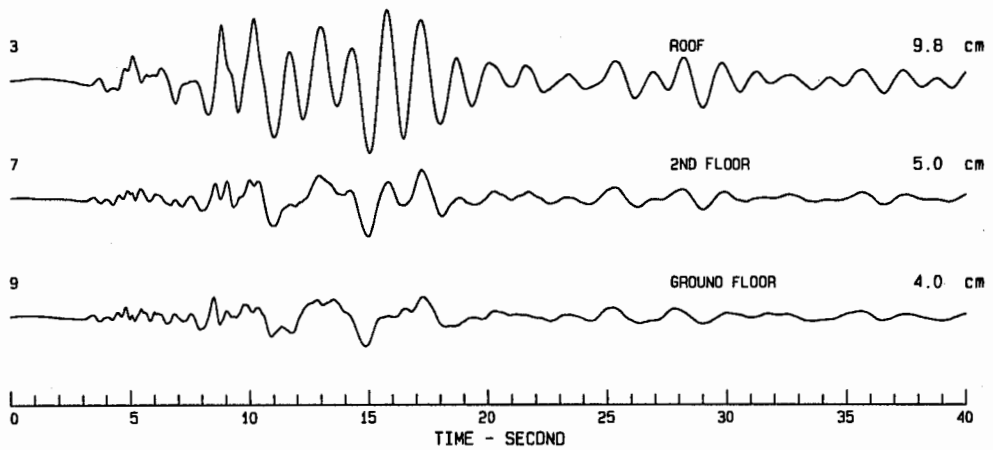


Fig. 17. Displacements corresponding to the accelerations in Fig. 16.

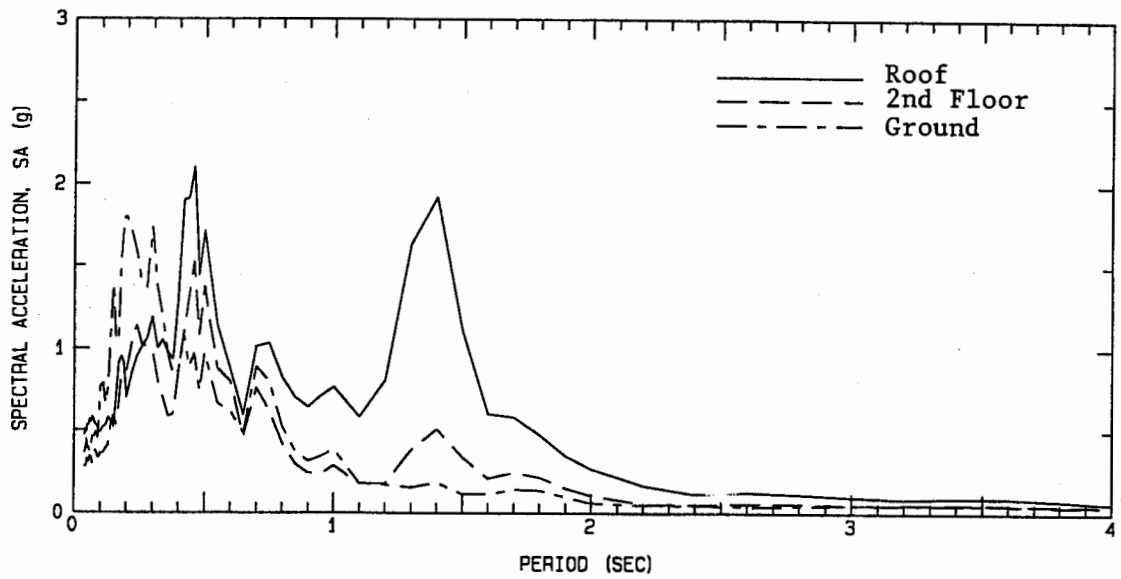


Fig. 18. Response spectra (2% damping) for the roof, 2nd and ground floors of the Burbank 6-story building corresponding to the accelerations in Fig. 16.

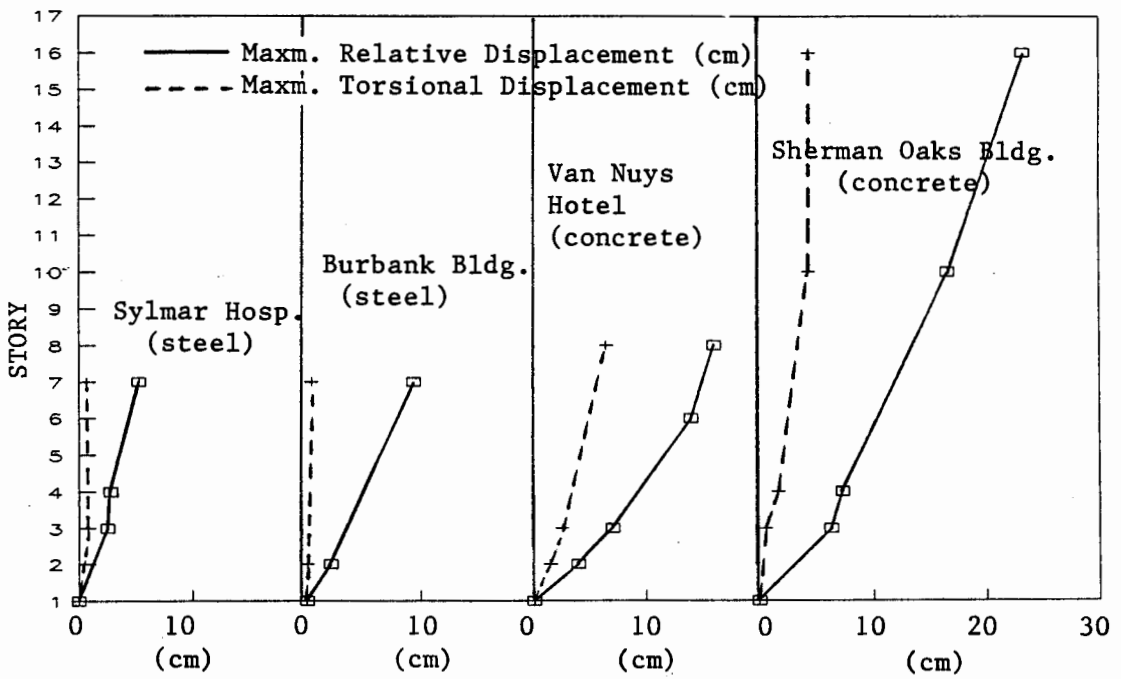


Fig. 19. Profile of drifts relative to the base in one direction and of torsional displacements in a) Sylmar Hospital, b) Burbank Building, c) Van Nuys Hotel, and d) Sherman Oaks Building for the Northridge earthquake.

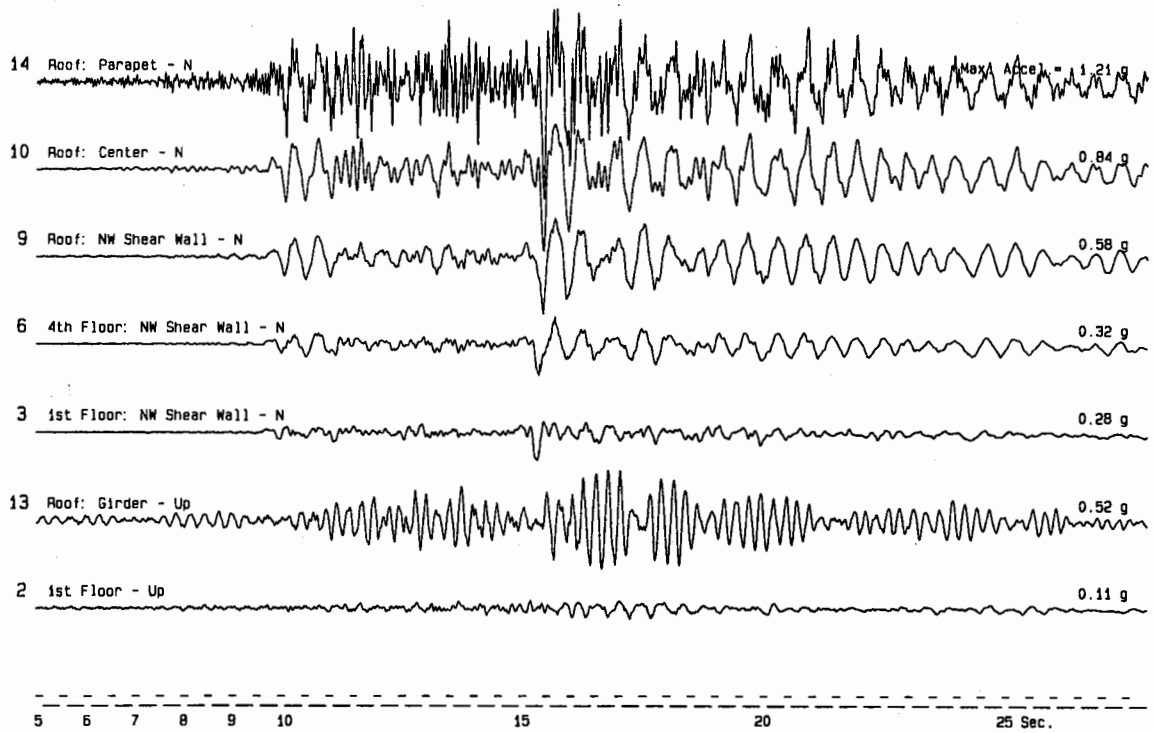


Fig. 20. Accelerations in the north-south and vertical directions recorded at the Los Angeles 6-story Parking Structure during the Northridge earthquake.

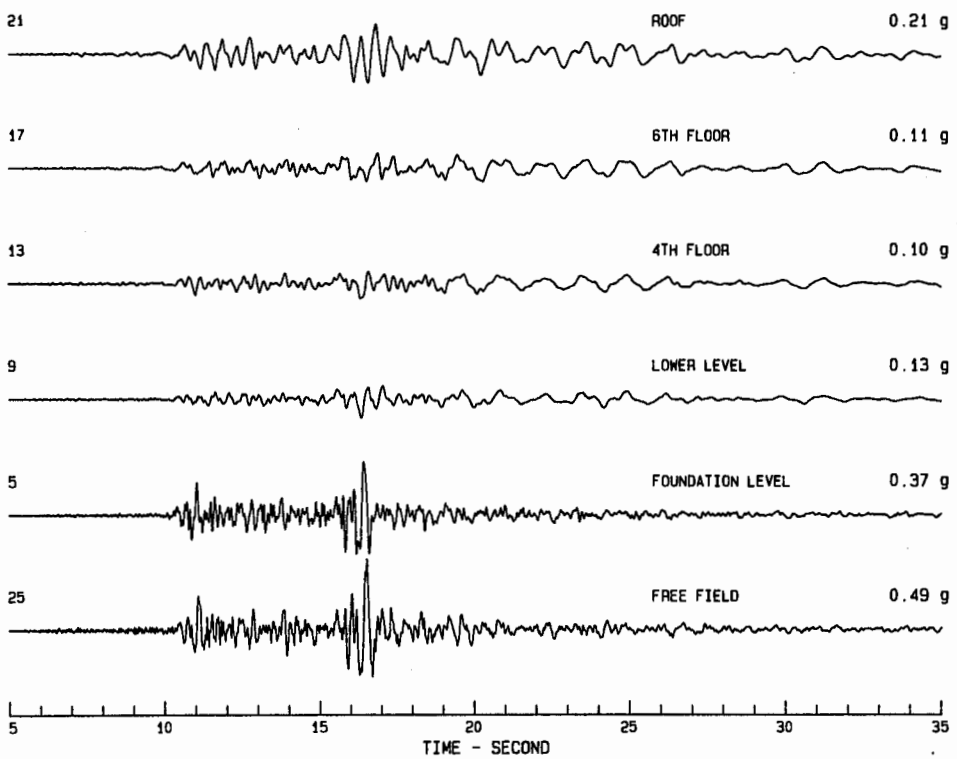


Fig. 21. Accelerations in the north-south (longitudinal) direction from the base-isolated University Hospital in Los Angeles for the Northridge earthquake.

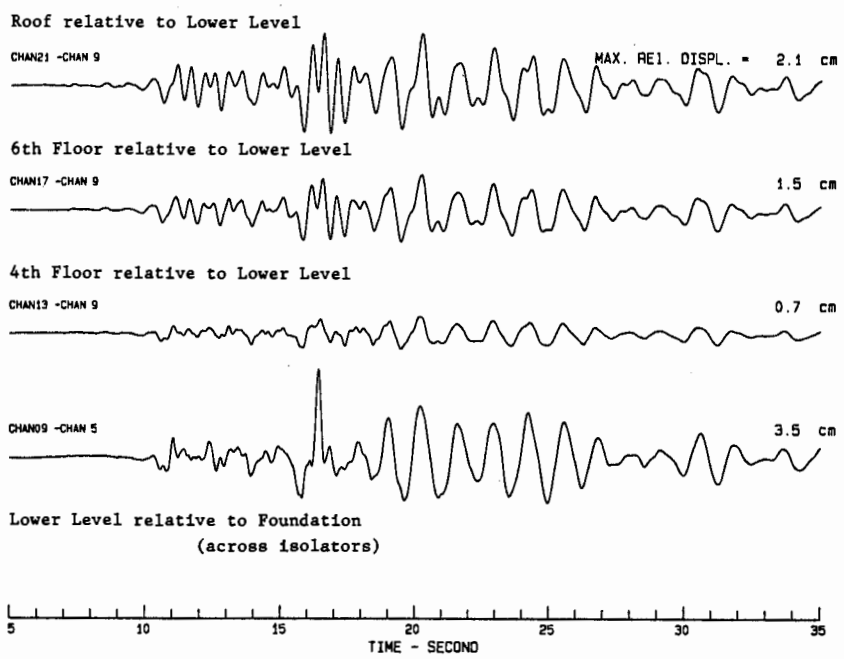


Fig. 22. Relative displacements in the north-south direction at the base-isolated University Hospital during the Northridge earthquake.

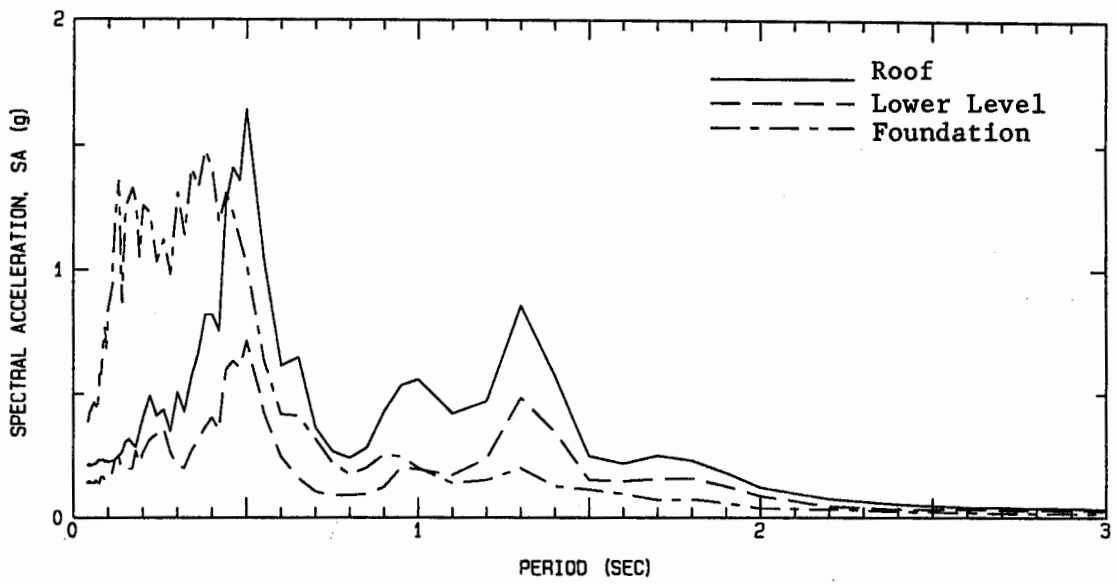


Fig. 23. Response spectra (2% damping) for the roof, lower level (above isolators) and foundation (below isolators) for the accelerations in Fig. 21.

# SITE RESPONSE STUDIES FOR PURPOSE OF REVISING NEHRP SEISMIC PROVISIONS

**C.B. Crouse and J.W. McGuire**

**Dames and Moore**
**Seattle, Washington**

## ABSTRACT

A strong-motion database was compiled for California earthquakes of surface-wave magnitudes, $M_S \geq 6$, occurring from 1933 through 1992. The database consisted of horizontal peak ground acceleration and 5 percent damped response spectra of accelerograms recorded on four different local geologies: bedrock (class A); soft rock or stiff soil (class B); medium stiff soil (class C); and, soft soil (class D). The results of regression analysis of the database within each of these site classes were used to derive a set of site-dependent spectral amplification factors for oscillator periods between 0.1 and 4.0 sec and ground acceleration levels between 0.1 and 0.4 g. The amplification factors at 0.3 and 1.0 sec periods are generally similar to those recommended during the 1992 NCEER Site Response Workshop.

## INTRODUCTION

The National Center for Earthquake Engineering Research (NCEER) held a workshop on site response in November 1992 (Martin, 1994). The primary objectives of the workshop were to develop revised site categories, site coefficients, and site-dependent spectra for inclusion in the 1994 National Earthquake Hazards Reduction Program (NEHRP) seismic provisions. The results of recent and ongoing research by several engineers and seismologists who attended the workshop provided valuable information for making the revisions. In reviewing this research, which was largely based on numerical model analysis using the computer program SHAKE (Schnabel et al., 1972) and on empirical studies of 1989 Loma Prieta earthquake data, it was discovered that a study of site response, using the wealth of strong-motion data recorded during the last 60 years, was not being conducted. This study was performed by the authors to compliment the results of the research completed to date and to provide to the revision process the necessary empirical component, which was currently lacking or underdeveloped.

The site-response parameters appearing in the 1991 NEHRP provisions were based mostly on the site-dependent spectra developed by Seed, et al. (1974) and Mohraz (1976), who used strong-motion data recorded through 1971. The abundant strong-motion accelerogram data recorded since the 1971 San Fernando earthquake offered the opportunity to improve the existing knowledge on site response gained since the Seed and Mohraz studies by conducting more thorough statistical studies of the strong-motion data.

The specific objectives of these statistical studies were to develop a set of site coefficients or amplification factors ($F_a$ and $F_v$), site-dependent spectra, and the associated site classifications for use in updating the NEHRP seismic provisions (Building Seismic Safety Council, 1991). The databases, analyses, and results of these studies are summarized in the remaining sections of this paper.

## DATABASES

Two databases were compiled: (1) geotechnical, geophysical and geological data for strong-motion stations, and (2) horizontal peak ground acceleration (PGA) and 5 percent damped pseudovelocity (PSV) response spectra of accelerograms recorded during central and southern California earthquakes of $M_s \geq 6.0$. Based on the local site data, four site classifications (A,B,C,D) were selected that were similar to those of Boore et al. (1993) and those recommended during the 1992 NCEER Site-Response Workshop (Martin, 1994). Abridged definitions of these site classes are as follows: A– rock, $\bar{V}_s \geq 2500$ fps; B– soft rock or stiff soil, $1200 \leq \bar{V}_s < 2500$ fps; C– medium stiff soils, $600 \leq \bar{V}_s < 1200$ fps; D– soft clay, $\bar{V}_s < 600$ fps, where $\bar{V}_s$ = average shear-wave velocity in the upper 100 feet of soil or rock.

After carefully searching the strong-motion and local geologic databases, a total of 238 records from 16 earthquakes were selected. With few exceptions, the data were recorded in small buildings up to three stories in height or in instrument shelters. The 238 records were distributed among the earthquakes and site classifications as shown in Table 1. Data from several $M_s > 6$ California earthquakes were not included. For example, accelerograms recorded in the Eureka-Ferndale area of Northern California were excluded because of the possible association of the causative earthquake with the southern Cascadia Subduction Zone, which represents a different tectonic environment than found in central and southern California. Accelerograms from the 1980 Mammoth Lakes sequence were excluded because this active volcanic region is atypical of the geological/tectonic regions of California where most of the accelerograms have been recorded. Accelerograms from the 1992 Big Bear earthquake were not available during the time the database was compiled.

A complete listing of the database used in the analysis will be provided in our final SMIP report to be submitted in June 1994. In addition to the information in Table 1, this listing will include: station name, location and type of structure recording ground motion; closest distance ($R$) from station to fault rupture of causative earthquake; PGA values for both horizontal and vertical components; site class; and, references for the information.

Plots of the $M_s$–$R$ distribution for the data within each site class in Table 1 are shown in Figure 1. Note that most of the data in each site class fall within the $M_s = 6 - 7.25$ and $R = 10 - 80$ km ranges.

**Table 1. Number of Accelerograms Used in Analysis**

| Date | Earthquake Name | $M_s$ | Type[1] | Soil Classification A | B | C | D |
|---|---|---|---|---|---|---|---|
| 1933.03.11 | Long Beach | 6.2 | S | | 1 | 1 | |
| 1940.05.19 | Imperial Valley | 7.1 | S | | | 1 | |
| 1952.07.21 | Kern County | 7.7 | R | | 3 | 1 | |
| 1966.06.28 | Central California | 6.1 | S | 1 | 3 | 3 | |
| 1966.08.07 | Baja | 6.3 | S | | | 1 | |
| 1968.04.09 | Borrego Mountain | 6.7 | S | | 2 | 5 | |
| 1971.02.09 | San Fernando | 6.5 | R | 6 | 13 | 8 | |
| 1979.10.15 | Imperial Valley | 6.8 | S | 1 | 1 | 23 | 3 |
| 1981.04.26 | Westmorland | 6.0 | S | 1 | 1 | 2 | 2 |
| 1983.05.02 | Coalinga | 6.7 | R | 1 | 13 | 6 | |
| 1984.04.24 | Morgan Hill | 6.1 | S | 1 | 7 | 6 | 4 |
| 1986.07.08 | Palm Springs | 6.0 | S | 4 | 3 | 4 | |
| 1986.07.21 | Chalfant Valley | 6.2 | S | 1 | | | |
| 1987.10.01 | Whittier | 6.1 | R | 3 | 14 | 13 | |
| 1989.10.17 | Loma Prieta | 7.1 | S | 11 | 20 | 18 | 7 |
| 1992.06.28 | Landers | 7.6 | S | 3 | 7 | 9 | |
| | Total | | | 33 | 88 | 101 | 16 |

[1] *Note:* S = *strike slip;* R = *reverse*

## ANALYSES

The numbers and distributions of accelerogram records in Table 1 suggested that the appropriate analysis procedure was to (1) conduct separate weighted nonlinear regressions of the more abundant class B and class C databases, and (2) compute factors to convert (i) class B response spectra to class A response spectra, and (ii) class C response to spectra to class D response spectra.

The regression model that was ultimately selected was

$$\ln Y = a + bM + d \ln\left(R + c_1 exp\{c_2 M\}\right) + eF$$

where: $Y$ is the ground-motion parameter (i.e., PGA or PSV); $M$ is surface-wave magnitude; $R$ is closest distance from the site to the fault rupture in km; $F$ is a binary fault-type parameter (1 for reverse earthquakes and 0 for strike-slip earthquakes) and $a$, $b$, $c_1$, $c_2$, $d$, and $e$ are the regression coefficients. The weighting scheme for the regression of each database was a modified form of one used by Campbell (1990), who defined distance intervals and gave the recordings from each earthquake within each interval the same total weight. In our weighing scheme, both magnitude and distance intervals were defined and the recordings within each magnitude-distance interval pair were given the same total weight. The magni-

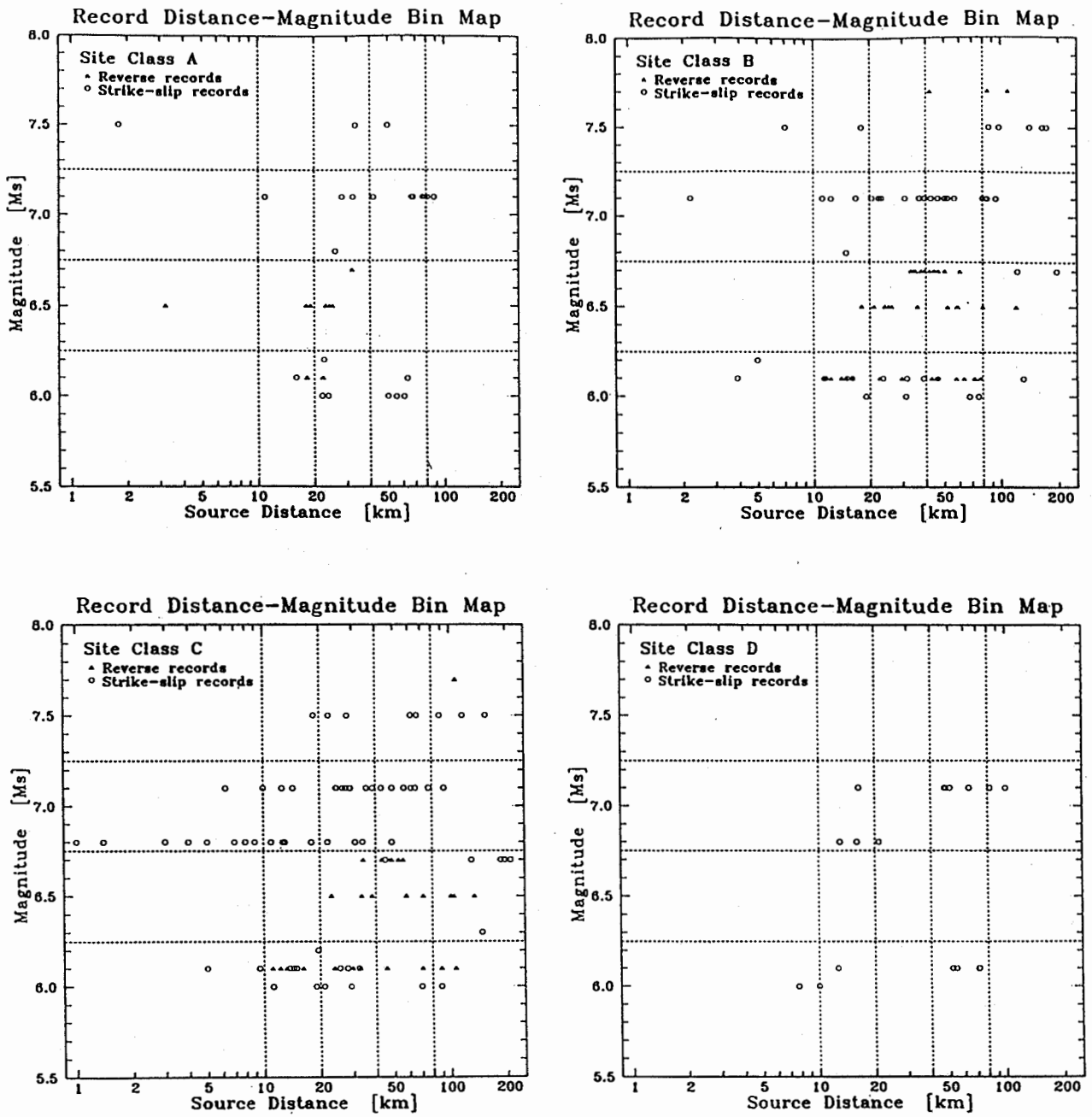


Figure 1. Distribution of Strong-Motion Data

tude–distance intervals are indicated with dashed lines in Figure 1. The geometric mean of both horizontal component values for each record was used in the regression analysis.

The nonlinear regressions on the class B and class C databases were performed using the BMDP Statistical Software program, 3R, (Dixon, 1986). Constraints involving the coefficients, $b$, $d$, $c_1$, and $c_2$, were introduced to ensure that $Y$ was an increasing function of $M$ for all $R \geq 0$. The coefficients, $a$, $b$, $c_1$, $c_2$, $d$, and $e$, and standard error, $\sigma_{\ell n Y}$ from the regressions are listed in Table 2. Plots of PGA and PSV ($T$ = 1 sec) attenuation curves for M = 6.0, 6.5, 7.0 and 7.5 strike-slip earthquakes are shown in Figure 2. These PGA and PSV figures are typical of the attenuation observed at short and long periods, respectively, where it can be seen that (1) the attenuation is slower for class C sites, and (2) the attenuation becomes slower with the increasing oscillator period, $T$.

Values of the coefficient, $e$, in Table 2 were used to plot the ratio of reverse to strike-slip ground motion versus $T$ (Figure 3) for class B and class C sites. The results for both site classes are similar in the sense that the ratios for $T < 1.0$ sec are generally greater that those for $T > 1.0$ sec, but the absolute values are different for the most part. Small values of $|e|$ (i.e., ratios ~ 1.0) were found statistically to not be significantly different from zero, but the general inconsistency in the class B and class C values makes it difficult to attach any significance of fault type on the level of ground motion from the results of this analysis.

The class B and class C regression equations were scaled to fit the class A and class D ground motion data. Specifically, the least-squares method was used to compute a factor $k_1$ such that $Y_A = k_1\ Y_B$. Similarly, a factor $k_2$ was computed such that $Y_D = k_2\ Y_C$. In these expressions, $Y_i$ denotes ground-motion parameters for site class $i$. The $k_1$ and $k_2$ values were computed as a function of $T$ and the median values are listed in Table 3. The possible dependence of $k_i$ with the acceleration level was not obvious based on a visual examination of the residuals from the regressions. Plots of the median $k_1$ and $k_2$ values (including the $\pm$ 1$\sigma$ limits) versus $T$ are shown in the upper and lower frames, respectively, of Figure 4. As expected from a visual examination of the results, the $k_i$ are not significantly different from 1.0 at the 95th percentile confidence level for the shorter periods (i.e., $T \leq 0.15$ sec for $k_1$ and $T \leq 0.50$ sec for $k_2$). Values of $k_1$ significantly less than 1.0 at longer periods are consistent with results of Boore et al. (1993) who show that longer period motions on rock sites are substantially less than those on soil sites. Similarly, values of $k_2$ significantly greater than 1.0 at longer periods are consistent with Borcherdt's (1994) results for the 1989 Loma Prieta earthquake data, which showed that longer period motion on the soft soils were greater than those on the stiff soil.

## AMPLIFICATION FACTORS AND RESPONSE SPECTRA

The PGA and PSV equations for site classes A, B, C and D were then used to generate amplification factors, $F_a$ and $F_v$ , analogous to those originally recommended during the 1992 NCEER workshop. The workshop values of $F_a$ and $F_v$ were primarily derived from the results of SHAKE computer analyses of soil profiles representative of the different site classes and to a lesser extent from empirical studies of the 1989 Loma Prieta earthquake ground motions (Borcherdt, 1994); these values were

**Table 2. Results of Regression Analyses**

$$\ell n\, Y^{\alpha,T} = a^{\alpha,T} + b^{\alpha,T} M + d^{\alpha,T} \ell n\left(R + c_1^{\alpha,T} exp\{c_2^{\alpha,T} M\}\right) + e^{\alpha,T} F$$

*Site Class B*

| Ground-Motion Parameter, $Y^{B,T}$ | Period $T$ [sec] | Predictor Equation Parameters $a^{B,T}$ | $b^{B,T}$ | $c_1^{B,T}$ | $c_2^{B,T}$ | $d^{B,T}$ | $e^{B,T}$ | $\sigma_{\ell n Y}^{B,T}$ |
|---|---|---|---|---|---|---|---|---|
| PGA | ... | –2.342699 | 1.091713 | 0.413033 | 0.623255 | –1.751631 | 0.087940 | 0.427787 |
| PSV($T$, $\xi$=5%) | 0.04 | –0.472585 | 1.036917 | 0.387669 | 0.612898 | –1.691826 | 0.108989 | 0.413926 |
| ⋮ | 0.10 | 7.571783 | 1.625135 | 4.612965 | 0.454664 | –3.574364 | 0.033013 | 0.467394 |
| ⋮ | 0.15 | 9.070027 | 1.601903 | 5.449227 | 0.434297 | –3.688497 | –0.014652 | 0.490720 |
| ⋮ | 0.20 | 7.408577 | 1.468556 | 3.775168 | 0.464040 | –3.164719 | 0.043634 | 0.472181 |
| ⋮ | 0.30 | 1.194880 | 1.086794 | 0.166050 | 0.706093 | –1.539165 | 0.128310 | 0.467039 |
| ⋮ | 0.40 | 0.887084 | 1.026752 | 0.083872 | 0.757907 | –1.354721 | 0.154355 | 0.495514 |
| ⋮ | 0.50 | 0.711154 | 1.055968 | 0.060623 | 0.788026 | –1.340017 | 0.153348 | 0.509970 |
| ⋮ | 0.60 | –0.070871 | 1.025031 | 0.048384 | 0.742853 | –1.104581 | 0.187939 | 0.529652 |
| ⋮ | 0.80 | –0.410607 | 0.936184 | 0.002278 | 1.044000 | –0.896728 | 0.330569 | 0.577221 |
| ⋮ | 1.00 | –1.829222 | 1.457603 | 0.008444 | 1.144165 | –1.273945 | 0.112767 | 0.592915 |
| ⋮ | 1.50 | –2.206094 | 1.262859 | 0.001634 | 1.287978 | –0.922951 | 0.032286 | 0.595854 |
| ⋮ | 2.00 | –3.886444 | 1.509735 | 0.000269 | 1.590216 | –0.949390 | 0.014204 | 0.561973 |
| ⋮ | 3.00 | –5.067456 | 1.651407 | 0.000080 | 1.807710 | –0.907890 | –0.135754 | 0.602980 |
| PSV($T$, $\xi$=5%) | 4.00 | –5.707326 | 1.745192 | 0.000070 | 1.844360 | –0.914570 | –0.245670 | 0.633340 |

*units of PGA:* [PGA] = $g$; *units of PSV:* [PSV] = cm/sec

*Site Class C*

| Ground-Motion Parameter, $Y^{C,T}$ | Period $T$ [sec] | Predictor Equation Parameters $a^{C,T}$ | $b^{C,T}$ | $c_1^{C,T}$ | $c_2^{C,T}$ | $d^{C,T}$ | $e^{C,T}$ | $\sigma_{\ell n Y}^{C,T}$ |
|---|---|---|---|---|---|---|---|---|
| PGA | ... | –2.353903 | 0.838847 | 0.305134 | 0.640249 | –1.310188 | –0.051707 | 0.416639 |
| PSV($T$, $\xi$=5%) | 0.04 | –0.316018 | 0.775418 | 0.317517 | 0.607199 | –1.277041 | –0.010872 | 0.424616 |
| ⋮ | 0.10 | 4.844192 | 0.668470 | 4.045981 | 0.352728 | –1.850579 | –0.091919 | 0.453879 |
| ⋮ | 0.15 | 12.359194 | 1.064481 | 16.158960 | 0.310128 | –3.432391 | –0.231488 | 0.435481 |
| ⋮ | 0.20 | 6.529981 | 1.249258 | 4.378859 | 0.443090 | –2.635199 | –0.041310 | 0.474415 |
| ⋮ | 0.30 | 2.043062 | 0.838572 | 0.884282 | 0.454604 | –1.285166 | 0.055896 | 0.496294 |
| ⋮ | 0.40 | –0.449217 | 1.103279 | 0.015008 | 0.978334 | –1.127712 | 0.227447 | 0.478698 |
| ⋮ | 0.50 | –1.079692 | 1.198570 | 0.006383 | 1.092807 | –1.096781 | 0.193853 | 0.468321 |
| ⋮ | 0.60 | –1.495757 | 1.172313 | 0.001802 | 1.232590 | –0.951097 | 0.159078 | 0.498147 |
| ⋮ | 0.80 | –3.567871 | 1.612229 | 0.000749 | 1.487888 | –1.083569 | 0.049774 | 0.558253 |
| ⋮ | 1.00 | –7.286583 | 2.563514 | 0.000557 | 1.716614 | –1.493355 | –0.102444 | 0.569552 |
| ⋮ | 1.50 | –6.200445 | 2.052788 | 0.000123 | 1.790362 | –1.146577 | –0.127769 | 0.545691 |
| ⋮ | 2.00 | –5.888256 | 1.974398 | 0.000155 | 1.748081 | –1.129466 | –0.279244 | 0.564984 |
| ⋮ | 3.00 | –6.088140 | 1.944268 | 0.000130 | 1.714319 | –1.134134 | –0.155093 | 0.692397 |
| PSV($T$, $\xi$=5%) | 4.00 | –7.441490 | 2.122133 | 0.000092 | 1.779805 | –1.119420 | –0.107566 | 0.745120 |

*units of PGA:* [PGA] = $g$; *units of PSV:* [PSV] = cm/sec

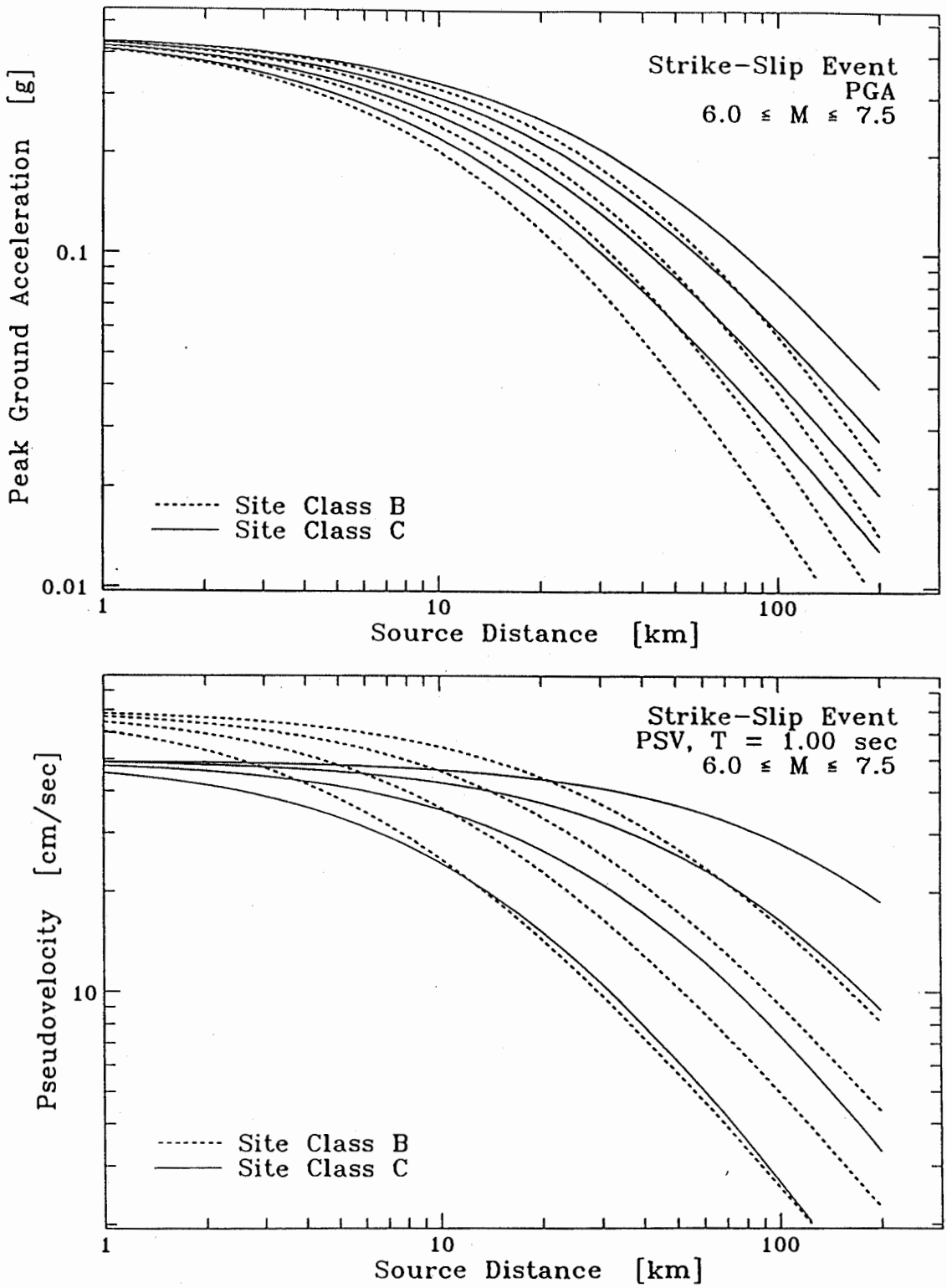


**Figure 2. Median PGA and PSV ($T$ = 1 sec) Attenuation Curves for $M$ = 6.0, 6.5, 7.0, and 7.5 Strike-Slip Events**

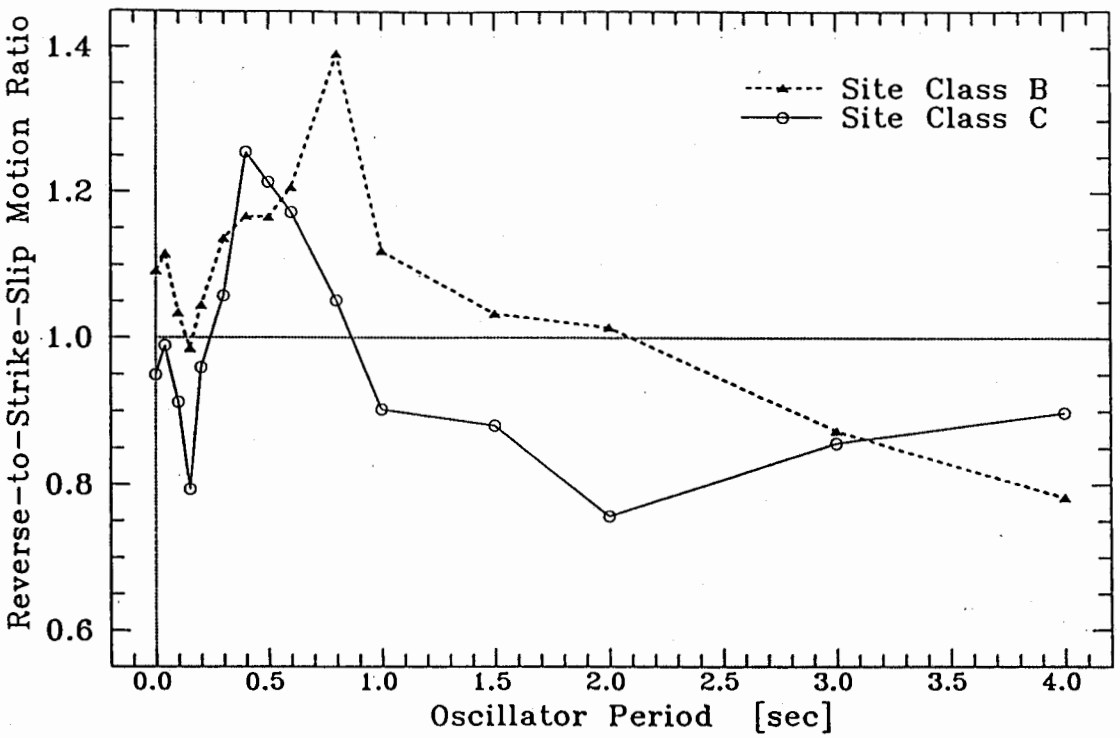


**Figure 3. Ratio of Reverse to Strike-Slip Earthquake Ground Motion**

**Table 3. Regression Results for $k_1$ and $k_2$**

$$Y^{A,T} = k_1^T\, Y^{B,T}$$
$$Y^{D,T} = k_2^T\, Y^{C,T}$$

| Ground-Motion Parameter, $Y^{\alpha,T}$ | Period $T$ [sec] | $k_1^T$ | $k_2^T$ |
|---|---|---|---|
| PGA | ... | 0.998638 | 1.200678 |
| PSV($T$, $\xi$=5%) | 0.04 | 1.023352 | 1.135611 |
| ⋮ | 0.10 | 1.144851 | 0.951057 |
| ⋮ | 0.15 | 0.952255 | 0.872571 |
| ⋮ | 0.20 | 0.817204 | 0.939360 |
| ⋮ | 0.30 | 0.753139 | 1.261232 |
| ⋮ | 0.40 | 0.719723 | 1.204849 |
| ⋮ | 0.50 | 0.620631 | 1.293272 |
| ⋮ | 0.60 | 0.600028 | 1.598795 |
| ⋮ | 0.80 | 0.629231 | 1.490827 |
| ⋮ | 1.00 | 0.572224 | 1.428036 |
| ⋮ | 1.50 | 0.529423 | 1.425156 |
| ⋮ | 2.00 | 0.578300 | 1.352620 |
| ⋮ | 3.00 | 0.589383 | 1.408488 |
| PSV($T$, $\xi$=5%) | 4.00 | 0.632419 | 1.300720 |

*units of PGA: g; units of PSV:* cm/sec

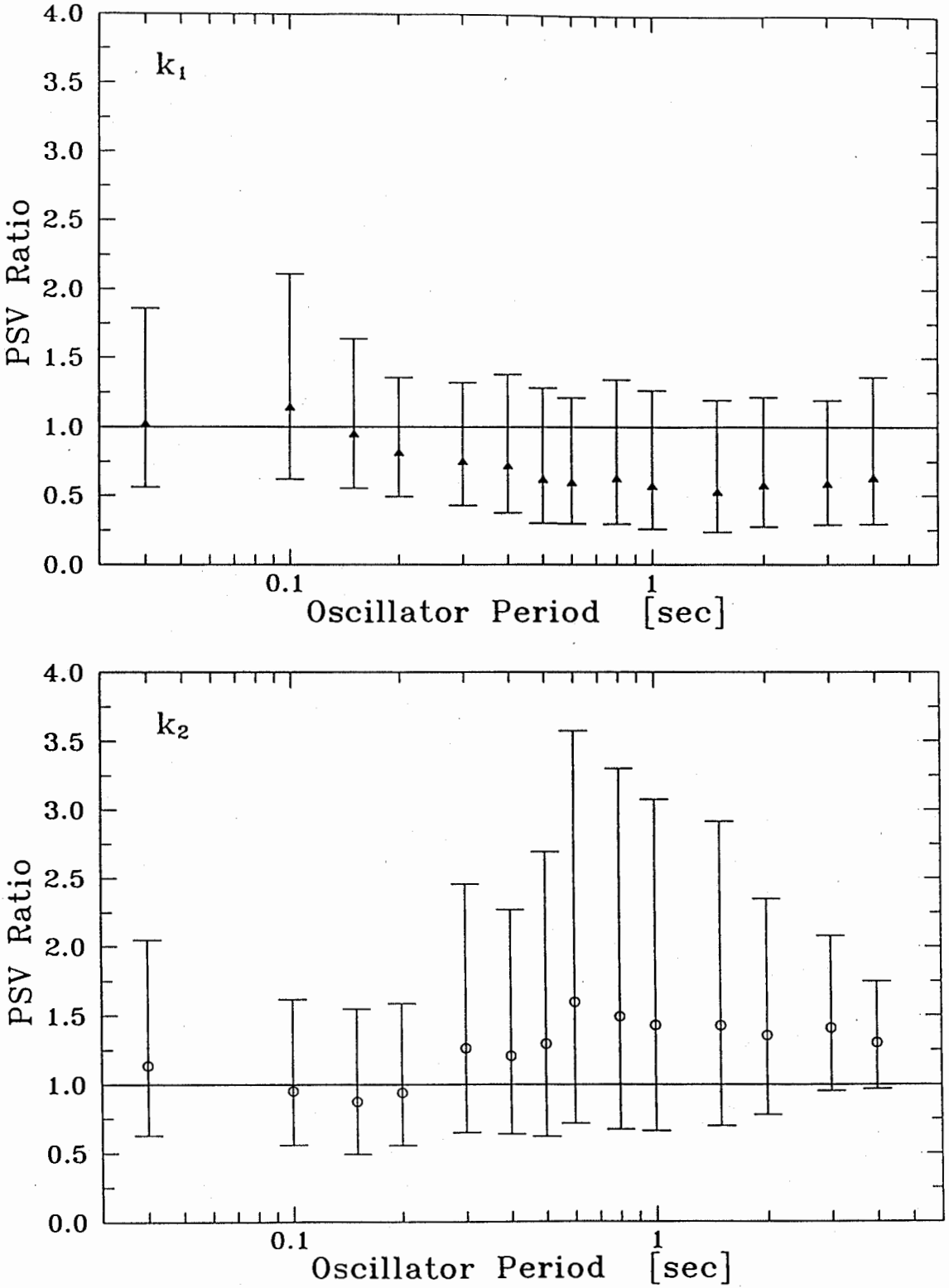


**Figure 4. Median Values and ± 1 Sigma Limits of $k_1$ and $k_2$**

functions of the ground acceleration level (0.1 g, 0.2 g, 0.3 g, 0.4 g, and 0.5 g). The $F_a$ values from the present study were derived from similar rock-site acceleration levels (median $PGA_A$ = 0.1 g, 0.2 g, 0.3 g, and 0.4 g) by computing the ratio $PSV_i / PSV_A$ (where $i$ = site classes B, C, and D) at period T = 0.3 sec for selected magnitude–distance combinations that yielded the proper acceleration values. Specifically, for each acceleration level $PGA_A$, three magnitude values ($M$ = 6.5, 7.0, and 7.5) and three acceleration values ($PGA_A$ and $PGA_A \pm 0.05$ g) were considered; for each magnitude, the value of $R$ required to yield each of the three acceleration values was computed. Thus, for a given acceleration level, nine ($M$, $R$) ordered pairs were used to compute nine values of $PSV_i / PSV_A$, which in turn were averaged to obtain the value of $F_a$ for a given site class $i$. In this manner, values of $F_a$ were determined at each acceleration level for site classes $i$ = B, C, and D.

The $F_v$ values were computed in a similar manner using the PSV ($T$ = 1 sec) predictions. The strong-motion data were insufficient to estimate factors for PGA = 0.5 g. Our computed $F_a$ and $F_v$ factors are summarized in Table 4; the adjacent values in parentheses are the recommendations from the 1992 NCEER workshop (Martin, 1994).

**Table 4. Amplification Factors, $F_a$ and $F_v$**

| Site Class | Acceleration Level 0.1 g | 0.2 g | 0.3 g | 0.4 g |
|---|---|---|---|---|
| Amplification Factor, $F_a$, at $T$ = 0.3 sec | | | | |
| A | 1.0 (1.0) | 1.0 (1.0) | 1.0 (1.0) | 1.0 (1.0) |
| B | 1.3 (1.2) | 1.3 (1.2) | 1.3 (1.1) | 1.3 (1.0) |
| C | 1.6 (1.6) | 1.5 (1.4) | 1.4 (1.2) | 1.3 (1.1) |
| D | 2.1 (2.25) | 1.9 (1.65) | 1.8 (1.2) | 1.7 (0.9) |
| Amplification Factor, $F_v$, at $T$ = 1.0 sec | | | | |
| A | 1.0 (1.0) | 1.0 (1.0) | 1.0 (1.0) | 1.0 (1.0) |
| B | 1.8 (1.7) | 1.8 (1.6) | 1.8 (1.5) | 1.8 (1.4) |
| C | 2.3 (2.4) | 1.7 (2.0) | 1.4 (1.8) | 1.2 (1.6) |
| D | 3.2 (3.5) | 2.5 (3.2) | 2.1 (2.8) | 1.8 (2.4) |

*Note: Values in ( ) are from the 1992 NCEER Workshop (Martin, 1994)*

To provide an indication of the differences in site-dependent spectra, response spectra for site classes A, B, C, and D were computed for several values of $M$ and $R$. A typical example is shown in Figure 5 for an $M$ = 7.0 strike-slip event at $R$ = 10 km. In this figure the differences in the spectra, which are representative of the 0.3 g acceleration level, are fairly consistent with the differences in the $F_a$ and $F_v$ values in Table 4. Note that at $T$ = 1.0 sec, the spectral acceleration for site class C is less than the spectral acceleration for site class B , which is consistent with the $F_v$ values for 0.3 g in Table 4 for

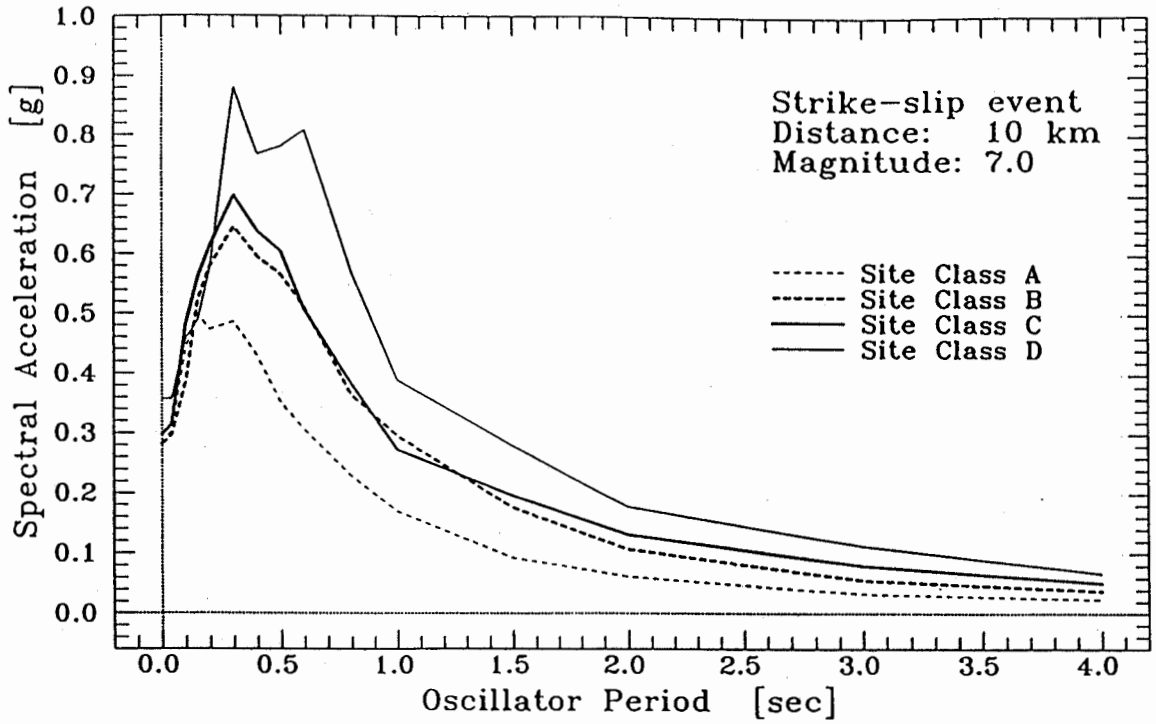


**Figure 5. Median Site-Dependent Response Spectra for 5% Damping**

classes B and C. However, in Figure 5 the class C spectra are larger than the class B spectra at $T > 1.0$ sec, which is intuitively expected and which was consistently observed in the spectra computed at other ($M$, $R$) values. Because the $F_v$ values proposed in the 1992 NCEER workshop were intended to represent the amplification over the intermediate period (constant spectral velocity) range of the spectrum, some revisions to the values in Table 4 are required. Factors of $F_v$ at other periods between 0.8 and 4.0 sec will be presented in our final SMIP report and used to develop our final recommendations.

Site-dependent response spectra estimated with the equations developed in this study were compared with spectra estimated from the attenuation equations recently published by Boore et al. (1993) and Campbell (1990). An example is shown in Figure 6 for the $M = 7.0$ strike-slip event at $R = 10$ km; the top and bottom plots show the spectra predicted for class A and class C sites, respectively. In an attempt to simulate site class A using Campbell's equations, the depth-to-basement-rock parameter ($D$) in his equations was set equal to zero; to simulate site class C, $D$ was set equal to 5 km. The differences among the spectra in Figure 6 are expected given the differences in databases, regression equations and analyses, and parameter definitions such as magnitude and distance. For example, for site class A, the Crouse and Boore et al. spectra are similar and both are significantly lower than Campbell's spectrum. The much larger Campbell spectrum is believed to be primarily the result of his rock database, which he defines as soft rock. Most of these soft rock data would fall into the site class B category rather than into site class A. Thus, Campbell's (1990) equations are not recommended for class A sites. Precise reasons for the differences in the class C spectra are less obvious, and further analysis would be required to explain them, which was outside the scope of this study.

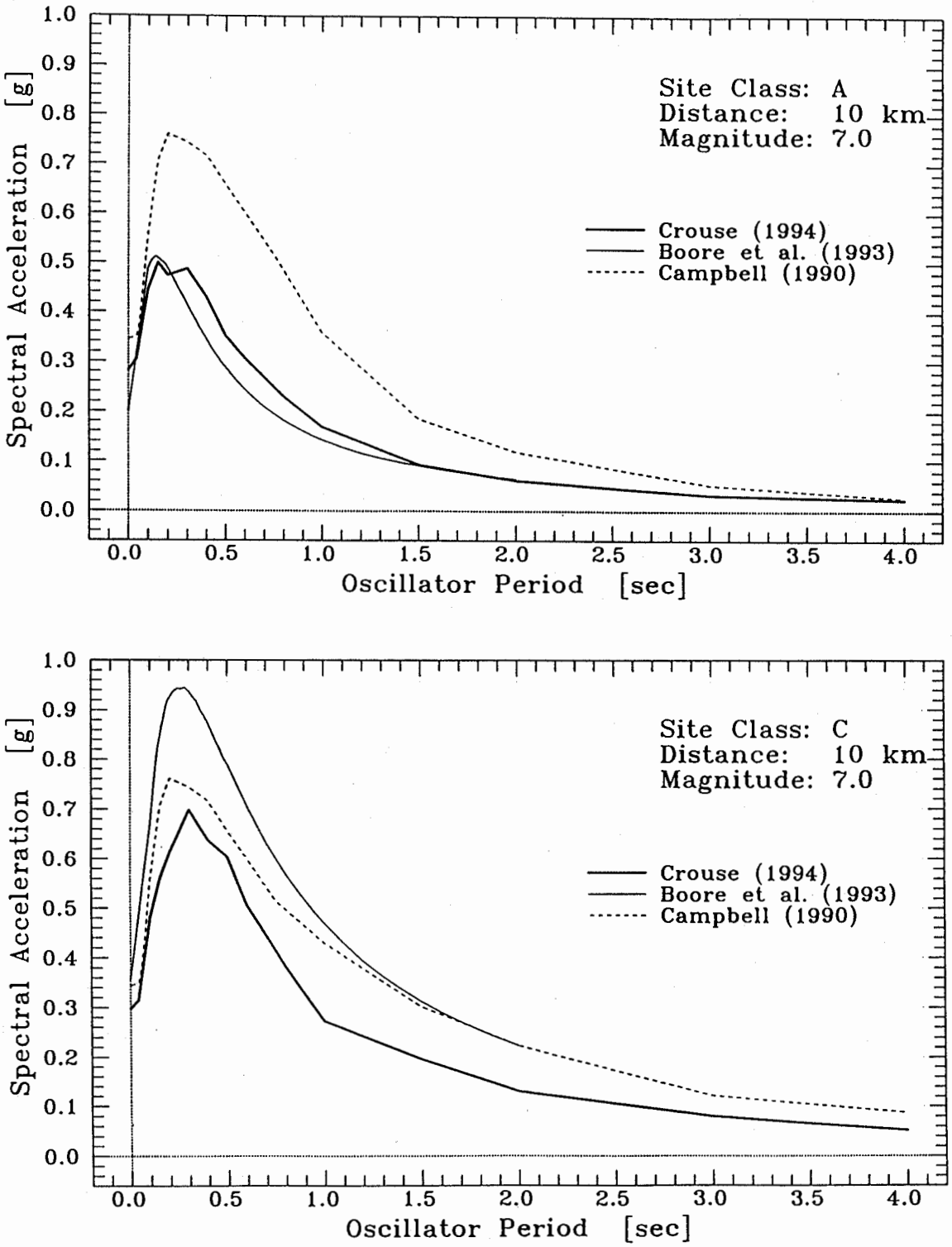


**Figure 6. Comparison of 5% Damped Median Response Spectra for Magnitude 7.0 Strike-Slip Earthquake**

## CONCLUSIONS

The results of this study provide estimates of the spectral amplification due to differences in local geology. The amount and distribution of the strong-motion data suggest that the results are more reliable for ground acceleration levels of approximately 0.1 to 0.3 g for class A, B, and C sites. These acceleration levels roughly correspond to the $M = 6 - 7.25$ and $R = 10 - 80$ km ranges where there is a reasonable amount of data. The results for 0.4 g and for class D sites at all acceleration levels are more uncertain. As a final note, the equations presented herein were developed to estimate site amplification factors and were not developed for seismic hazard analyses. The authors caution potential users of these equations for such analyses, especially for near-field conditions ($R < 10$ km), where the database used to derive the equations is recognized as being limited.

## ACKNOWLEDGEMENTS

The authors wish to thank J. Egan and M. Power of Geomatrix, P. Grant of Shannon and Wilson, and C. Thiel for providing data on the local geology of many of the strong-motion stations. Mr. T. Price, former staff engineer at Dames & Moore and currently a graduate student at the University of Washington, participated in the initial phases of the study. This project was funded by grants from the National Science Foundation, Nuclear Regulatory Commission, and the California Division of Mines and Geology. Their support is greatly appreciated.

## REFERENCES

Boore, D.M., Joyner, W.B., and Fumal T.E. (1993). Estimation of Response Spectra and Peak Accelerations from Western North America Earthquakes: An Interim Report: *USGS Open-File Report 93-509.*

Borcherdt, R.D.(1994). New developments in estimating site effects on ground motion: *Proceedings ATC-35-1.*

Building Seismic Safety Council (1991). *NEHRP Recommended Provisions for the Development of Seismic Regulations for New Buildings, Part 1, Provisions.*

Campbell, K.W. (1990). Empirical prediction of near-source soil and soft-rock ground motion for the Diablo Canyon Power Plant Site, San Luis Obisbo County, California: *Dames and Moore report to Lawrence Livermore National Laboratory*, September 1990 110p.

Crouse, C.B. (1994). Site response studies for purpose of revising NEHRP seismic provisions: *Dames and Moore report to be submitted to NSF, NCR and CDMG*, June 1994.

Dixon, W.J.(Editor) (1986). BMDP Statistical Software: *University of California Press*, 733p.

Martin, G., ed., (1994). *Proceedings NCEER, SEAOC, BSCC Workshop on site response during earthquakes and seismic code provisions*: University of Southern California, Los Angeles, California, November 1992.

Mohraz, B. (1976). Earthquake response spectra for different geologic conditions: *Bull. Seism. Soc. Am.*, v.66, p.915–935.

Schnabel, P.B., Lysmer, J. and Seed, H.B. (1972). SHAKE: A Computer Program for Earthquake Response Analysis of Horizontally Layered Sites: *Report No. EERC 72-12*, Earthq. Engr. Res. Center, Univ. of Calif. at Berkeley.

Seed, H.B., Ugas, C., and Lysmer J. (1974). Site dependent spectra for earthquake resistant design: *Report No. EERC 74-12*, Earthq. Engr. Res. Center, Univ. of Calif. at Berkeley.

# ANALYSIS OF STRONG MOTION RECORDS FROM NON-DUCTILE CONCRETE MOMENT FRAME BUILDINGS

David Bleiman[1], S.E., Simon Kim[2], Ma-Chi Chen, Ph.D.[3]

**Abstract**

The California Strong Motion Instrumentation Program has obtained significant records of earthquake motions of non-ductile concrete moment frames in Southern California. This research was performed to verify or develop methods for better understanding and prediction of the seismic performance of these buildings.

Three dimensional models of non-ductile reinforced concrete buildings were developed to test a variety of analytic techniques and materials assumptions against the recorded data. Linear elastic models which explicitly account for the stiffness contribution of diaphragms, in addition to the building frames, provided fairly accurate prediction for the low to moderate levels of earthquake motions.

## Introduction

This study is part of the Data Interpretation Project of the California Strong Motion Instrumentation Program (CSMIP) in the Department of Conservation, Division of Mines and Geology. The purpose of this study is to use strong motion records from non-ductile concrete moment frame buildings to verify or develop methods for better understanding and prediction of the seismic performance of these buildings.

The three subject buildings for this study are:

| Van Nuys Bldg. | Pasadena Bldg. | Sherman Oaks Bldg. |
|---|---|---|
| CSMIP Sta. #24386 | CSMIP Sta. #24571 | CSMIP Sta. #24322 |

All three buildings are fairly regular in plan and represent a good range of typical mid-height non-ductile concrete moment frame buildings, thus allowing some generalizations from this research for non-ductile concrete frame buildings as a class. See Table 1 and Figures 1,2, and 3 for building descriptions.

The strong-motion records available for this research represent low to moderate input earthquake motions. The input base accelerations ranged from a maximum of 0.25g to a low of 0.024g, and the majority of the records show peak input base accelerations of less than 0.10g (see Table 2). None of the subject buildings exhibited residual displacements from these earthquakes, or indicated significant nonlinear behavior.

Two types of dynamic analysis were tested to verify their ability to predict the building response: Three Dimensional Linear Analysis and Three Dimensional Nonlinear Analysis. The linear analysis was further subdivided into two types, according to modeling assumptions: Rigid Diaphragms and Flexible Diaphragms.

## Analytical Techniques

The initial models used the simplest and most common assumptions used to analyze concrete frames. These models were developed using the computer program "ETABS"[1]. The ETABS models assumed rigid diaphragms so that the story stiffnesses were condensed into three degrees of freedom per floor: two translational and one rotational. Floor diaphragm rotational stiffness was

---

[1]Project Manager, Cygna Group, Inc., 1800 Harrison Street, Oakland CA 94612

[2]Engineer, Cygna Group, Inc., 1800 Harrison, Oakland CA 94612

[3] Principal, Collaborative Engineering Service, 20430 Towne Center Lane #5E-1, Cupertino CA 95014

neglected. In addition, section properties were based on $I_{gross}$, and damping was assumed to be 5% of critical for all earthquakes. Our next refinement of the models used the linear computer program "SAP90"[2]. Here the diaphragms were explicitly modeled as shell elements to include shear and bending deformations, and $I_{effective}$ and damping were varied. Lastly, a highly refined, three dimensional nonlinear analysis using the computer program "DRAIN-3DX"[3] was performed for the only structure with a building response above 0.3g (Pasadena Bldg.).

**Linear Analysis with Rigid Diaphragms - "ETABS Analysis"**

Structural Models

All necessary structural information was obtained from the structural drawings provided by CSMIP. The member sizes for beams and columns were obtained from the design drawings. The floor slab bending stiffness was ignored. Shear deformations in beams and columns were included, and the rigid joint offsets were modeled.

The masses of the buildings were computed including the floor slabs, columns, beams, and exterior skin. Penthouse and mechanical room masses were lumped to the roof. Young's modulus was calculated using the ACI section 8.5.1. For the time history analysis, a standard 5% damping ratio was assumed. Soil-structure interaction effects were ignored.

Analysis Results

A single earthquake record was selected for the linear time history analysis of each building. The calculated and recorded values for peak accelerations and time history displacements were compared. As shown in Tables 3,4 and 5, the peak accelerations results differed by as much as 60%. Comparisons of recorded and calculated displacement time histories (not included in this paper) show that phase and amplitudes were not in agreement, indicating that the model stiffnesses and dampings were incorrect.

**Linear Analysis with Flexible Diaphragms - "SAP90 Analysis"**

Because of the poor match between the recorded and calculated peak acceleration and displacement responses, further refinement was required to accurately predict the response of the buildings. The models were refined by including the flexible floor diaphragms and by calibrating the structural periods and damping.

Structural Model Refinements

Starting with the previously developed linear models, the flexible diaphragms were added by modeling the roof/slabs with shell elements. The gross sections of the slabs were used. The model stiffness was "calibrated" using the building responses from one arbitrarily chosen earthquake. To perform this calibration, we carefully examined the time histories, Fourier spectra, and response spectra provided by CSMIP to determine the fundamental periods of vibration of the buildings. The model response periods were then calibrated to match the recorded periods by adjusting the frame stiffnesses and roof/slab stiffnesses.

After calibrating the structural periods, the damping values were adjusted by comparing the calculated and recorded peak responses (acceleration and displacement), using the same earthquake that was used for the period calibration. Effective damping values were determined in the long and short directions of buildings. Only one effective damping per direction was assumed, and the selected damping values remained constant for all other earthquake records.

Van Nuys - 7-story Hotel

From the Big Bear records, the fundamental periods of 1.2 seconds (long) and 1.3 seconds (short) were estimated. Effective damping values of 9% and 15%

were determined in the long and short directions, respectively. Both damping values seem quite high for the low amplitude of vibration. Possible reasons for the high values include soil-structure interaction and participation of the nonstructural elements (partitions, etc.).

The slab bending stiffness significantly affected the transverse mode. By including 62% of the slab shell in the short direction, the transverse mode period decreased from 1.7 seconds to 1.3 seconds. Although there are no interior beams in the transverse direction, the thick slabs contribute partial frame action with the columns. In the longitudinal direction, slabs provided only a small increase in the longitudinal stiffness.

Time History Analysis Results

The building was subjected to three recorded base accelerations: The Big Bear Earthquake, The Landers Earthquake, and The Whittier Earthquake. (See Table 2.) Comparisons of calculated and recorded peak accelerations in the long direction of the building show an agreement within 10% (see Table 6). In the short direction, the maximum accelerations generally agree within 25%. The Whittier results cannot be directly compared, for only the base input in the short direction was used. (The base sensors failed in the long direction during the earthquake.)

Displacement time history plots provide a more complete basis for comparing the performance of the model than peak accelerations. Comparisons of displacement time histories also show very close agreement; the displacement response frequencies and amplitudes matched quite well between the recorded and calculated values for all earthquake record (see Figures 4 and 5).

Pasadena - 9-story Commercial Building

The Sierra Madre Earthquake was used to determine the fundamental periods of vibration of 1.2 seconds (long dir.) and 2.0 seconds (short dir.). Effective damping values of 3% and 4% were selected for the long and short directions.

The modal analysis results indicated that the bending stiffness of the slab does not affect the fundamental modes, since the building has complete frames in both directions. The stiffness calibration required a stiffness reduction of 25% in frames in the longitudinal direction.

Time History Analysis Results

The building was subjected to three recorded base accelerations: the Big Bear Earthquake, the Landers Earthquake, and the Sierra Madre Earthquake. Comparisons of calculated and recorded peak accelerations in the longitudinal direction are within 20% (see Table 6). In the short direction, the maximum accelerations generally agree within 20%.

Comparisons of displacement responses during the Sierra Madre Earthquake, which produced the highest recorded accelerations in the building, yield interesting observations: The calculated and recorded roof displacements in the long direction of the building match well for the first 6 seconds. Then, the recorded data shows an increase in the structural period between 6 and 30 seconds of the strong motion. In the last 10 seconds of the earthquake,the two responses match again. This observation suggests that the structure softened due inelastic behavior. (This was verified by the nonlinear analysis of the building.) However, the degree of nonlinearity was not severe enough to cause a significant deviation between the recorded and calculated displacements (see Figure 5).

Overall, the calculated and recorded displacement responses matched fairly well (see Figures 5 and 6).

Sherman Oaks - 13-story Commercial Building

The Whittier Earthquake records indicate the fundamental periods of vibration of 2.2 seconds (long dir.) and 2.4 seconds (short dir.). The modal analysis

results indicated that the bending stiffness of the slab did not affect the fundamental modes, since the building has complete frames in both directions, and the slab is relatively thin. The period calibration required a frame stiffness reduction of about 15% in both directions.

Effective damping values of 5% were determined in both the long and short directions. Although the selected damping value matched the displacements, the peak accelerations could not be matched as well. Time history acceleration and displacement responses show that the peak acceleration occurs at the beginning of the strong motion, and appears to be associated with high frequency motions. [4]

Time History Analysis Results

The building was subjected to two recorded base accelerations: the Whittier Earthquake and the Landers Earthquake. Comparisons of displacements during the Whittier Earthquake show good agreement in frequency and amplitude.

Results from the Landers Earthquake are quite interesting. Time histories, Fourier spectra, and response spectra of the recorded motions indicate that the building's fundamental periods are 2.8 seconds in both directions. This is significantly different from the periods 2.2 seconds (long) and 2.4 seconds (short) during the Whittier Earthquake. Since the model was "calibrated" to the Whittier Earthquake, calculated and recorded responses do not match well for the Landers Earthquake. Figure 7 shows that the calculated and recorded roof displacements do not agree in frequency and amplitude. The change in structural periods, perhaps, may be due to soil-structure interaction. The soil-structure interaction can change the fundamental structural periods. [5]

**Non-Linear Analysis - "DRAIN-3DX Analysis"**

As a final phase of the research, the importance of the material nonlinearity was explored. The Pasadena 9-story Commercial Building and the Sierra Madre Earthquake records were selected for detailed nonlinear analysis. The choices were based on the peak building acceleration responses. During the Sierra Madre Earthquake, the Pasadena building experienced the maximum base acceleration of 0.23g, and the maximum structural response acceleration of 0.43g. This was the highest recorded acceleration of all three selected buildings in this research.

The three dimensional nonlinear finite element model used fiber beam-column elements to model member nonlinearities. Each fiber beam-column element consisted of an elastic bar element in the middle, and nonlinear fiber hinges at each end. The assembly of fiber beam-column elements allowed nonlinear actions at every joint in the model.

The non-linear moment curvature relationship for each fiber hinge was developed using the program "BIAX" [6]. The non-ductile concrete stress strain relationship was developed using the Shiehk-Uzumeri relation [6]. The column moment curvature relationships were developed using the unfactored dead load as the axial load to capture the P-M interaction. The developed nonlinear moment curvature relationships were, then, idealized as bilinear stress-strain relations for the fiber hinges. In addition to the material nonlinearity, the geometric nonlinearity due to the P-delta effect was included in the time history analysis. The nonlinear time history analyses were performed using the Rayleigh damping equivalent to the 5% viscous damping.

Two models were tested for the nonlinear dynamic analysis, with the elastic portion of the fiber beam-column elements varied in each model. The moment of inertia for the elastic portion of the beams and columns was varied from $1.0xI_{gross}$ to $0.5xI_{gross}$ in two separate models. The use of $I=0.5xI_{gross}$ provided a fairly accurate match of displacements to the recorded responses in the longitudinal direction. (See Figure 8.)

Time history analysis results in the long direction, the predominant

earthquake input direction, show that only a small number of beam/column joints experienced minor incursions into the inelastic region. From this observation we concluded that the material nonlinearity was not a significant factor for predicting the responses of the buildings in this study.

Nonlinear (DRAIN-3DX) and SAP90 Compared

Figure 8 shows the roof displacement time histories in the long direction of the Pasadena Building during the Sierra Madre Earthquake. The DRAIN-3DX calculated displacements match the recorded displacements fairly well. SAP90 calculated displacements, on the other hand, match the beginning portion of the time history and "misses" the stiffness change in the structure. Thus the linear model, which was "calibrated" to the initial elastic stiffness of the structure, remained elastic while DRAIN-3DX model updated the minor stiffness degradation experienced by the structure.

With the exception of the frequency of motion, the linear analysis results produced satisfactory results. Since the nonlinearities experienced by the structure were minor due to the relative low base input accelerations, the deviations between the two analyses results were not significant. However, if the earthquake motions were stronger, we would expect that only nonlinear analysis will accurately predict the behavior of the structure. (Only the nonlinear analysis is capable of updating the stiffness changes taking place, and of predicting the structural capacity limit during strong earthquake motions, i.e., the Northridge Earthquake of January 17, 1994.)

## Conclusions

Important findings of this research are:

- Linear analysis can be "calibrated" to accurately predict motions of nonductile reinforced concrete moment frame structure during small to moderate earthquake strong motions.
- Two parameters available for "calibrating" the linear model are the frame stiffness and damping ratio.
- In-situ concrete frame member stiffnesses varies between 75% to 85% of the $I_{gross}$, and the viscous damping varied between 3% to 15% of critical.
- Floor slab bending stiffness should be included in the model.

## Bibliography

[1] Ashraf Habibullah, ETABS, Three Dimensional Analysis of Building Systems, Version 5.4, Computers and Structures, Inc. Berkeley, CA, August, 1992

[2] E.L. Wilson and Ashraf Habibullah, SAP90, A Series of Computer Programs for the Static and Dynamic Finite Element Analysis of Structures, Ver. P5.4, Computers and Structures, Inc., Berkeley, CA, July 1989

[3] V. Prakash, G.H.Powell, and F.C. Filippou, DRAIN-3DX, Version 1.03: Base Program User Guide, Structural Engineering Mechanics and Materials Report No. UCB/SEMM-92/30, December 1992

[4] CSMIP, CSMIP Strong Motion Records from the Whittier California Earthquake of 1 October, 1987, California Department of Conservation, Division of Mines and Geology, Office of Strong Motion Studies, Report OSMS 87-05

[5] Gregory L. Fenves and Georgio Serino, "Evaluation of Soil-Structure Interaction in Buildings During Earthquakes", Data Utilization Report CSMIP/92-01, CSMIP Sacramento, CA, June 1992

[6] John W. Wallace, BIAX: Revision 1, A Computer Program for the Analysis of Reinforced Concrete and Reinforced Masonry Sections, Dept. of Civil Engineering, Clarkson University, Report No., CU/CEE-92/4, Potsdam, New York, Feb. 1992

Table No. 1: Description of Building

| Name SMIP Station | Date of Construct. | Plan Dimensions | Stories Above Ground/ Below Ground | Foundation System |
|---|---|---|---|---|
| Pasadena Bldg. Sta. #24571 | 1964 | 213'x86' | 9/1 | Spread Ftgs. |
| Sherman Oaks Bldg. Sta. #24322 | 1965 | 193'x75' | 13/2 | Concrete Piles |
| Van Nuys Bldg. Sta. #24386 | 1966 | 151'x63' | 7/0 | Concrete Pile |

Table 2: Earthquake Records used in Research

| Building | Record Name | Richter Magnitude | Peak Base Accel. | Peak Building Accel. |
|---|---|---|---|---|
| Pasadena Building Sta. #24571 | Landers EQ of 28 June, 1992 | 7.4 | .047g | .23g |
| | Big Bear EQ of 28 June, 1992 | 6.4 | .039g | .09g |
| | Sierra Madre EQ of 28 June, 1991 | 5.8 | .23g | .43g |
| Sherman Oaks Bldg. Sta. #24322 | Landers EQ of 28 June, 1992 | 7.4 | .045g | .11g |
| | Whittier EQ of 1 October, 1987 | 5.9 | .25g | .21g |
| Van Nuys Bldg. Sta. #24386 | Landers EQ of 28 June, 1992 | 7.4 | .042g | .19g |
| | Big Bear EQ of 28 June, 1992 | 6.4 | .024g | .06g |
| | Whittier EQ[1] of 1 October, 1987 | 5.9 | .16g | .20g |

[1] This input earthquake record was incomplete in one direction.

Table 3: Pasadena Bldg. ETABS Peak Accelerations for Sierra Madre E.Q.

| FLOOR | RESPONSE (PREDICTED/RECORDED absolute g) | | | % DIFFERENCE |
|---|---|---|---|---|
| 2nd | Channel | 6 | 0.300/0.344 | -13 |
| | | 8 | 0.112/0.092 | +22 |
| 5th | Channel | 9 | 0.234/0.291 | -20 |
| | | 10 | 0.078/0.067 | +17 |
| | | 11 | 0.086/0.091 | -10 |
| Roof | Channel | 12 | 0.361/0.425 | -15 |
| | | 13 | 0.086/0.091 | -6 |
| | | 14 | 0.113/0.100 | +12 |

Table 4: Sherman Oaks Bldg. ETABS Peak Accelerations for Whittier E.Q.

| FLOOR | RESPONSE (PREDICTED/RECORDED absolute g) | | | % DIFFERENCE |
|---|---|---|---|---|
| 2nd | Channel | 1 | 0.1268/0.14 | -9 |
| | | 2 | 0.1034/0.14 | -26 |
| | | 3 | 0.1128/0.197 | -43 |
| 8th | Channel | 4 | 0.0758/0.107 | -29 |
| | | 5 | 0.062/0.114 | -46 |
| Roof | Channel | 7 | 0.0718/0.109 | -34 |
| | | 8 | 0.0789/0.171 | -54 |

Table 5: Van Nuys Bldg. ETABS Peak Accelerations for Big Bear E.Q.

| FLOOR | RESPONSE (PREDICTED/RECORDED absolute g) | | | % DIFFERENCE |
|---|---|---|---|---|
| 2nd | Channel | 7 | .0227/0.03 | -24 |
| | | 12 | 0.037/.03 | +23 |
| 3rd | Channel | 5 | 0.0244/0.046 | -39 |
| | | 11 | 0.0492/0.03 | +64 |
| 6th | Channel | 4 | 0.039/0.04 | -3 |
| | | 10 | 0.0586/0.05 | +1 |
| Roof | Channel | 3 | 0.0614/0.04 | +54 |
| | | 9 | 0.084/0.06 | +40 |

Table 6: SAP90 Peak Accelerations

| Building | Earthquake Record Name | Floor Level | Recorded/ Predicted Accel. Long Dir. | Recorded/ Predicted Accel. Short Dir. |
|---|---|---|---|---|
| Pasadena Building Sta. #24571<br><br>Model Damping: Long=3% Short=4% | Landers EQ of 28 June, 1992 | Roof | 0.23/0.21 | 0.07/0.08 |
| | | 5th | 0.19/0.17 | 0.05/0.07 |
| | | 2nd | 0.13/0.11 | 0.04/0.04 |
| | Big Bear EQ of 28 June, 1992 | Roof | 0.09/0.10 | 0.04/0.04 |
| | | 5th | 0.06/0.06 | 0.03/0.03 |
| | | 2nd | 0.04/0.05 | 0.03/0.03 |
| | Sierra Madre EQ of 28 June, 1991 | Roof | 0.41/0.43 | 0.09/0.11 |
| | | 5th | 0.29/0.26 | 0.07/0.07 |
| | | 2nd | 0.34/0.32 | 0.09/0.10 |
| Sherman Oaks Bldg. Sta. #24322<br><br>Model Damping: Long=5 % Short= 5% | Landers EQ of 28 June, 1992 | Roof | 0.09/0.06 | 0.09/0.06 |
| | | 8th | 0.06/0.05 | 0.06/0.04 |
| | | 2nd | 0.04/0.03 | 0.04/0.03 |
| | Whittier EQ of 1 October, 1987 | Roof | 0.14/0.11 | 0.14/0.09 |
| | | 8th | 0.11/0.06 | 0.11/0.06 |
| | | 2nd | 0.10/0.07 | 0.17/0.09 |
| Van Nuys Bldg. Sta. #24386<br><br>Model Damping: Long=9% Short=15% | Landers EQ of 28 June, 1992 | Roof | 0.13/0.12 | 0.11/0.08 |
| | | 6th | 0.09/0.10 | 0.09/0.06 |
| | | 2nd | 0.05/0.05 | 0.05/0.04 |
| | Big Bear EQ of 28 June, 1992 | Roof | 0.06/0.05 | 0.04/0.05 |
| | | 6th | 0.05/0.05 | 0.04/0.04 |
| | | 2nd | 0.03/0.03 | 0.03/0.03 |
| | Whittier EQ[1] of 1 October, 1987 | Roof | N.A. | 0.15/0.10 |
| | | 6th | N.A. | 0.08/0.06 |
| | | 2nd | N.A. | 0.14/0.10 |

[1] This input earthquake record was incomplete in one direction.

Van Nuys - 7-story Hotel
(CSMIP Station No. 24386)

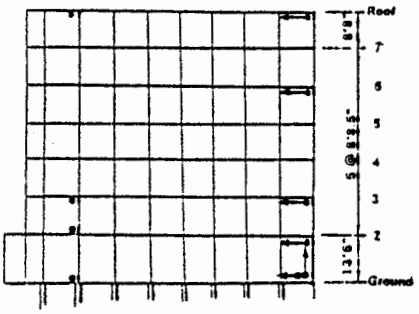


W/E Elevation

Figure 1: Van Nuys - 7 Story Hotel

Pasadena - 9-story Commercial Bldg.
(CSMIP Station No. 24571)

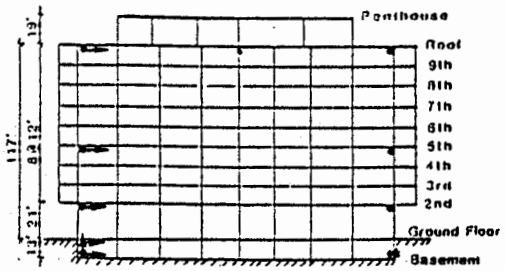


N/S Elevation

Figure 2: Pasadena - 9-story Commercial Bldg.

Sherman Oaks - 13-story Commercial Bldg.
(CSMIP Station No. 24322)

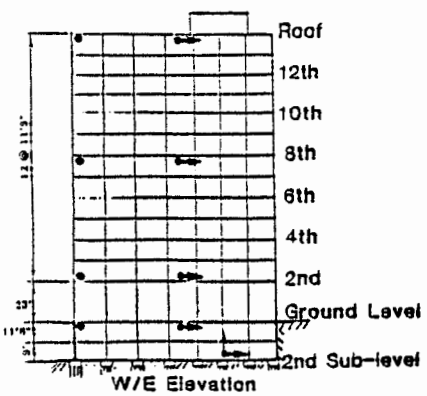


W/E Elevation

Figure 3: Sherman Oaks - 13-story Commercial Bldg.

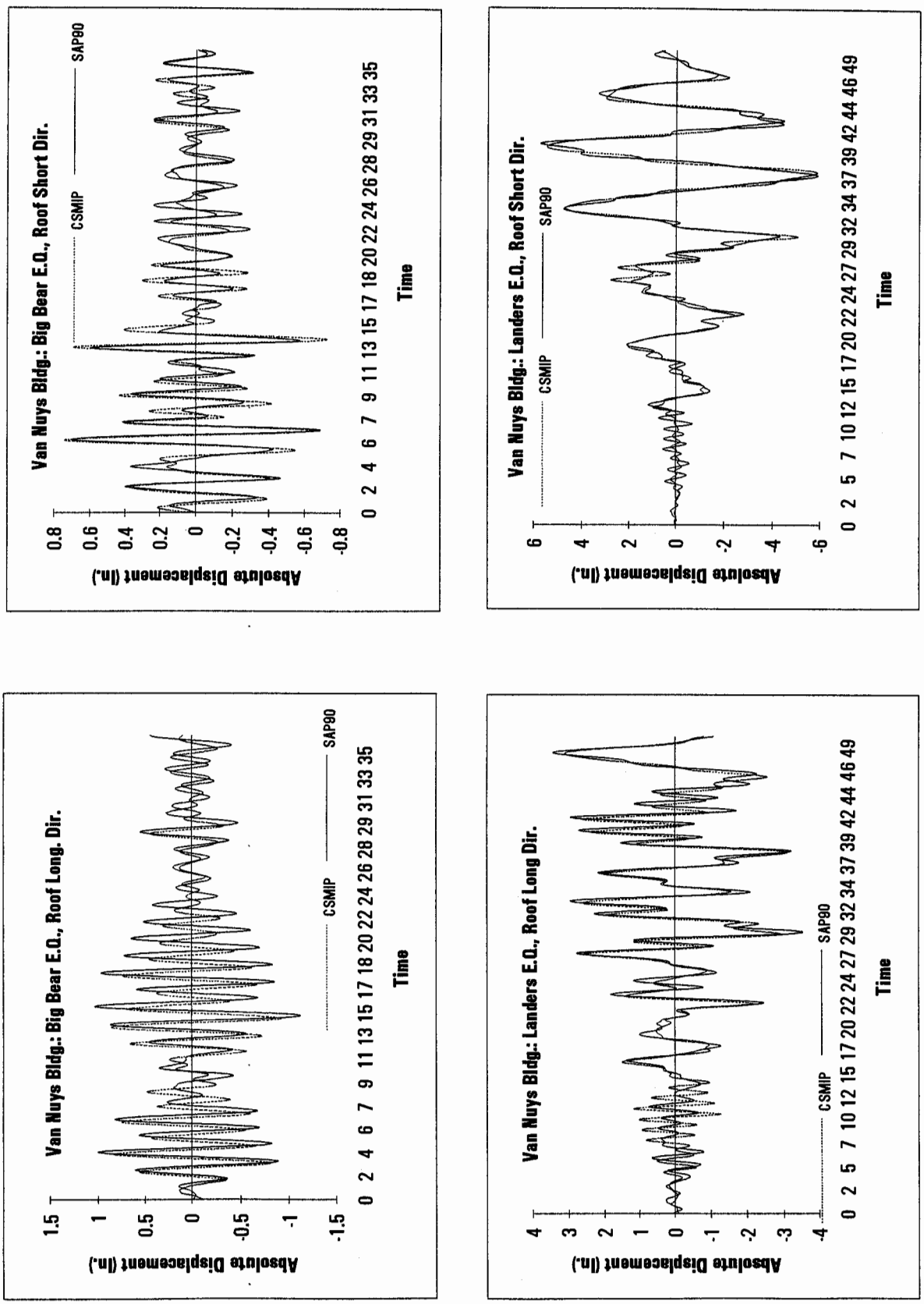


Figure 4: SAP90 Time History Displacement Plots

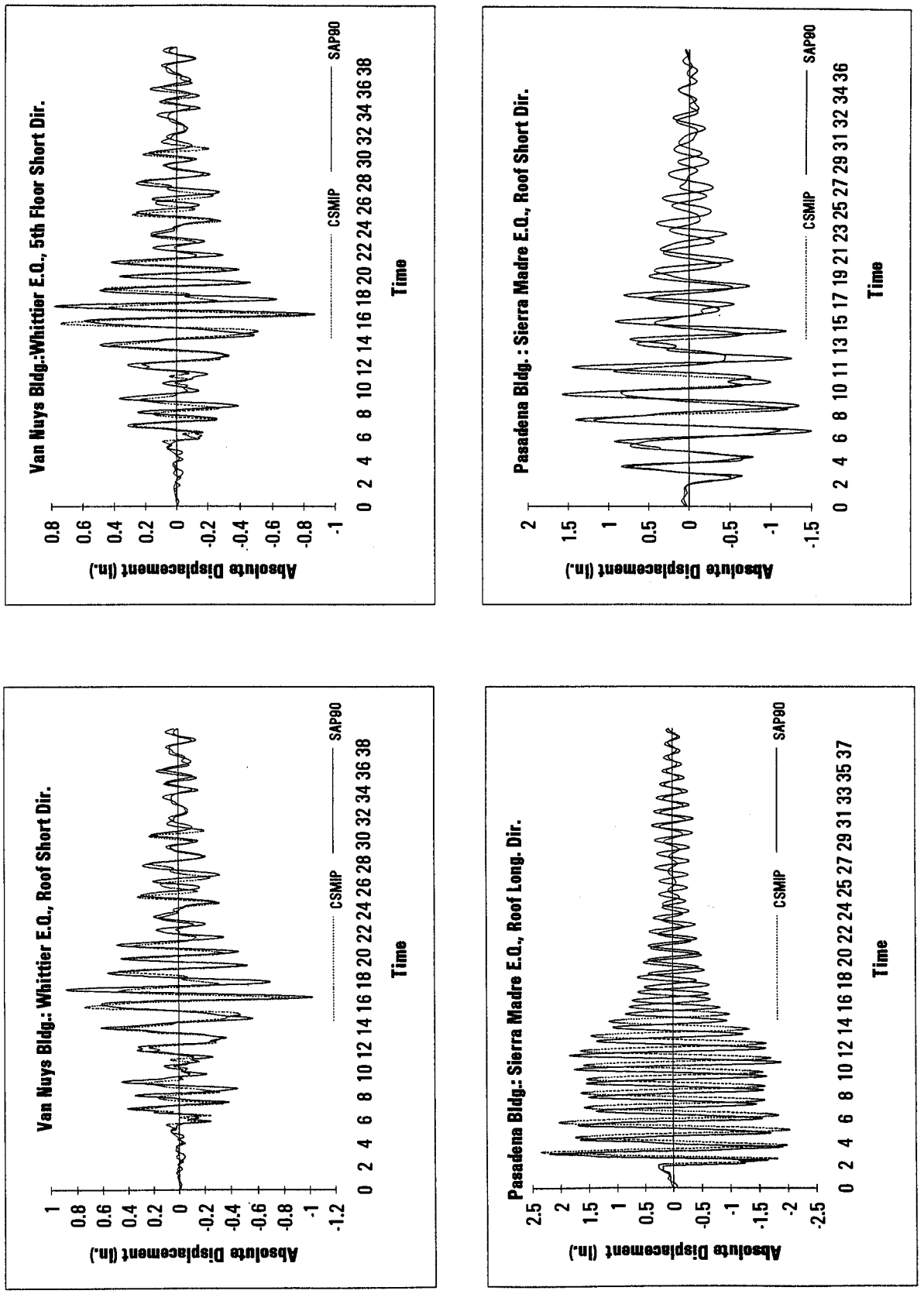


Figure 5: SAP90 Time History Displacement Plots

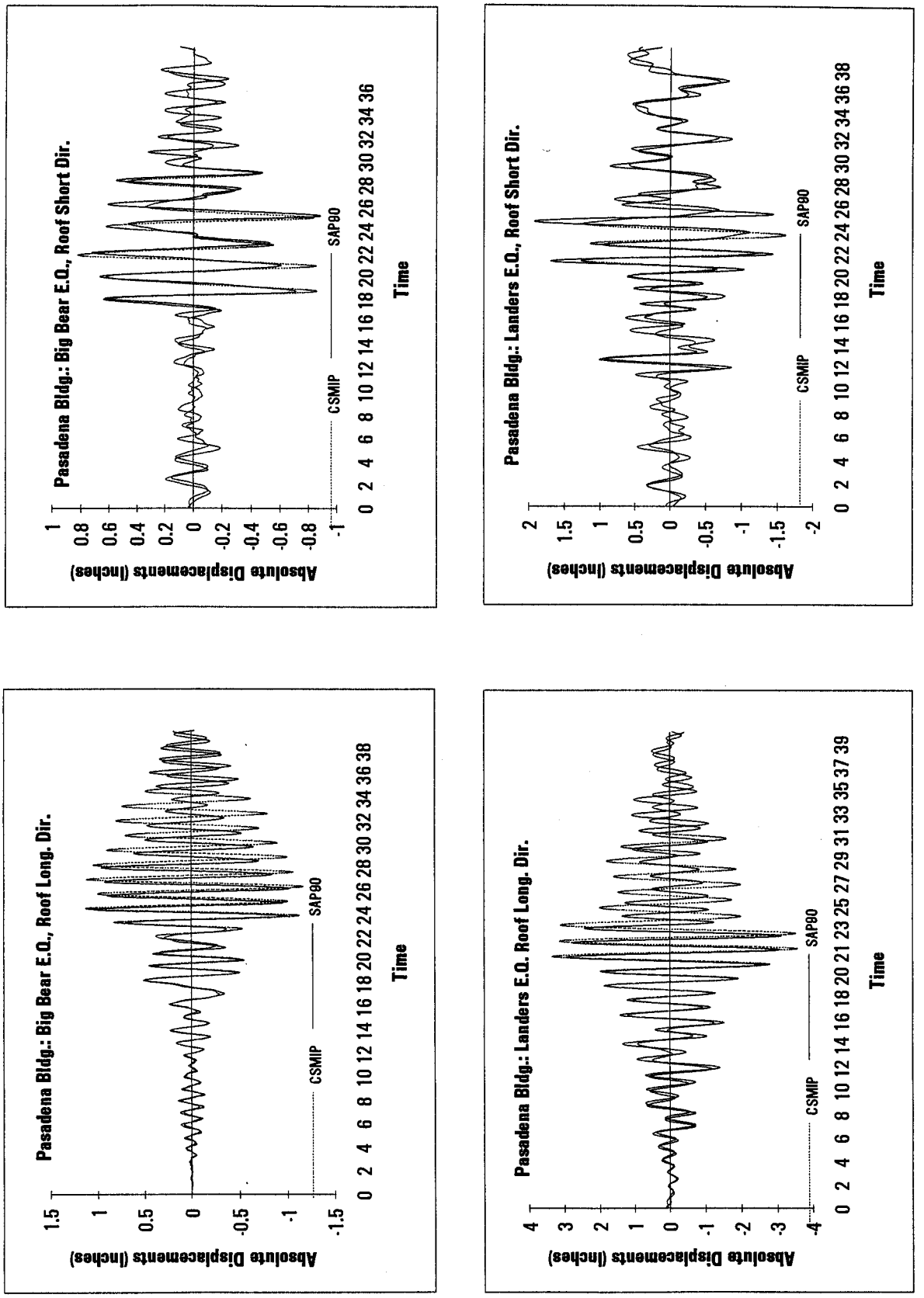


Figure 6: SAP90 Time History Displacement Plots

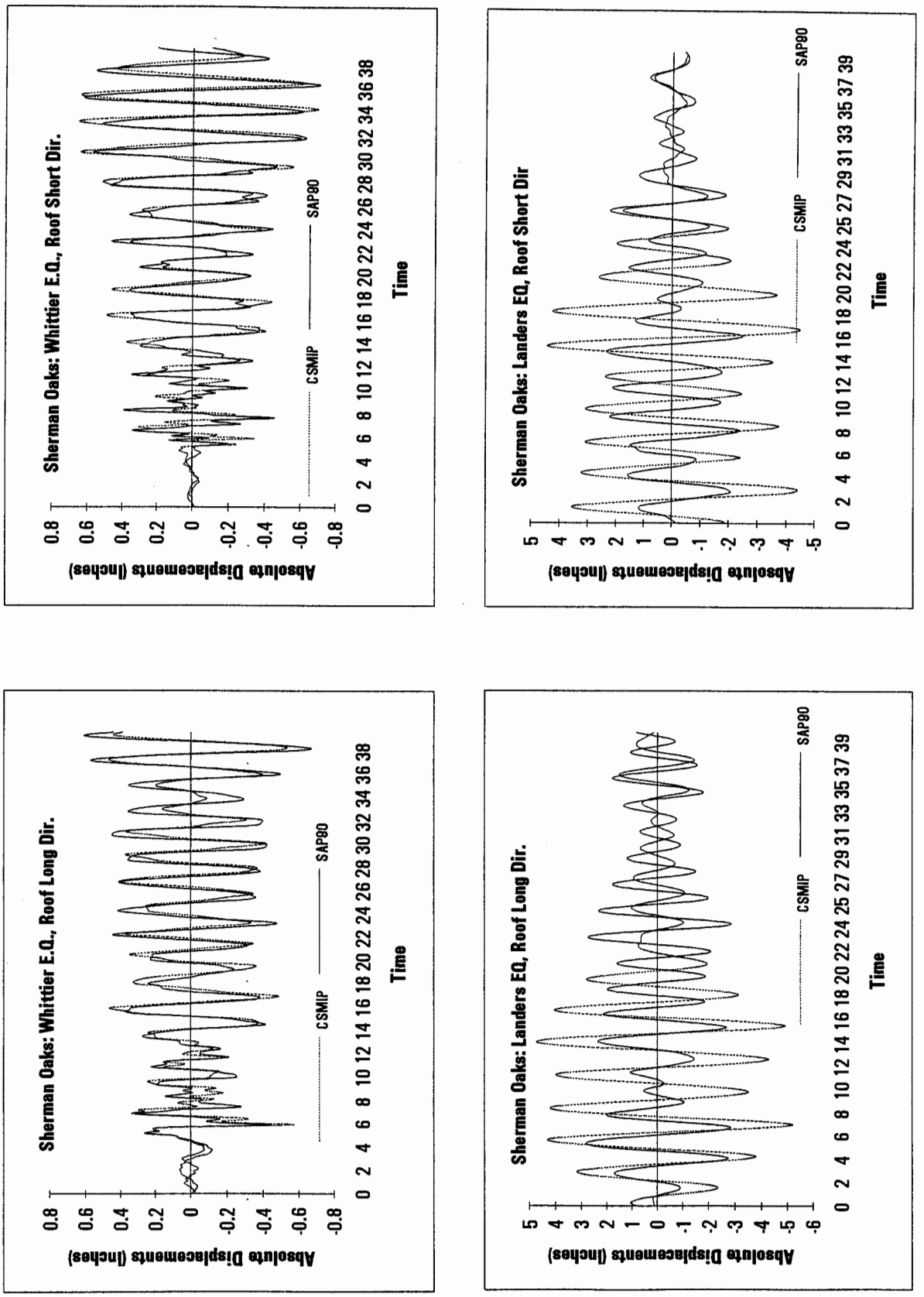


Figure 7: SAP90 Time History Displacement Plots

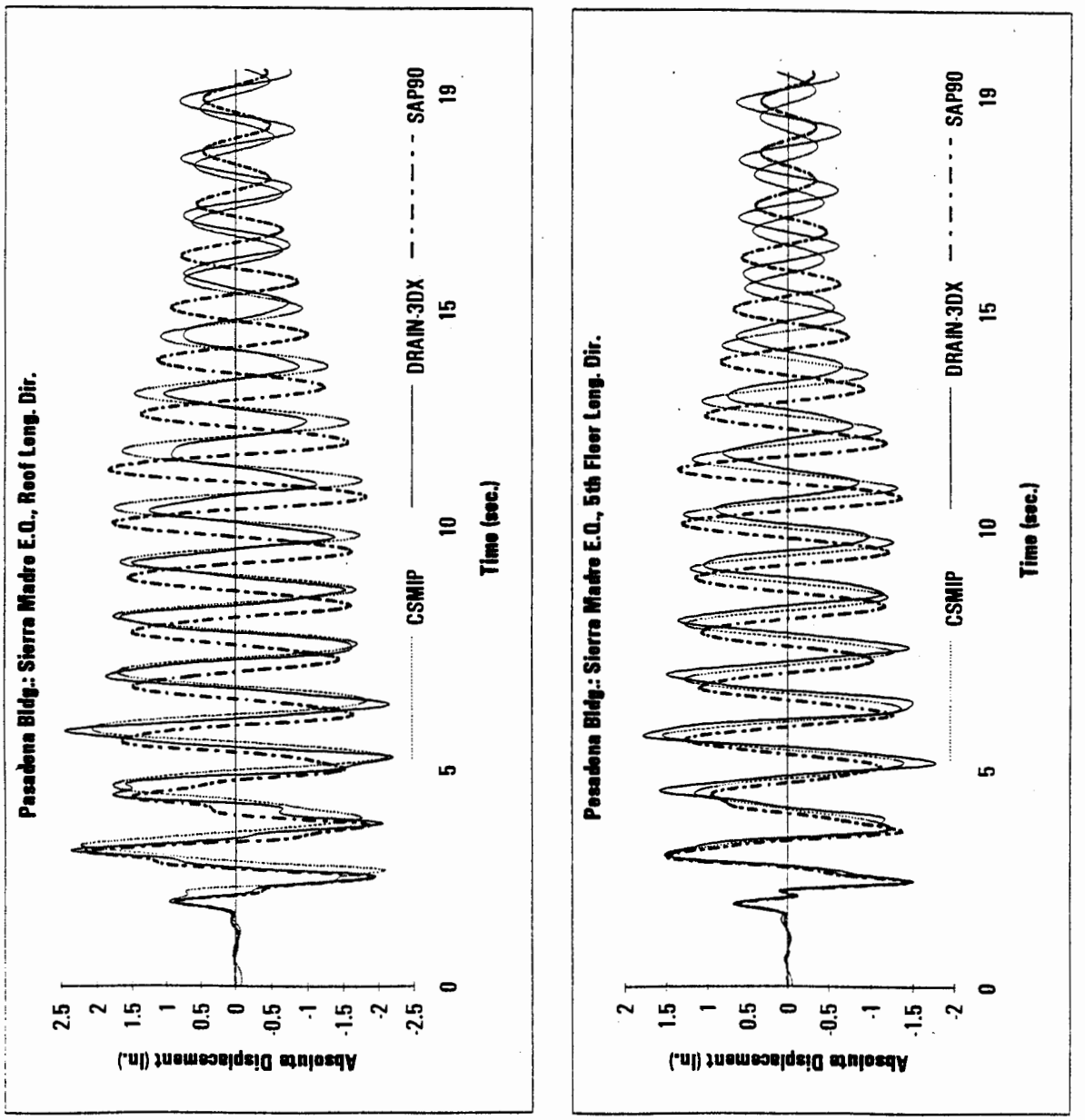


Figure 8: DRAIN-3DX & SAP90 Time History Displacement Plots

# INTERACTION AT SEPARATION JOINTS OF THE I10/215 BRIDGE DURING EARTHQUAKES

P. K. Malhotra, M. J. Huang and A. F. Shakal

California Strong Motion Instrumentation Program
Division of Mines and Geology, California Department of Conservation

## ABSTRACT

A multi-span, curved, concrete box-girder bridge has been extensively instrumented by the California Strong Motion Instrumentation Program (CSMIP) in cooperation with the California Department of Transportation (Caltrans). On June 28, 1992, the bridge was shaken by the magnitude 7.5 Landers and magnitude 6.6 Big Bear earthquakes in Southern California. The epicenters of these earthquakes were 50 and 29 miles (81 and 46 km) from the bridge, respectively. All thirty-four strong-motion sensors installed on the bridge recorded its response to these earthquakes and provided an insightful set of response data. A striking aspect of the response is the presence of intermittent sharp spikes in nearly all of the acceleration records from sensors on the deck of the bridge. Among these the highest spike was $0.80g$ for the Landers and $1.00g$ for the Big Bear earthquake. The peak ground acceleration at the bridge site was only about $0.10g$ for both these earthquakes. With the aid of visual examination and simple analysis it is deduced that: (i) the spikes were caused by forces generated at separation joints between adjacent bridge segments by impacts and stretching of the cable restrainers; and (ii) the forces of impacts and cable stretching are directly proportional to the size of the spikes and can be estimated by the use of a simple formula.

## INTRODUCTION

The California Strong Motion Instrumentation Program (CSMIP) of the Division of Mines and Geology in the Department of Conservation is installing strong-motion sensors on different structures and ground sites in California. The bridge structure examined here is one of the more than 100 stations from which strong-motion records were obtained during the June 28, 1992 Landers and Big Bear earthquakes in California.

### Bridge Structure

The instrumented bridge (shown in Figure 1) is a multi-span, concrete structure that connects highways I-10 and I-215 in Southern California, approximately 53 miles (85 km) from downtown Los Angeles. The bridge is curved in plan with radii of 1,200 and 1,300 ft (365 and 396 m), and has a total length of 2,540 ft (774 m). The superstructure consists of a 41 ft (12.5 m) wide, 4-cell concrete box-girder that carries two lanes of traffic from eastbound I-10 to northbound I-215. There are five separation joints (hinges) in the box-girder that divide the bridge into six structures of different lengths and number of spans. The hinges are numbered 3, 7, 9, 11 and 13 in Figure 1. The box-girder is supported on single-column concrete bents and abutments that are monolithic with it. The columns are octagonal in shape and $8 \times 5.5$ ft ($2.4 \times 1.7$ m) in size. Their height ranges from 24 to 76 ft (7.3 to 23.2 m).

The bridge was designed by the California Department of Transportation (Caltrans) in 1969 and the construction was completed in 1973. During 1991-92 the bridge was retrofitted by Caltrans under a program to seismically upgrade bridges with single-column bents. One of the tasks of this retrofitting effort was to improve the connection at the hinges by tying the adjacent segments of the box-girder with new cable restrainers. A typical cable restrainer unit, shown in Figure 2, consists of twenty 0.75 in (1.9 cm) diameter cables, between 16 and 21 ft (4.9 and 6.4 m) long.

### Strong-Motion Instrumentation and Earthquake Records

Seismic instrumentation of the bridge by CSMIP was completed in early 1992. A total of thirty-four strong-motion sensors (accelerometers) were installed to measure the motions of selected points at the base of concrete columns, the abutments, and the bridge deck. Of particular interest in this instrumentation was the response at the hinges. Sensors were installed at each of the five hinges to measure the transverse motions of the adjacent bridge segments. At some hinges the longitudinal and vertical motions are also measured. Only selected sensors are shown by numbered arrows in Figure 1, where the arrows indicate the positive direction of motion measured by the sensors. Sensor 6, for example, measures the transverse motion at the base of Bent 3, and Sensor 10 measures the longitudinal motion of the left segment at Hinge 3. The positive motion measured by Sensors 6, 7 and 8 is in the radially inward direction. The positive motion measured by Sensor 10 is tangential to the bridge in the clockwise direction. The complete instrumentation scheme is discussed in detail by Huang and Shakal (1994).

The acceleration records for the Landers and Big Bear earthquakes from all thirty-four sensors on the bridge were included in three CSMIP data reports (Shakal et al., 1992; Huang et al., 1992; Darragh et al., 1993). The records obtained from sensors near the hinges were of special significance because of intermittent sharp spikes, as high as $1.00g$. The peak ground accelerations, however, were only about $0.10g$.

### Scope and Objectives

The objectives of this paper are: (i) to identify the mechanism(s) responsible for the observed spikes, and (ii) to estimate the magnitude of the forces involved. For this purpose records obtained during the Landers earthquake, only from Sensors 6, 7, 8 and 10, are studied here. These records are shown in Figure 3.

## SEISMIC INTERACTION AT A HINGE

A vertical section through Hinge 3 in Figure 2 shows that the right segment is supported by the left segment and rests on an elastomeric bearing pad. There is a horizontal separation between the two segments, provided to accommodate temperature-induced expansion; the separation gap had a width of 2 in (5 cm) at the time of construction. The actual width of the gap at the time of the earthquakes might have been different depending upon the effect of aging on concrete and temperature at the time of earthquakes. According to Caltrans design drawings, the cable restrainers were given an initial slack of approximately 2 in (5 cm) to allow free movement of the bridge segments during temperature variations.

At Hinge 3 the transverse motions of the left and the right segments of the box-girder are measured by Sensors 7 and 8, respectively. In addition, the longitudinal motion of the left segment is measured by Sensor 10. The acceleration records of these sensors, shown in Figure 3, contain a series of sharp spikes. These spikes are more clearly visible in the smaller, 9 second, segments of these records that are shown in Figure 4. Note that:

- The spikes appear in sets, occurring simultaneously in each of the three records in Figure 4; seven sets of spikes appeared during the 18.5 to 27.5 second interval.
- With the exception of Spike 3, the transverse spikes (in the records of Sensors 7 and 8) are equal in magnitude and opposite in direction to each other; the 3rd spike in these two records points in the same direction.

Spikes of similar nature can be observed in the published data from all hinges of the bridge during both Landers and Big Bear earthquakes (Shakal et al., 1992; Huang et al., 1992; Darragh et al., 1993).

Due to the absence of spikes in the base input motion, measured by Sensor 6 (see Figure 3), it is apparent that the observed spikes are not directly caused by the ground input motion. Whereas, the response without the spikes is a direct result of the amplification of ground motion through the height of the bridge, the spikes are caused by interaction between the adjacent bridge segments at the hinges. Three different mechanisms that might be responsible for the observed spikes are discussed below.

### Interaction Mechanisms

The equal and opposite transverse spikes (1, 2, 4, 5, 6 and 7 in Figure 4) are the result of a pair of self-balancing transverse forces generated at Hinge 3. Two mechanisms (Mechanisms 1 and 2) that may give rise to these forces are as follows:

Mechanism 1–Frictional Contact. In this mechanism, illustrated in Figure 5(a), the two adjacent segments of the box-girder, undergoing predominantly transverse motion, come in contact with each other. Upon contact a pair of equal and opposite frictional forces, $F_T$, are generated in the transverse direction. These forces are in turn responsible for the observed equal and opposite spikes in the transverse direction. Note that an axial compressive force, $F_L$, is also generated in this mechanism. This force is responsible for the longitudinal spike.

Mechanism 2–Cable Restraint. In this mechanism, illustrated in Figure 5(b), the two adjacent segments, undergoing predominantly transverse motion, move far enough away from one another that the cable restrainers between them become engaged and pull the two segments back toward each other. In this case the component of the cable forces in the transverse direction, $F_T$, is responsible for the spikes in that direction. The axial tensile force, $F_L$, equal in magnitude to the longitudinal component of the cable force, is responsible for the longitudinal spike in this mechanism.

After analyzing the longitudinal spikes in the next section it is deduced that the Spikes 1, 2, 5 and 6 were caused by Mechanism 1, and Spikes 4 and 7 were caused by Mechanism 2.

The 3rd set of spikes in Figure 4 can not be explained by either Mechanism 1 or 2 because the transverse spikes in this set are not equal and opposite to each other. A clue to the mechanism that might have given rise to the 3rd set of spikes is provided by the large longitudinal response corresponding to this set of spikes (see $A_{10}(t)$ in Figure 4). This mechanism is as follows:

**Mechanism 3–Head-on Impact**. Spikes in this mechanism are generated by a head-on impact between adjacent bridge segments undergoing predominantly longitudinal motion. The response in this case is, therefore, predominantly longitudinal, although a certain amount of transverse response is also generated. One possible cause of the transverse response is illustrated is Figure 6 in which two adjacent segments are shown to impact against each other at a slight angle. Upon impact a pair of transverse forces, $F_T$, pointing in the same transverse direction is generated which is responsible for nearly identical transverse spikes.

## FORCES OF INTERACTION

As already noted, each spike in the transverse direction is accompanied by a spike in the longitudinal direction, which should, more appropriately, be called a doublet because of its shape. Upon closer examination of the longitudinal response, $A_{10}(t)$ in Figure 4, it is seen that for Doublets 1, 2, 3, 5 and 6 a positive peak is followed by a negative peak, while for Doublets 4 and 7 it is vice-versa–a negative peak followed by a positive peak. The sign reversal of the doublet peaks is more clearly visible in Figure 7 where the lower two plots of Figure 4 are redrawn to a larger horizontal scale in the vicinity of Doublets 2 and 7. The shape of Doublet 2 in the record of Sensor 10 may be approximated by a single cycle of sinusoidal function, i.e.

$$A(t) = A_{max} \sin\left(\frac{2\pi t}{\tau}\right) \tag{1}$$

where $\tau$=the duration of the doublet and $A_{max}$=its amplitude. As previously mentioned, Doublet 2 was caused by an axial force generated by Mechanism 1 or 2. Whether the axial force is compressive or tensile will determine if the doublet was caused by Mechanism 1 or by Mechanism 2.

A simple model is used to determine the shape and size of the axial force pulse that produced Doublet 2, given by equation (1). In this model, shown in Figure 8(a), the segment of the box-girder to the left of Hinge 3 is represented by a semi-infinite rod of uniform cross-section area $\bar{A}$. An unknown axial force $F(t)$ is suddenly applied at the right end of this rod which produces an acceleration response at that end of the rod of the form given by equation (1) and shown in Figure 8(b). The objective is to determine the force $F(t)$ from this acceleration response. With the help of an analysis that made use of the one-dimensional wave propagation theory it is shown by Malhotra et al. (1994) that the axial force $F(t)$ has the following form:

$$F(t) = A_{max} \frac{c\rho\tau}{\pi} \left[\frac{1}{2}\left(1 - \cos\frac{2\pi t}{\tau}\right)\right] \times \bar{A} \tag{2}$$

in which $c$=the compression wave velocity is given by the following expression (Clough and Penzien 1993):

$$c = \sqrt{\frac{E}{\rho}} \tag{3}$$

where $E$=the Young's modulus of elasticity, and $\rho = w/g$=its mass density, obtained by dividing the weight density $w$ by the acceleration due to gravity $g$. The force $F(t)$ is plotted in Figure 8(c), below the assumed acceleration form shown in Figure 8(b). During time $\tau$ the force builds up from zero to a maximum value and then drops to zero again. Its positive sign implies that the force is compressive. Since the assumed acceleration form (Figure 8(b)) was chosen to approximate the shape of Doublet 2 in Figure 4, the doublet was, therefore, produced by a compressive force generated by impacts between the adjacent segments in Mechanism 1.

The results of the above analysis are summarized in the top row of Table I which essentially states that Mechanism 1 produces equal and opposite spikes in the transverse direction and a sinusoidal doublet in the longitudinal direction. Spikes 1, 2, 5 and 6 in Figure 4 were, therefore, caused by Mechanism 1. Rows two and three of Table I are generated by simple deduction. It is stated in the second row that Mechanism 2, similar to Mechanism 1, produces equal and opposite spikes in the transverse direction but a reverse sinusoidal doublet in the longitudinal direction (caused by an axial tensile force). Spikes 4 and 7 were, therefore, caused by Mechanism 2. In the third row of Table I, Mechanism 3 is shown to produce transverse spikes that are nearly equal to each other, and a longitudinal doublet that has a sinusoidal shape similar to Mechanism 1. Spike 3 was, therefore, caused by Mechanism 3.

**Forces of Impact**

Substituting the term in the square brackets in equation (2) by its maximum value of unity, the expression for the maximum value of the force $F_{max}$ is obtained as follows:

$$F_{max} = A_{max}\frac{c\tau\rho}{\pi} \times \bar{A} \tag{4}$$

By making use of equation (4) one can compute the forces generated at Hinge 3 from the size (amplitude and duration) of the longitudinal doublets. For Doublet 2 (Figure 6), $A_{max}$=0.24$g$, and $\tau$=0.04 sec. The compression wave velocity $c$, obtained from equation (3) by using Young's modulus of elasticity $E$=3,400 ksi (23.4 GPa) and weight density $w=\rho g$=145 lb/ft$^3$ (22.8 kN/m$^3$) is 10,400 ft/sec (3,200 m/sec). The cross-section area of the box-girder, estimated from construction drawings is $\bar{A}$=10,000 in$^2$ (6.45 m$^2$). Upon substituting the values of various quantities in (4) one obtains, $F_{max}$=320 kips (1,450 kN). Assuming that the entire cross-section of the box-girder comes in contact when the two segments collide, the maximum compressive stress $\sigma_{max}=F_{max}/\bar{A}$=32 psi (220 kPa).

The largest doublet in the record of Sensor 10 is Doublet 3 (see Figure 4). Its large size is not unexpected because it is associated with Mechanism 3 in which a head-on impact occurs between the adjacent bridge segments. Although the shape of Doublet 3 is not strictly sinusoidal a rough estimate of the force responsible for this doublet can still be obtained by

the use of the simple formula given by (4). This force is nearly ten times (≈3,000 kips) the force that caused Doublet 2, and the corresponding stress $\sigma_{max}$=300 psi.

### Tensile Forces in Cable Restrainers

As previously noted, Doublets 7 in Figure 7 was caused by Mechanism 2 by sudden engagement of the cable restrainers between the adjacent segments. Equation (4) can also be used to estimate the cable forces from the size of Doublet 7, for which $A_{max}$=−0.10$g$ and $\tau$=0.10 sec. Upon substituting these into (4), one obtains the net maximum tensile force in the box-girder and hence in the cable restrainers to be 330 kips (1,470 kN). This gives an average tensile force in each of the twenty cables to be 16.5 kips (73.5 kN). The actual force in a cable may be significantly larger since not all the cables are necessarily engaged at the same time. The stress in a 0.75 in diameter cable corresponding to a tensile force of 16.5 kips is 37.4 ksi (257 MPa).

### Actual vs. Allowable Stresses

In accordance with Caltrans "Bridge Design Specifications" (1990) the allowable compressive stress for concrete is 2 ksi (13.8 MPa), and the cracking stress is 530 psi (3.65 MPa). The maximum value of the compressive stress pulse generated by impacts in Mechanism 3 was estimated to be approximately 300 psi (2.07 MPa). This value is only 15% of the allowable value. A compressive pulse is, however, reflected as a tensile pulse, of equal magnitude, from the free end of the medium in which it travels (Clough and Penzien 1993). In other words, a compressive pulse generated at Hinge 3 is reflected as a tensile pulse from Hinge 7. A tensile stress of 300 psi is quite considerable for concrete, but still only 57% of the cracking stress.

As noted above the maximum stress induced in the cable restrainers was estimated to be 37.4 ksi (257 MPa). This value is 21% of the yield stress $F_y$=176 ksi (1,220 GPa) given by the Caltrans "Bridge Design Aids" (1991).

## CONCLUSIONS

This paper was focused on the interpretation and analysis of sharp spikes in the acceleration records obtained during a recent California earthquake from an instrumented concrete bridge. The principal conclusions are as follows:

1. The spikes were caused by forces generated at the separation joints (hinges) by the interaction of adjacent segments of the box-girder. The interaction between adjacent segments occurred both by impacts and by engagement of the cable restrainers that tie them together.

2. The forces of impact and cable restraining can be estimated from the amplitude and duration of the acceleration spikes using a simple formula. Results obtained from the strong-motion records indicate that reasonably high forces were generated at the hinges during the 1992 Landers earthquake. However, the resulting stresses estimated were below the yield values for the cable restrainers and concrete.

## REFERENCES

"Bridge Design Aids (14-16)," (1991) California Department of Transportation.

"Bridge Design Specifications (9-7)," (1990) California Department of Transportation.

Clough, R. W., and Penzien, J. (1993) "Dynamics of Structures," McGraw-Hill, Inc., 2nd Edition.

Darragh, R., Cao, T., Huang, M., Shakal, A. (1993) "Processed CSMIP Strong-Motion Records From the Landers and Big Bear, California Earthquakes of 28 June 1992: San Bernardino–I10/215 Interchange," California Department of Conservation, Division of Mines and Geology, Office of Strong Motion Studies, Report OSMS 93-08.

Huang, M., Shakal, A., Cao, T., Sherburne, R., Sydnor, R., Fung, P., Malhotra, P., Cramer, C., Su, F., Darragh, R., and Wampole, J. (1992) "CSMIP Strong Motion Records From the Big Bear, California Earthquake of 28 June 1992," California Department of Conservation, Division of Mines and Geology, Office of Strong Motion Studies, Report OSMS 92-10.

Huang, M., and Shakal, A. (1994) "CSMIP Strong-Motion Instrumentation and Records from the I10/215 Interchange Bridge near San Bernardino," *Earthquake Spectra*, submitted for publication.

Shakal, A., Huang, M., Cao, T., Sherburne, R., Sydnor, R., Fung, P., Malhotra, P., Cramer, C., Su, F., Darragh, R., and Wampole, J. (1992) "CSMIP Strong Motion Records From the Landers, California Earthquake of 28 June 1992," California Department of Conservation, Division of Mines and Geology, Office of Strong Motion Studies, Report OSMS 92-09.

Malhotra, P. K., Huang, M. J., Shakal, A. F. (1994) "Seismic Interaction at Separation Joints of an Instrumented Concrete Bridge," *Journal of Earthquake Engineering and Structural Dynamics*, submitted for publication.

Table I. Identification of spike-causing mechanisms in records of Sensors 7, 8 and 10 shown in Figure 4.

| Mechanism | Transverse spikes in records of Sensors 7 & 8 | Shape of longitudinal doublet in record of Sensor 10 | Shape of axial force pulse* | Spike No. |
|---|---|---|---|---|
| 1 | Equal & opposite | | + | 1, 2, 5 & 6 |
| 2 | Equal & opposite | | − | 4 & 7 |
| 3 | Equal & same polarity | | + | 3 |

* + = compressive; − = tensile

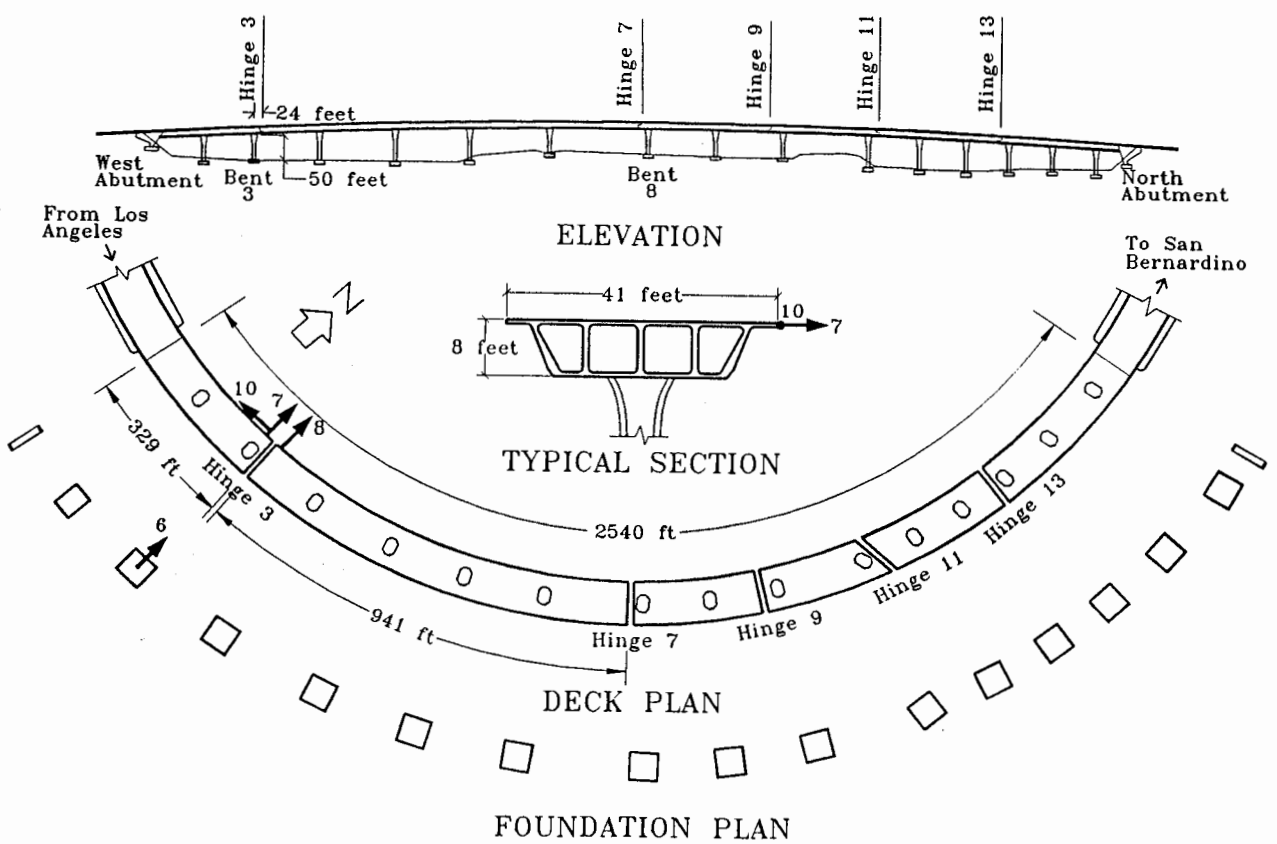


Figure 1. Plan and elevation of the Caltrans I-10/215 interchange bridge in San Bernardino, California showing locations of selected seismic sensors. Only four (6, 7, 8 and 10) of the total thirty-four sensors are shown here. Arrows indicate the positive direction of motion measured by the sensors.

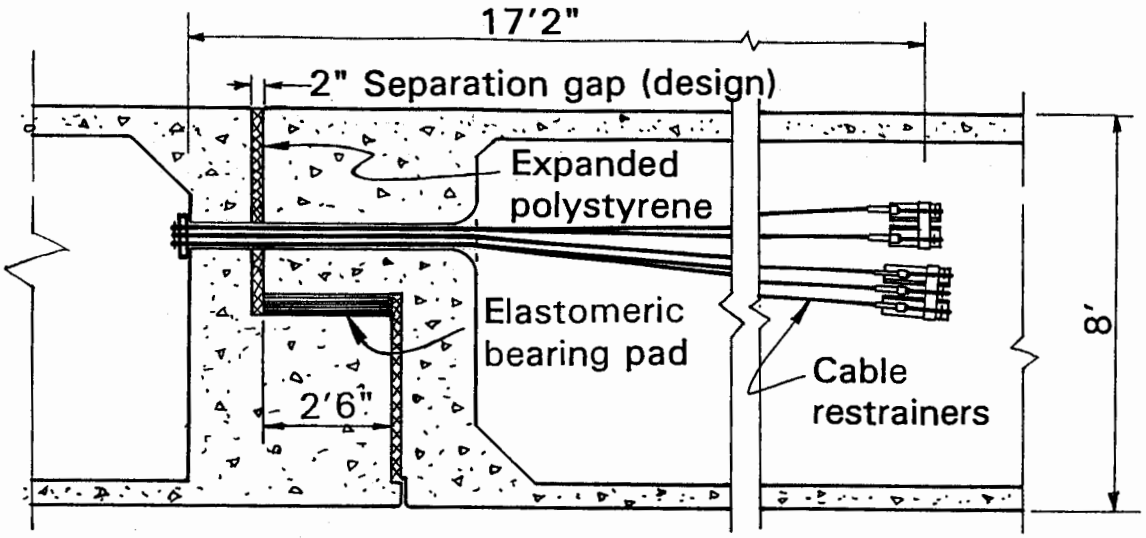


Figure 2. Vertical sections at Hinge 3 showing the separation gap, cable restrainers, and elastomeric bearing pad (from Caltrans construction drawings).

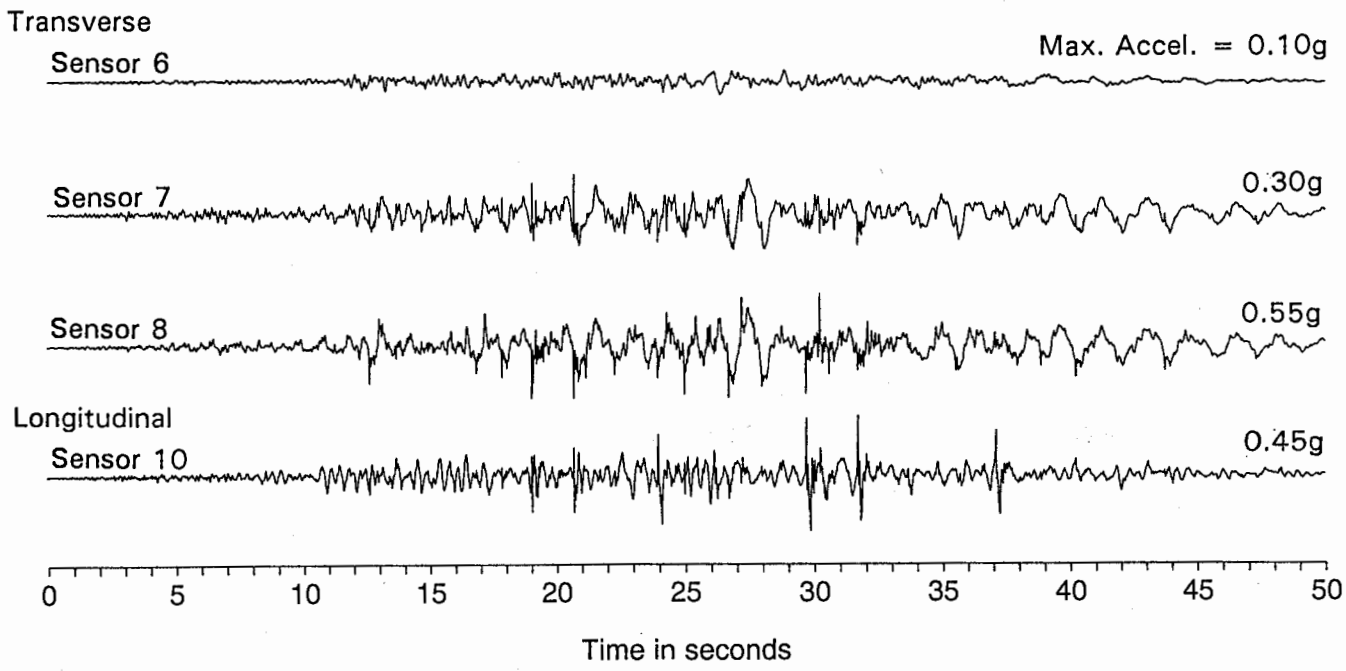


Figure 3. Acceleration records of Sensors 6, 7, 8 and 10 (Figure 1) obtained during the June 28, 1992 Landers earthquake in Southern California.

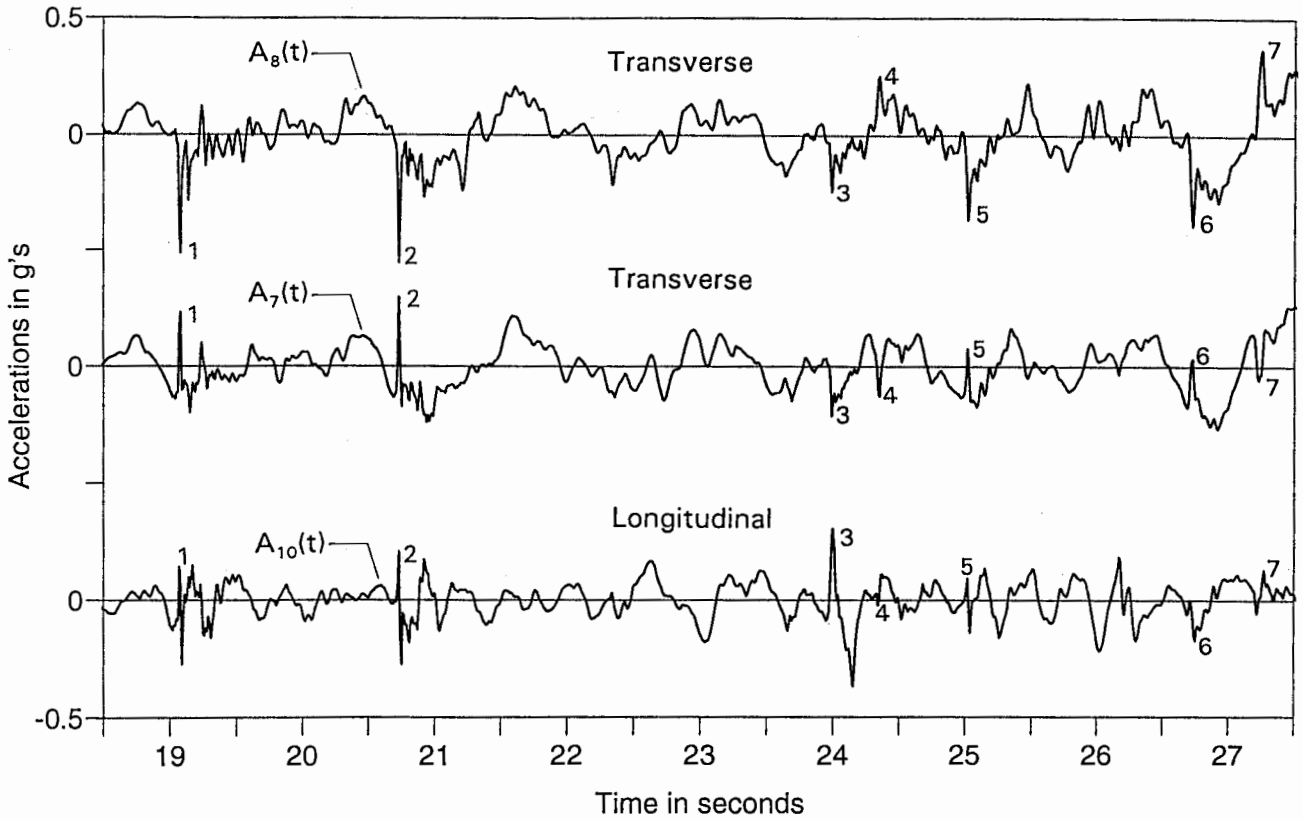


Figure 4. Acceleration records at Hinge 3 from 18.5 to 27.5 seconds into the record, showing simultaneous occurrence of spikes in the transverse, $A_7(t)$ and $A_8(t)$, and longitudinal, $A_{10}(t)$, directions.

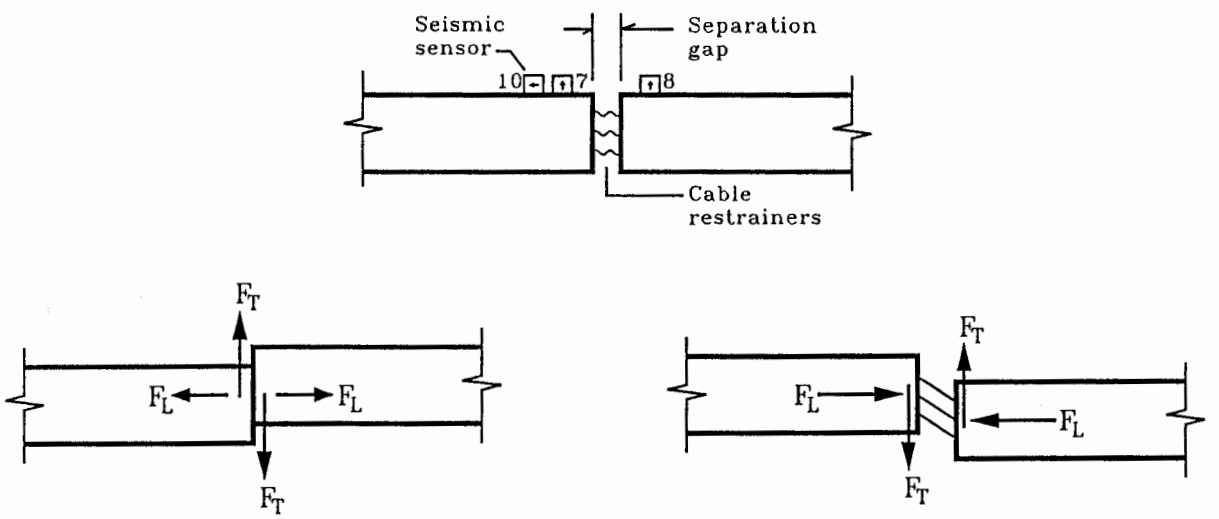


(a) Mechanism 1–Frictional Contact (b) Mechanism 2–Cable Restraint

Figure 5. Plan views at Hinge 3 illustrating interaction Mechanisms 1 and 2. $F_T$=transverse force, $F_L$=longitudinal force; arrows indicate the direction of forces generated.

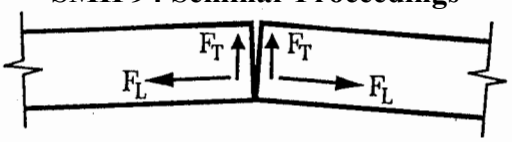


Mechanism 3 Head-on Impact

Figure 6. Plan views at Hinge 3 illustrating interaction Mechanism 3.

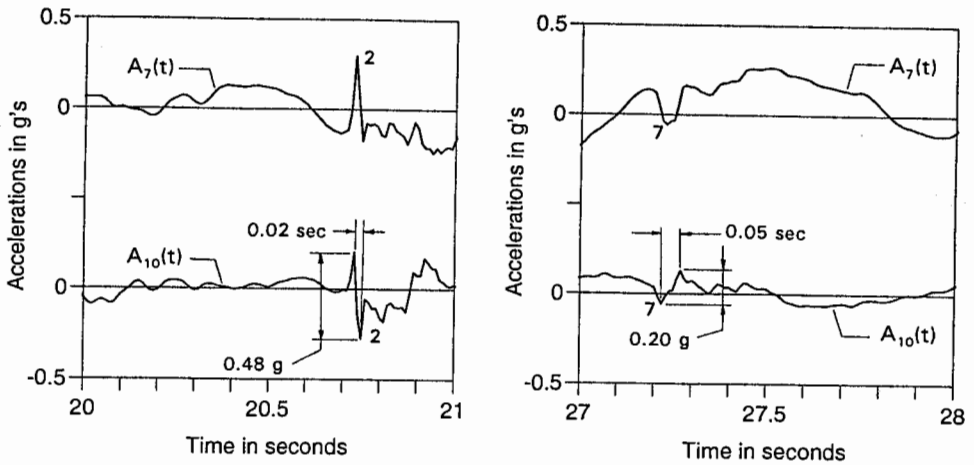


Figure 7. Acceleration records in the vicinity of Spikes 2 and 7 in Figure 4 in the transverse, $A_7(t)$, and longitudinal, $A_{10}(t)$, directions.

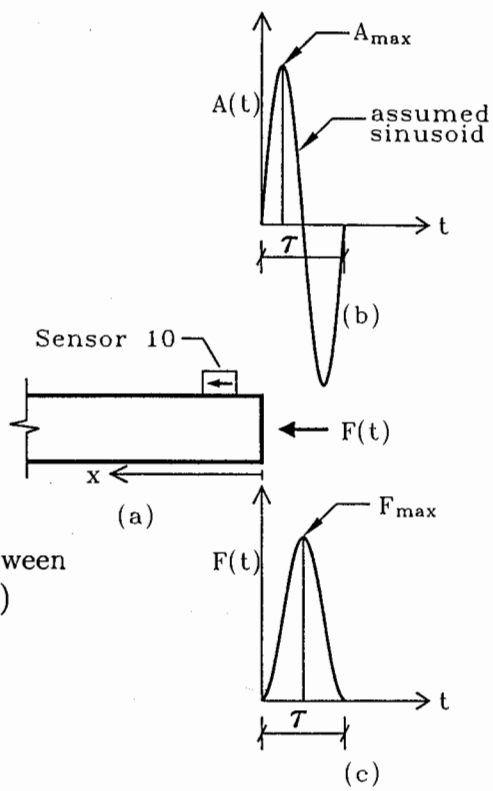


Figure 8. (a) Plan view of the box-girder model used to study the relationship between (b) a hypothetical acceleration spike $A(t)$ similar to those measured by Sensor 10, and (c) the axial force pulse $F(t)$ that would be generated at the end of the box-girder model.

# RESPONSE OF THE NORTHWEST CONNECTOR IN THE LANDERS AND BIG BEAR EARTHQUAKES

Gregory L. Fenves and Reginald DesRoches

Department of Civil Engineering
University of California at Berkeley

## ABSTRACT

The strong motion records from the Northwest Connector (located in Colton, Calif.) in the 1992 Landers and Big Bear earthquakes provide valuable information about the seismic behavior of this common type of freeway bridge. Modeling of the bridge with reasonable estimates of the column stiffness and pile foundation properties and with gap elements for the intermediate hinges provides a good correlation between the computed and the recorded earthquake response of the bridge. Pounding of the hinges produces large acceleration spikes, causing sharp increases in the column shear forces. Since modeling the hinge opening–closing is relatively simple, this type of analysis is recommended for the design of multiple–frame bridges.

## INTRODUCTION

Connectors are elevated, curved bridges that allow traffic to travel between freeways at an interchange. Interest in the seismic behavior of connectors began when the 1971 San Fernando earthquake caused severe damage to several bridges. As shown in an experimental study conducted nearly twenty years ago (Williams and Godden, 1976), the curved superstructure of a connector can be very effective in resisting seismic loads. The intermediate hinges between the frames, however, reduce the stiffness of the box girder and are susceptible to local damage.

The Landers and Big Bear earthquakes on June 18, 1992, triggered an extensive strong motion instrumentation network at the Northwest Connector, a bridge at the Interstate 10/215 interchange in Colton, Calif. (see Fig. 1). The Connector is a 2540 ft long, curved, concrete box girder bridge with sixteen spans supported by single column bents and diaphragm abutments.

This paper summarizes a study of the seismic response of the Northwest Connector in the two 1992 earthquakes. The objectives of the study are to use the strong motion data recorded at the Connector to improve the understanding of the behavior of this common type of freeway bridge and calibrate the modeling and analysis procedures used in bridge design.

## DESCRIPTION OF SITE, BRIDGE AND INSTRUMENTATION

The elevation and plan of the Connector, including the strong motion instrumentation, are shown in Fig. 2. Although the design was completed in 1969, the need to identify the causes for the failure of connectors in the 1971 San Fernando earthquake, and incorporate the lessons into new bridge construction, delayed completion of the Colton interchange until 1973. While the interchange was under construction, the San Jacinto fault zone was mapped in close proximity to the structures. The location of the fault in relation to the interchange is indicated in Fig. 1.

The fault acts as a barrier against ground water flow, causing a drop in the water table on the southwest side of the fault compared with the northeast side. The foundation soils consist of

slightly compact to dense sand in the upper layer underlain by compact to dense sand, silty sands, and sand and gravel mixtures (Jackura, 1991). The sandy soils and high ground water table present a potential for liquefaction during an earthquake.

The structural system for the bridge consists of six frames, connected at five intermediate hinges. The hinges are designated by the spans in which they are located: H3, H7, H9, H11, and H13. The frames have a cast in–place box girder superstructure supported by two to four single column bents. The box girder is 8 ft deep, and the original columns have 8 ft by 5.5 ft octagonal sections. The box girders in two of the frames (H3 to H7, and H9 to H11) are post–tensioned in the longitudinal direction. The spans of the four conventionally reinforced frames range from 75 ft to 155 ft. The spans of the two post–tensioned frames range from 183 ft to 204 ft. The column height (from top of pile cap to the box girder soffit) varies from 24 ft for Bent 16 to 77 ft for Bent 5. Most of the bents are oriented without skew, with the exception of Bents 11 to 14.

The five intermediate hinges in the superstructure have a seat width of 32 in. or 36 in., of which 2 in. is expanded polystyrene joint seal. The hinge support for the girders is provided by elastomeric bearing pads. Although it was not possible to determine material specification for the pads, the plans show they are 4 to 5.5 in. thick. Relative transverse displacement at a hinge is prevented by a 1 ft shear key, with a specified 1/4–in. joint filler.

The original foundations for the single column bents consist of a pile cap (without top reinforcement) and reinforced concrete piles. The largest foundations (for Bents 4, 5, and 7) have a 24 ft by 23 ft pile cap, 6.75 ft thick, and 48 piles. At the diaphragm abutments, the box girder is integral with a 13 ft high backwall.

The decision to retrofit the Northwest Connector was based on the importance of the bridge, known deficiencies in the original design (Roberts, 1991), and the fact that it crosses a mapped fault. The features of the extensive retrofit are field–welded steel jackets on all the bent columns, strengthened pile caps and foundations for most of the bents, new cable restrainer units for the hinges, and supplemental support beams under the box girder near the abutments.

The Northwest Connector was instrumented with a network of strong motion accelerometers by the California Division of Mines and Geology, in conjunction with Caltrans. The instrumentation consists of 34 force–balance accelerometers, as shown in Fig. 2. In this paper the directions based on the chord of the bridge are called the global longitudinal and global transverse directions. The tangential and radial directions of the curved bridge are called the longitudinal and transverse directions, respectively. A sheltered free–field ground motion station is located approximately 1400 ft from Bent 8.

## EARTHQUAKES RECORDED AT THE CONNECTOR

Within a year of the seismic retrofit, the Connector withstood three earthquakes in the Landers sequence, as summarized in Table 1. The plots of the processed records are available in the DMG reports (Darragh, Cao et al., 1993). During the current study, the Connector was subjected to the Northridge earthquake. Table 1 also summarizes the maximum free–field ground motion at the bridge site.

After the two earthquakes on June 28, 1992, Caltrans personnel inspected the Connector. The left barrier (inside edge of deck) near Hinge 3 had spalled an area 8 in. by 6 in. with a depth of 6 in., exposing steel reinforcing bars. The seat of Hinge 3 had three hairline cracks radiating from the reentrant corner. Another inspection report described settlement at the hinges, possibly caused by earthquake damage to the elastomeric bearing pads (Yashinksy, Maulchin et al., 1992).

Table 1. Earthquakes and Free–Field Ground Motion Recorded at the Northwest Connector

| Event | Date | Magnitude $M_S$ | Epicentral Distance (miles) | Peak Free–Field Ground Acceleration (g) | | Bracketed Duration[b] (sec) |
|---|---|---|---|---|---|---|
| | | | | Horizontal[a] | Vertical | |
| Joshua Tree[c] | 4/22/92 | 6.3 | 52 | | | |
| Landers | 6/28/92 | 7.6 | 50 | 0.089 | 0.062 | 26 |
| Big Bear | 6/28/92 | 6.6 | 28 | 0.112 | 0.073 | 14 |
| Northridge[d] | 1/17/94 | 6.8 | 72 | 0.10 | 0.04 | |

[a]Instantaneous peak horizontal acceleration.
[b]Time the ground acceleration peaks exceed 0.05 g.
[c]Joshua Tree record was not available from DMG.
[d]Based on unprocessed records.

## FREE–FIELD AND INPUT MOTION

The pseudo–acceleration response spectra, with 5% damping, for the horizontal free–field ground acceleration in the principal axes are shown in Fig. 3. The Big Bear earthquake has larger spectral ordinates than the Landers earthquake for vibration periods less than 1 sec. For periods greater than 3 sec, the spectral ordinates for Landers are about twice that for Big Bear. The spectra for both earthquakes have a peak near a period of 1.8 to 1.9 sec. This peak may be associated with the characteristic vibration period of the deep alluvial site.

The response spectra for ground motion in the principal axes can be compared with the smooth design response spectrum used by Caltrans, as shown in Fig. 4. The S.7GD51 ARS spectrum corresponds to a 0.7g peak ground acceleration and an alluvial site with soil depth greater than 150 ft (Caltrans, 1990). Also shown in Fig. 4 is the ARS spectrum reduced by a Z factor of four, a typical reduction factor to account for inelastic behavior and seismic risk of single column bents. In the short period range, less than 1 sec, the spectra for the earthquakes exceed the reduced ARS/Z spectrum. For longer periods the design spectrum envelopes the spectra for the two earthquakes, except for one peak for Landers near 1.9 sec. The important vibration modes of the Connector have periods between 1.0 and 1.7 sec. There is not a large difference between the reduced ARS/Z spectrum and the recorded spectra in this period range, so the forces developed in the columns during the two earthquakes may have approached the nominal design strength.

The free–field ground motion records were not time synchronized with the records from the Connector. The time lag between vertical Channel 23 relative to the vertical free–field channel is determined by computing the correlation coefficient between the processed displacement records. Based on the correlation coefficients, it is assumed that the Connector records started 1.96 sec after the free–field records for Landers and 0.64 sec for Big Bear.

The input motion for the Connector was recorded at four supports: Abutments 1 and 17, and Bents 3 and 8. Figures 5 and 6 show the displacement histories at the four supports in the global longitudinal direction and global transverse direction for the two earthquakes. The heavy line is the free–field displacement histories in the same directions, accounting for the aforementioned time lags. The displacement histories are similar at the four supports and the free–field location, indicating that the pseudo–static effects of multiple–support excitation are not large. In the long period range, the dynamic effects of multiple–support excitation are not large either.

## RECORDED DISPLACEMENT RESPONSE

The processed acceleration and integrated displacement records allow evaluation of the superstructure displacements relative to the supports and opening–closing displacements of the hinges by subtraction of two displacement records. The baseline correction and high–pass filtering obscures any residual displacement.

### Bent 8 Response

The instruments at Bent 8, near the center of the Connector, provide detailed response of the bent. The displacement at the top of the column is computed considering the rotation of the box girder, the pile cap rotation, and deformation of the column, as shown in Fig. 7. The dotted line is the displacement at the top due to the pile cap rotation, and the solid line is the displacement at the top due to column deformation and pile cap rotation. The rotation of the pile cap is in–phase with the transverse displacement. The difference in the two histories is the deformation of the column, which is a maximum of 4.76 in. for Landers (drift=0.86%), and 2.98 in. for Big Bear (drift=0.54%).

The pile cap rotation produces displacements at the top of the column as a result of soil–structure interaction: 0.63 in. for Landers and 0.47 in. for Big Bear. For Landers, the ratio of the rotational soil stiffness to transverse stiffness of the column is 0.13, and the period is lengthened by a factor of 1.06 due to soil–structure interaction. For Big Bear, the stiffness ratio is 0.16 and the period ratio is 1.08. It is difficult to estimate the stiffness of the structure to within about 15%, but these soil–structure interaction effects are at about the limit for which they should be considered in the analysis of the bridge.

### Hinge Response

The longitudinal acceleration records show several large spikes that are caused by pounding of adjacent frames at the hinges. The longitudinal opening–closing displacements at Hinge 7 and Hinge 11 (inside edge of the deck) are shown in Figs. 8 and 9 for the two earthquakes. Hinge 7 has the largest opening: 1.41 in. for Landers and 1.70 in. for Big Bear. The closing of the hinge (negative displacement) is harder to discern. Hinge 7 closes about 1/2–in. during the first 25 sec of the Landers earthquake. Later the maximum closing displacement is about 1 in., indicating that filler material in the hinge may have crushed during the strong motion response later in the earthquake. The opening at Hinge 11 is less than the opening of Hinge 7, and the maximum closing displacement is 0.86 in. Hinge 7 opens more in the Big Bear earthquake than in Landers. The maximum closing displacement is nearly 1.5 in., possibly indicating accumulated pounding damage at the hinge in the second earthquake. The response of Hinge 11 is similar for the two earthquakes. The opening displacements are well below the yield displacement of the restrainers (4.2 in.), even neglecting the initial slack in the cables.

As shown in Fig. 10, the maximum transverse displacement for Hinge 3 is 0.35 in. for Landers. The relative transverse displacement of Hinge 7 is substantially different than for Hinge 3. There is little displacement for the first 18 sec in Landers. However, there are then larger displacement excursions at a frequency of approximately 0.5 Hz. The maximum relative displacement is 0.47 in. The relative transverse displacement is slightly larger for Big Bear.

One concern about the seismic performance of hinges is the possibility that torsion of the box girder may cause vertical lift–off and pounding on the elastomeric bearing pads. The relative vertical displacement at the outside edge of Hinge 7 is less than 0.20 in. opening and 0.27 in. closing for both earthquakes, and it is most likely caused by deformation of the pads. In contrast, the relative vertical displacements at the inside edge are larger. The maximum relative opening is 0.34 in. and 0.39 in. for Landers and Big Bear, respectively. The maximum relative closing is

0.55 in. and 0.36 in. for Landers and Big Bear, respectively. It is possible that lift–off and pounding occurred on the inside edge of the Connector, with rotation about the outside edge. The drawings for the bridge do not show vertical tie–down restrainers.

## VIBRATION PROPERTIES OF CONNECTOR

The transmissibility functions are computed from an input acceleration in one direction relative to the output acceleration at various locations in the superstructure using power and cross–power spectral density functions. Since the predominant input motion is in the transverse direction, two transverse input motions are used to compute transmissibility functions: the support acceleration for Bent 8 (Channel 24), and the free–field ground acceleration. Because of space limitations, Figs. 11 and 12 show some of the transmissibility functions for transverse channels using the Bent 8 motion for the two earthquakes.

Based on the spectral analysis and additional identification using an auto–regressive analysis (Ljung, 1987), the vibration periods and damping ratios for the lower vibration modes of the Connector are listed in Table 2. The most significant finding is the increase in the fundamental mode period of the Connector from 1.56 sec in the Landers earthquake to 1.75 sec in the Big Bear earthquake. The period lengthening and the increase in damping may indicate that the structure or foundation softened in the first earthquake.

Table 2. Vibration Periods and Damping Ratio Identified from Recorded Motion

| Mode | Landers Earthquake | | Big Bear Earthquake | |
|---|---|---|---|---|
| | Period (sec) | Damping Ratio | Period (sec) | Damping Ratio |
| 1 | 1.56 | 0.03 | 1.75 | 0.08 |
| 2 | 1.30 | 0.11 | 1.29 | 0.02 |
| 3 | 0.98 | 0.05 | 1.09 | 0.15 |
| 4 | 0.83 | 0.07 | 0.97 | 0.07 |

## MODELING OF THE CONNECTOR

Structural modeling and earthquake analysis are a central step in the design of new bridges and evaluation of existing bridges. There are always questions about how well the models predict the response of an actual bridge. An objective of the current study is to develop a model of the Northwest Connector and use the model to compute the response of the bridge to the earthquakes, and compare the computed response with the recorded response. The approach is to use methods of modeling and dynamic analysis typically available for bridge design. The details of the modeling will be available in the final report.

Since the Connector did not experience inelastic deformation in the earthquakes, it is appropriate to use linear, elastic models for the structural components. The foundations are modeled as linear, elastic springs. The opening and closing of the intermediate hinges, however, is nonlinear and that behavior is represented in the model of the Connector. The dynamic analyses

are performed using the computer program SADSAP (Wilson, 1992). The program includes standard linear frame elements, non–linear one–dimensional elements for gaps, tension–only elements, and compression–only elements. Models of the intermediate hinges are constructed using the nonlinear elements.

One of the parameters in the model is the factor by which the gross moments of inertia for the columns are reduced to represent the level of deformation. The reduction factor is selected as the primary parameter to match the computed response with the recorded response in the two earthquakes. Based on interpretation of the test data for steel jacketed columns (Priestly, Seible et al., 1992), the moments of inertia for a column are increased 20% or 10%, depending on the full or partial jacket retrofit, to account for the stiffening effect of the jacket.

The stiffness of the pile foundations are represented by translational and rotational springs at the pile cap. The translational spring stiffness is based on a lateral stiffness of 65 kip/in per pile, which is 30% of the stiffness based on the gross properties of the piles using the small strain estimate of shear wave velocity for the soil. The reduction accounts for pile cracking, larger soil strains, soil gapping, and group effect. The rotational stiffness of the pile cap was determined from the displacements of Bent 8 described previously. The rotational stiffness of $4 \times 10^7$ k–ft/rad is also about 30% of the rotational stiffness of the pile group using the axial stiffness of the piles.

The three–dimensional model of the Connector consists of approximately 300 frame elements and 40 nonlinear elements with 1500 degrees–of–freedom. The model is illustrated in Fig. 13 with the first four vibration modes of the bridge. The properties are calibrated for the Landers response, in which the column stiffness is based on the gross section properties. The model is modified for the Big Bear earthquake by multiplying the stiffness of the columns by a factor of 0.65 and the springs for the pile foundations by a factor of 0.50. The first four vibration periods for the modified model are: 1.74 sec, 1.44 sec, 1.36 sec, and 1.12 sec.

Comparison of the calculated periods with the identified periods in Table 2 shows a good match for the first mode, but differences in the higher modes. More detailed study is required to determine the cause of the discrepancy. As discussed in the next section, the correlation of computed and recorded response is fairly good.

## RESPONSE COMPARISON

The models are analyzed using the recorded Bent 8 support motion as uniform input motion. The use of the recorded free–field motion as uniform input gives similar results. For Landers, the model is assumed to have a damping ratio of 3% in all modes, and for Big Bear the damping is assumed to be 5% in all modes.

The comparison of computed and recorded total displacements at selected channels is shown in Figs. 14 and 15 for the Landers and Big Bear earthquakes, respectively. In general, the models represent the overall dynamic response of the Connector recorded in the earthquakes. Although there are some differences in the peaks, the correlation is generally good for both earthquakes, particularly in regard to the phasing of the displacements.

The ability of the gap elements to model the hinge opening and closing is of particular interest. Figure 16 shows the longitudinal displacement of Hinge 7 and Hinge 11 for the two earthquakes. The simple hinge modeling represents the hinge displacements fairly well.

Since bridge design is currently based on linear models for earthquake analysis, the effects of intermediate hinges are bounded by a "tension model" and a "compression model." The former

includes linear elements representing the restrainers with no longitudinal constraint at the hinges. The latter model connects the frames with moment releases at the hinges. Figure 17 shows the maximum longitudinal shear force in the columns computed from the tension model, compression model, and the nonlinear model with hinge opening–closing. The two linear models underestimate the shear force at several of the columns, mostly the short ones. The larger shear forces develop because of pounding at nearby hinges, which is not captured in the linear models.

## CONCLUSIONS

The strong motion response of the Northwest Connector in the 1992 Landers and Big Bear earthquakes provides valuable information about the dynamic response of this common type of bridge. The intermediate hinges opened as much as 1.7 in., which is well below the yield displacement of the cable restrainers. Typical modeling of the bridge with estimates of the column stiffness and pile foundation properties provide a reasonable correlation between the computed and the recorded responses, although there are some errors in the periods of the higher modes. Pounding of the hinges produces large acceleration spikes, which causes increased shear forces in the columns. Since modeling the hinge opening–closing is relatively simple using gap elements, this type of analysis is recommended for the design of multiple–frame bridges.

## ACKNOWLEDGMENTS

This work was sponsored by the California Division of Mines and Geology under Interagency Agreement 1093–546. The assistance of the program director, Moh Huang, is appreciated. Many engineers at Caltrans provided assistance that was invaluable, including Pat Hipley, James Gates, Kelly Holden, Ken Jackura, and Mark Yashinsky.

## REFERENCES

Caltrans (1990). "Bridge Design Specifications Manual," California Department of Transportation.

Darragh, R., T. Cao, et al. (1993). "Processed CSMIP Strong–Motion Records from the Landers and Big Bear, California, Earthquakes of 28 June 1992 —— San Bernardino, I10/215 Interchange," *Report No. OSMS 93–08*, Office of Strong Motion Studies, Division of Mines and Geology.

Jackura, K. A. (1991). "Study of Liquefaction Potential at the I–10/I–215 Interchange in San Bernardino County," California Department of Transportation.

Ljung, L. (1987). *System Identification*, Prentice–Hall, Englewood Cliffs, NJ.

Priestly, M. J. N., F. Seible, et al. (1992). "Seismic Retrofit of Bridge Columns Using Steel Jackets," Tenth World Conference on Earthquake Engineering, Vol. 9, Madrid, Spain, pp. 5285–5290.

Roberts, J. E. (1991). "Research Based Seismic Design and Retrofit of California Bridges," First Annual Seismic Research Workshop, Sacramento, CA, pp. 1–10.

Williams, D. and W. G. Godden (1976). "Experimental Model Studies on Seismic Response of High Curved Overcrossings," *Report No. UCB/EERC–76/18*, Earthquake Engineering Research Center, University of California at Berkeley.

Wilson, E. L. (1992). "SADSAP: Static and Dynamic Structural Analysis Programs," Structural Analysis Programs, Inc.

Yashinksy, M., L. Maulchin, et al. (1992). "Performance of Bridges During the Landers and Big Bear Earthquakes, Post–Earthquake Investigation Team Report," Division of Structures, California Department of Transportation.

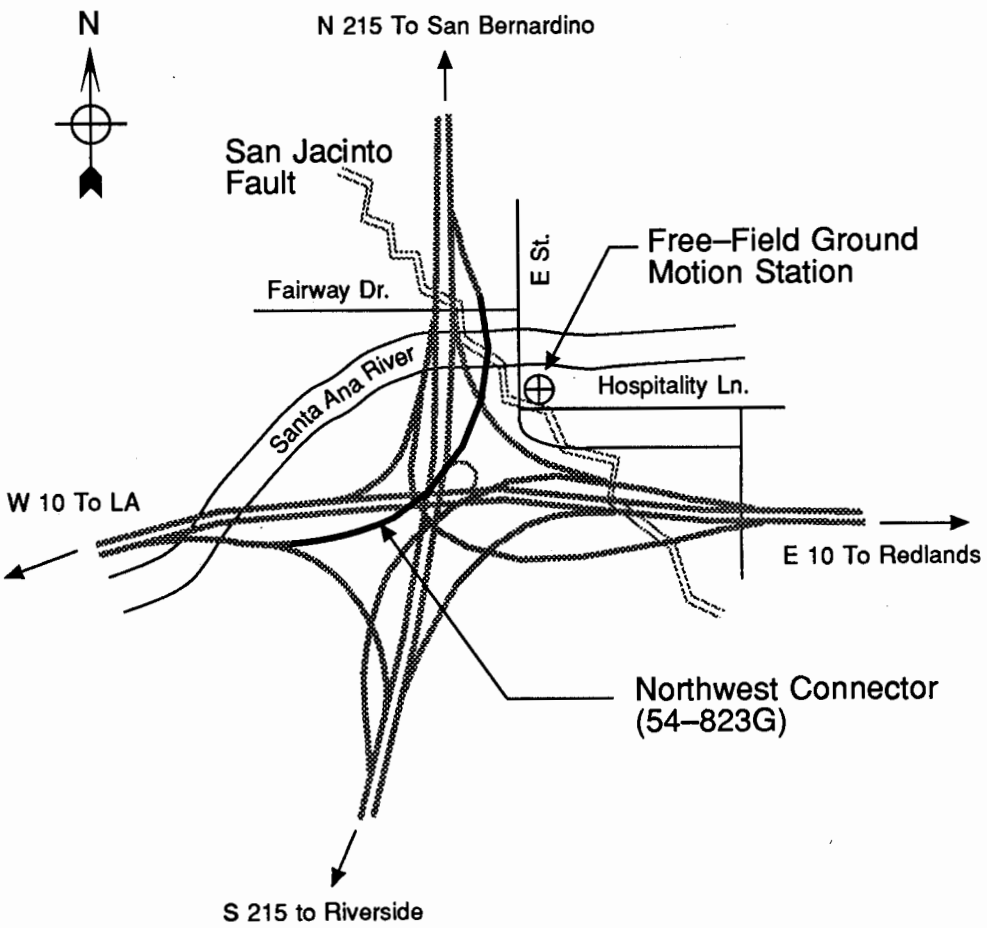


Fig. 1 Interstate 10/215 Interchange in Colton, CA.

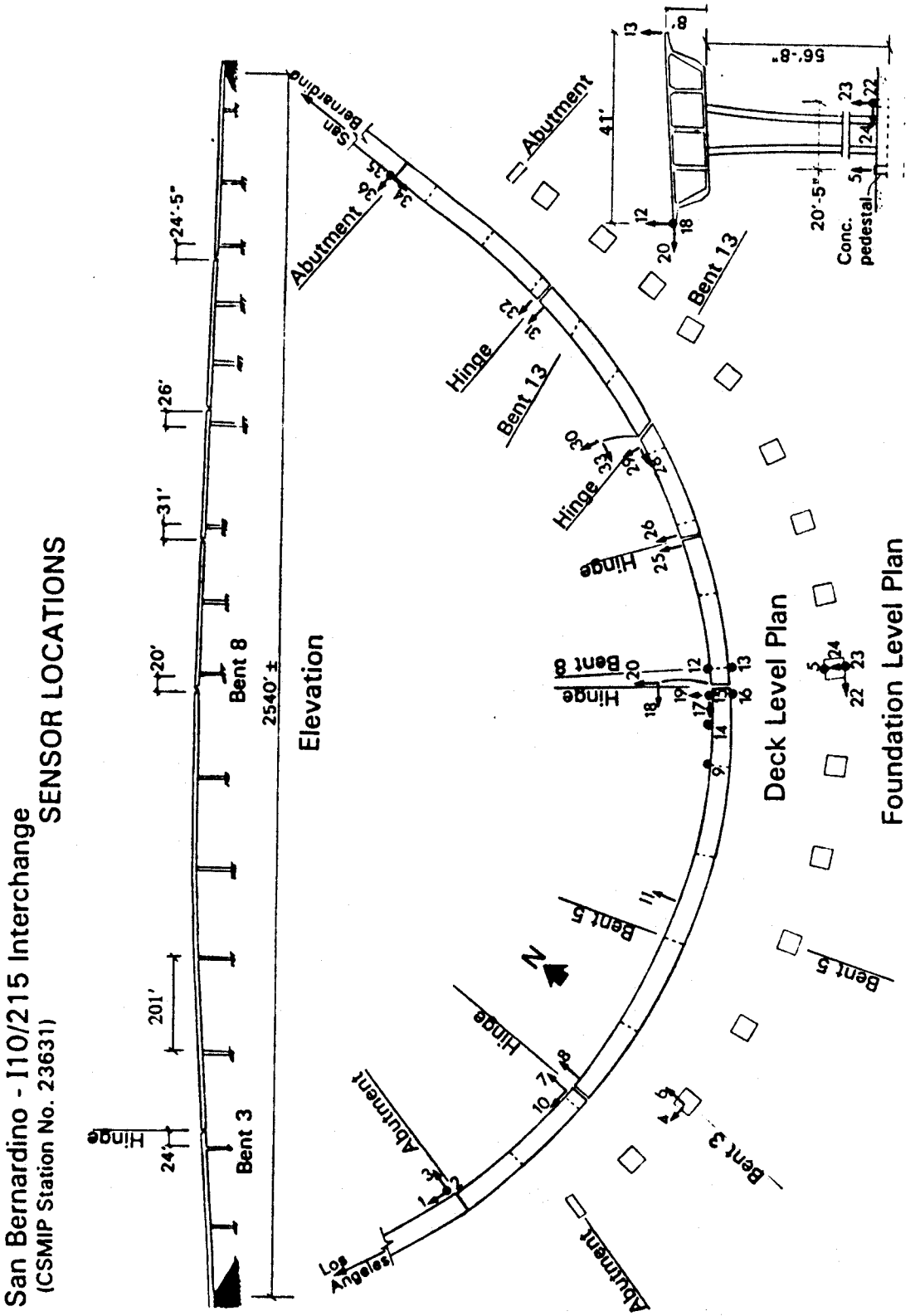


Fig. 2 Strong–Motion Instrumentation Plan for the Northwest Connector (Darragh, Cao et al., 1993).

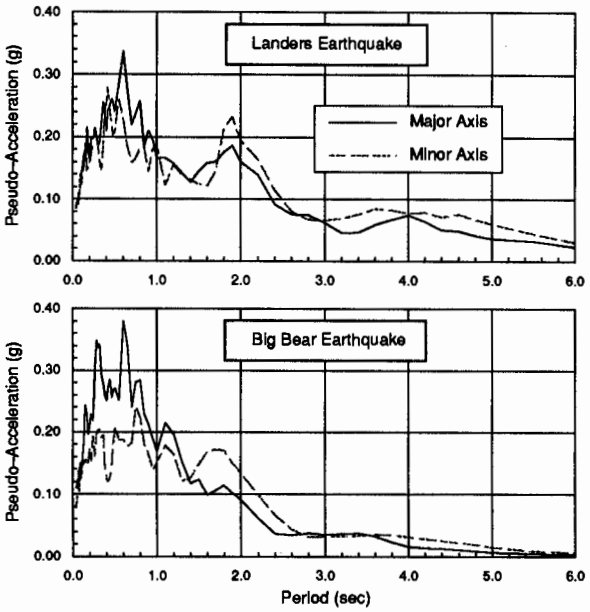


Fig. 3 Response Spectra for Free–Field Ground Motion (5% Damping).

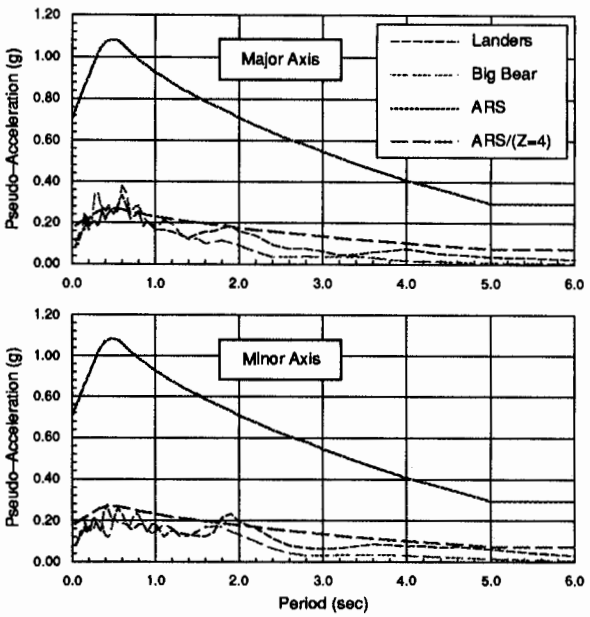


Fig. 4 Response Spectra for Free–Field Ground Motion Compared with ARS Design Spectra (5% Damping).

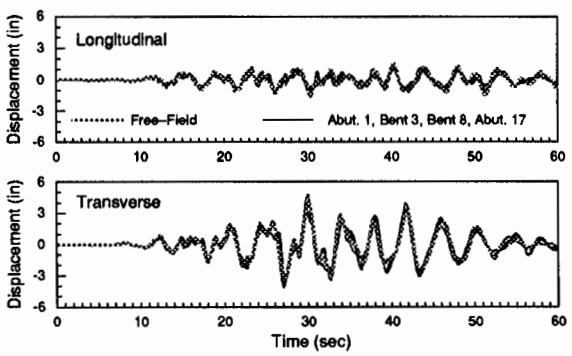


Fig. 5 Input Motion in Global Directions for Landers Earthquake.

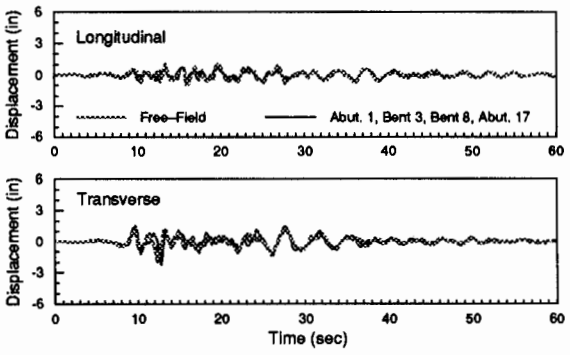


Fig. 6 Input Motion in Global Directions for Big Bear Earthquake.

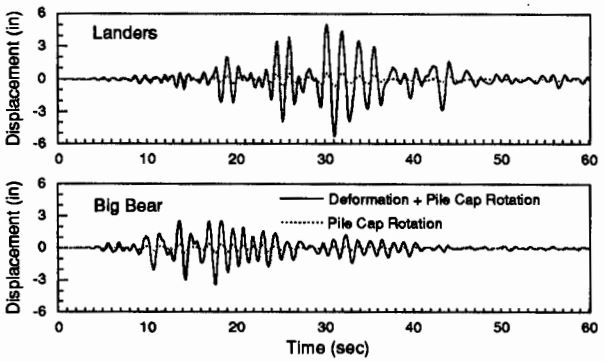


Fig. 7 Transverse Displacements of Bent 8 Column.

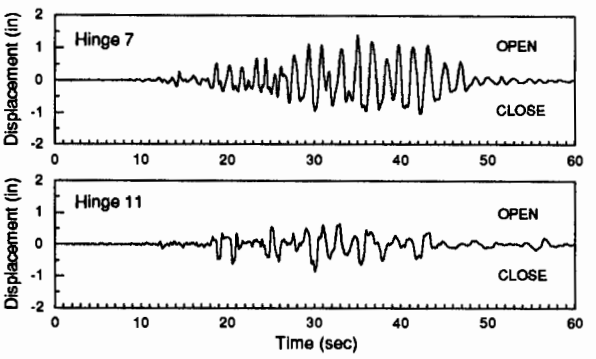


Fig. 8 Longitudinal Displacement of Hinges in Landers Earthquake.

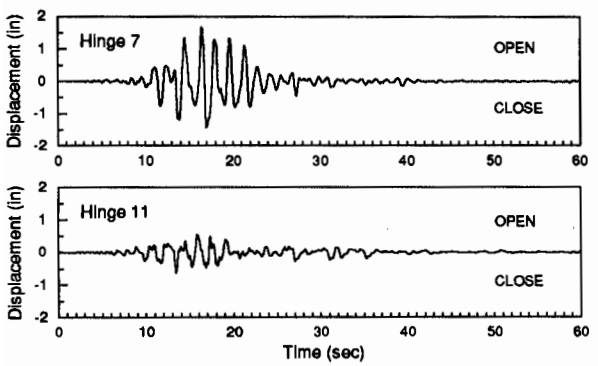


Fig. 9 Longitudinal Displacement of Hinges in Big Bear Earthquake.

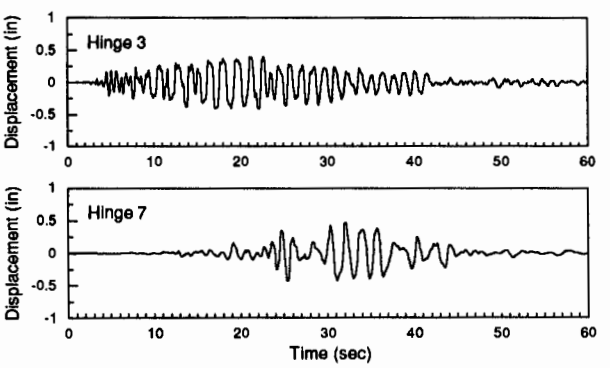


Fig. 10 Transverse Displacement of Hinges in Landers Earthquake.

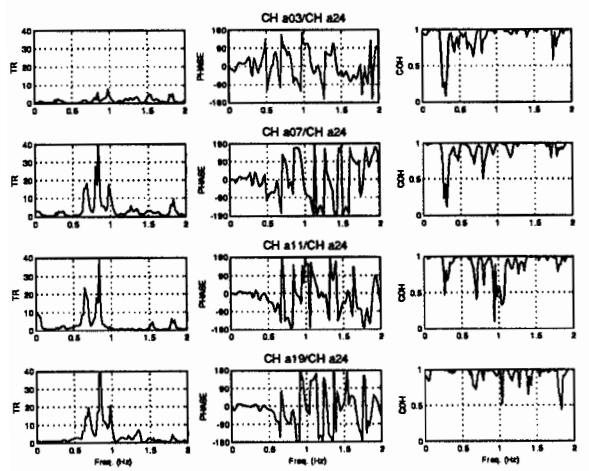


Fig. 11 Spectral Response Using Bent 8 Input Motion in Landers Earthquake.

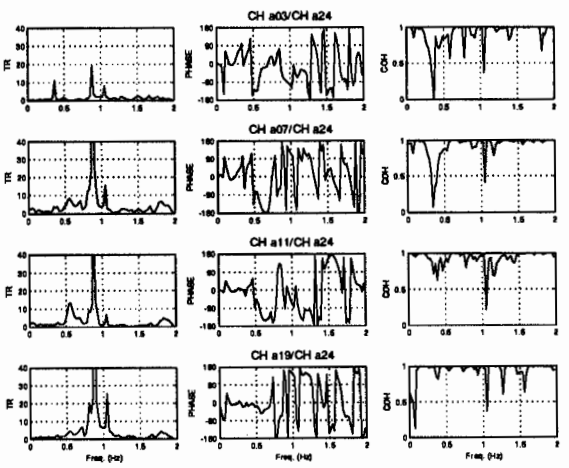


Fig. 12 Spectral Response Using Bent 8 Input Motion in Big Bear Earthquake.

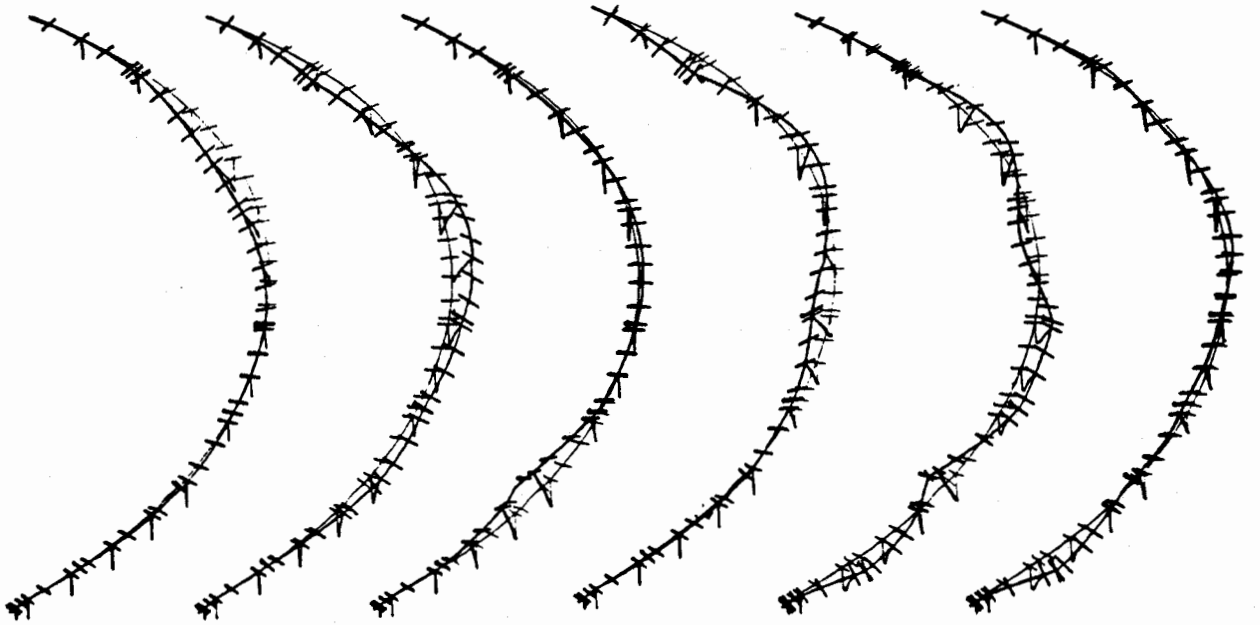

$T_1$=1.51 sec $T_2$=1.24 sec $T_3$=1.17 sec $T_4$=0.97 sec $T_5$=0.82 sec $T_6$=0.76 sec

Fig. 13 First Four Vibration Modes of the Model for the Northwest Connector.

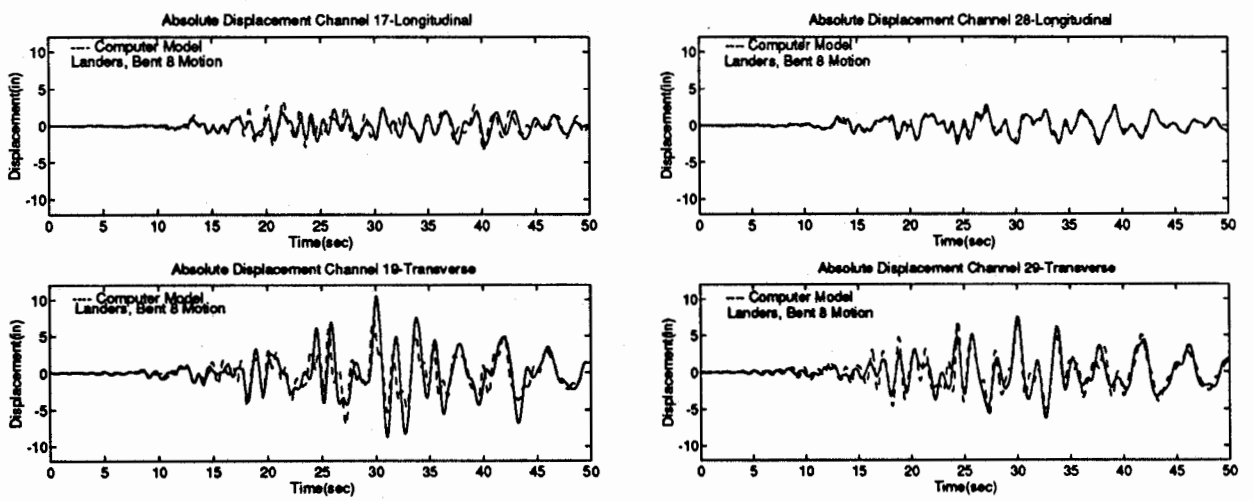


Fig. 14 Comparison of Recorded and Computed Response in Landers Earthquake.

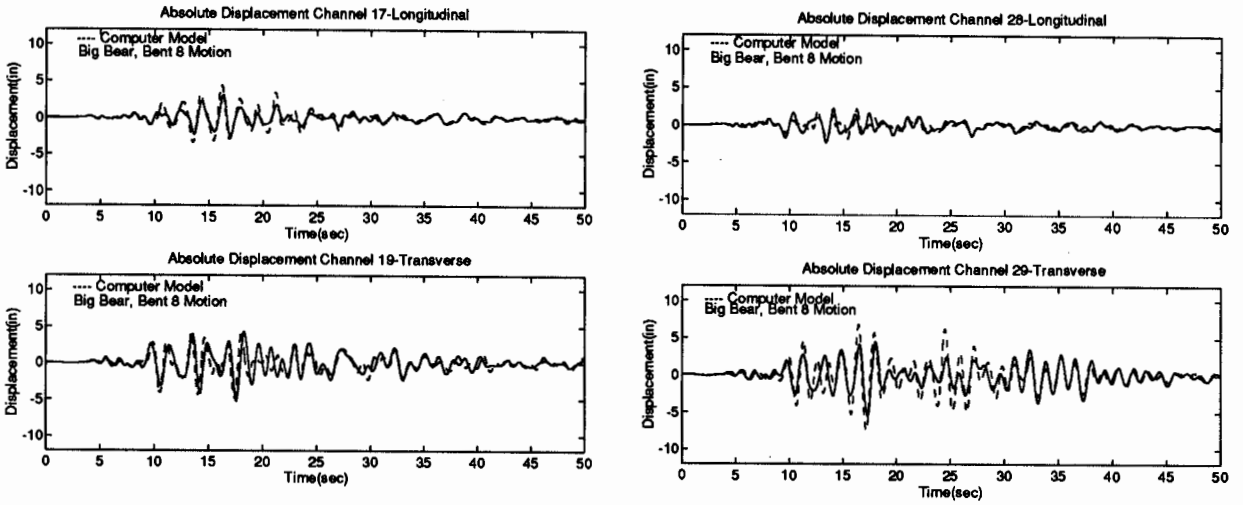


Fig. 15 Comparison of Recorded and Computed Response in Big Bear Earthquake.

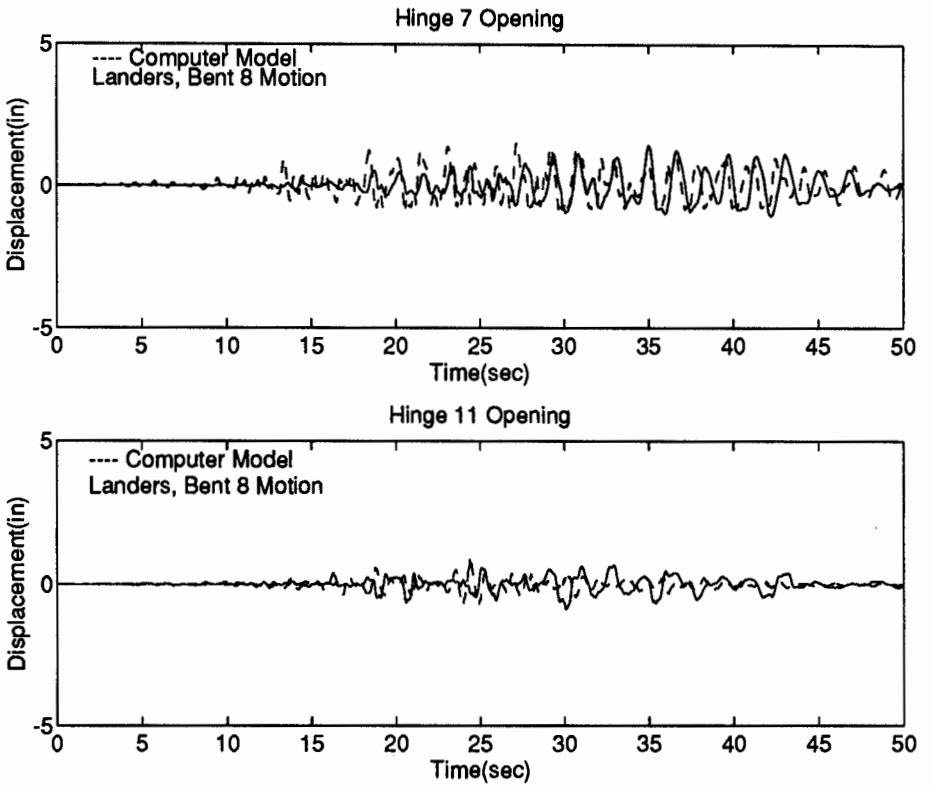


Fig. 16 Comparison of Recorded and Computed Longitudinal Hinge Displacement in Landers Earthquake.

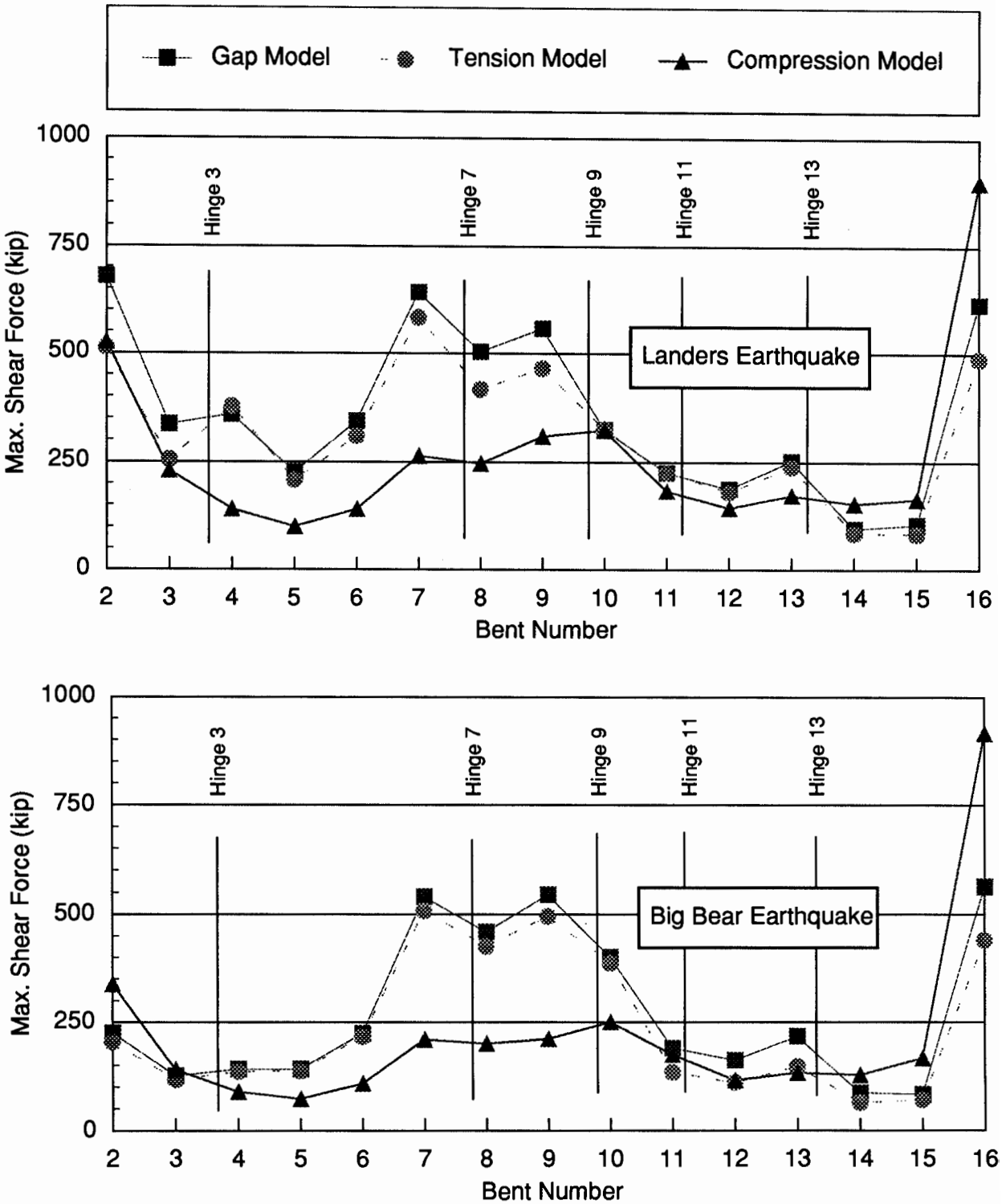


Fig. 17 Maximum Longitudinal Shear Force in Columns for Three Models.

# SEISMIC RESPONSE STUDY OF THE US 101/ PAINTER STREET OVERPASS USING STRONG MOTION RECORDS

Rakesh K. Goel and Anil K. Chopra

Department of Civil Engineering
University of California at Berkeley

## ABSTRACT

Abutment stiffnesses are determined directly from the earthquake motions recorded at the US 101/ Painter Street Overpass using a simple equilibrium-based approach without finite-element modeling of the structure or the abutment-soil systems. The calculated abutment stiffnesses, which include the effects of soil-structure interaction and nonlinear behavior of the soil, are used to investigate variation of the abutment stiffness with its deformation during the earthquake and torsional motions of the road deck. Also evaluated are the CALTRANS, ASSHTO-83, and ATC-6 procedures for estimating the abutment stiffness. It is demonstrated that stiffness of the abutment depends significantly on its deformation during the earthquake: larger is the deformation, smaller is the stiffness. The road deck of this structure experienced significant torsional motions in part because of eccentricity created by different transverse stiffnesses at the two abutments. It is also shown that the CALTRANS procedure leads to good estimate of the abutment stiffness provided the deformation assumed in computing the stiffness is close to actual deformation during the earthquake, and ASSHTO-83/ATC-6 procedure results in stiffer initial estimate of the abutment stiffness.

## INTRODUCTION

The 1971 San Fernando earthquake clearly demonstrated the importance of abutment-soil systems in earthquake response of short bridges (Jennings and Wood, 1971). Recognizing this importance, most earthquake design codes for highway bridges require that the abutment-soil systems be included in the structural idealization as equivalent discrete springs (CALTRANS, 1990; ATC-6, 1981; AASHTO-83, 1988). Needed for such code-based earthquake analyses of short bridges are the stiffness values of the abutment-soil springs. In the design profession, these values are selected based on some simplified rules and trial-and-error process. It is not entirely clear how well the stiffness values thus determined represent the complex behavior of the abutment-soil systems, such as soil-structure interaction and nonlinear behavior of the soil, during actual ground shaking. It is therefore important to determine the stiffness values directly from the motions recorded during actual earthquakes.

This investigation is aimed at filling this need. The primary objective of this investigation is to determine the stiffness values of the abutment-soil systems from the earthquake motions recorded at the US 101/ Painter Street Overpass without any finite-element modeling of the structure or abutment-soil systems. The approach adopted in this investigation involves estimating the stiffness

of the abutment-soil systems from their force-deformation loops, which are determined from the recorded motions using the dynamic equilibrium of the road deck. This simple approach is possible because the US 101/ Painter Street Overpass can be idealized by just a few stiffness parameters -- springs along the east abutment, normal to the east abutment, and along the west abutment; for simplicity, the stiffness values of two columns in the central bent are assumed to be known and are determined from their structural details. The calculated abutment stiffnesses, which include the effects of soil-structure interaction and nonlinear behavior of the soil, are used to investigate variation of the abutment stiffness with its deformation during the earthquake and torsional motions of the road deck of this structure. Also evaluated are the CALTRANS, ASSHTO-83, and ATC-6 procedures for estimating the abutment stiffness.

## STRUCTURE AND RECORDED MOTIONS

Identified as CSMIP Station No. 89324, the US 101/ Painter Street Overpass (Figure 1) is located in Rio Dell, California. This 265 ft long bridge consists of a continuous reinforced-concrete (R/C) multi-cell box-girder road deck supported on integral abutments at the two ends and on an R/C two-column bent, which divides the bridge into two unequal spans of 119 ft and 146 ft. Both abutments and bent are skewed at an angle of 38.9°. The east abutment is supported on 14 driven 45-ton concrete friction piles. The west abutment rests on a neoprene bearing strip that is part of a designed thermal expansion joint of the road deck. The foundation of this abutment consists of 16 driven 45-ton concrete friction piles. This bridge is typical of short bridges in California spanning two or four lanes separated highways.

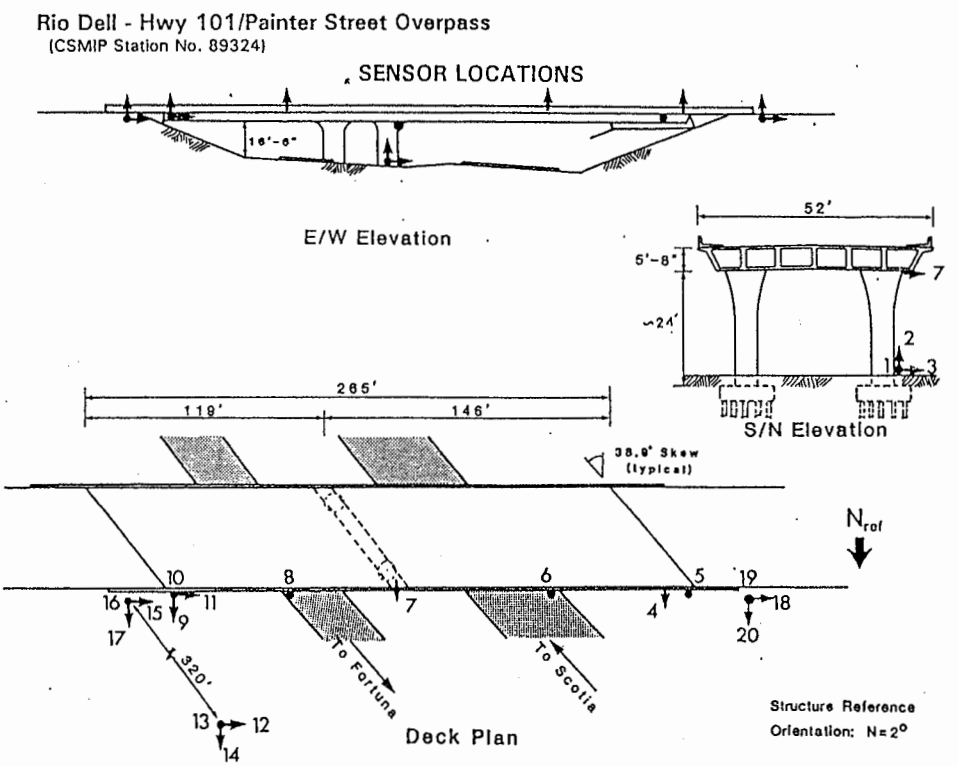


Figure 1. US 101/ Painter Street Overpass (Shakal et al., 1992)

The US 101/ Painter Street Overpass was instrumented by California Strong Motion Instrumentation Program (CSMIP) in 1977. Figure 1 shows locations of the instruments and identifies the channels on this structure. Since this overpass was instrumented, it has yielded strong motion records during nine earthquakes (Table 1). For the purpose of this research investigation, we have selected motions recorded during two earthquakes: the main shock of the April 25, 1992, Cape Mendocino/ Petrolia earthquake which produced the maximum free-field acceleration of 0.543g that was amplified to 1.089g at the structure; and the second event of the November 21, 1986, Cape Mendocino earthquake that caused much smaller motions of 0.144g and 0.35g at the free-field and the structure, respectively.

Table 1. List of recorded motions at the US 101/ Painter Street Overpass

| No. | Earthquake | Depth (Km.) | Mag. $M_L$ | Dist. (Km.) | Max. FF Acc. (g) | Max. Str. Acc. (g) |
|---|---|---|---|---|---|---|
| 1. | Trinidad Offshore 8 Nov, 1980 | 19 | 6.9 | 82 | 0.147 | 0.169 |
| 2. | Rio Dell 16 Dec, 1982 | 5 | 4.4 | 15 | -- | 0.420 |
| 3. | Eureka 24 Aug, 1983 | 30 | 5.5 | 61 | -- | 0.215 |
| 4. | Cape Mendocino 21 Nov, 1986 (First Event) | 17 | 5.1 | 32 | 0.432 | 0.399 |
| 5. | Cape Mendocino 21 Nov, 1986 (Second Event) | 18 | 5.1 | 26 | 0.144 | 0.350 |
| 6. | Cape Mendocino 31 Jul, 1987 | 17 | 5.5 | 28 | 0.141 | 0.335 |
| 7. | Cape Mendocino/ Petrolia Apr 25, 1992 | 15 | 6.9 | 6.4 | 0.543 | 1.089 |
| 8. | Cape Mendocino/ Petrolia Apr 26, 1992 (AS # 1) | 18 | 6.2 | 6.2 | 0.516 | 0.757 |
| 9. | Cape Mendocino/ Petrolia Apr 26, 1992 (AS # 2) | 21 | 6.5 | 6.4 | 0.262 | 0.311 |

## ANALYSIS PROCEDURE

### Structural Idealization

Figure 2 shows the free-body diagram of an idealized model of the US 101/ Painter Street Overpass. The model consists the road deck with three spring-dampers, which represent the abutment-soil systems along the east abutment, normal to the east abutment, and along the west abutment. The spring represents the stiffness of the abutment and the damper accounts for material and radiation damping of the abutment-soil system. Each column in the central bent is represented by two simple linear elastic springs -- one normal to and other along the bent. The stiffness values of these springs are computed by frame analysis of the bent using the cracked stiffness of each column with inertia values determined from its moment-curvature relationship.

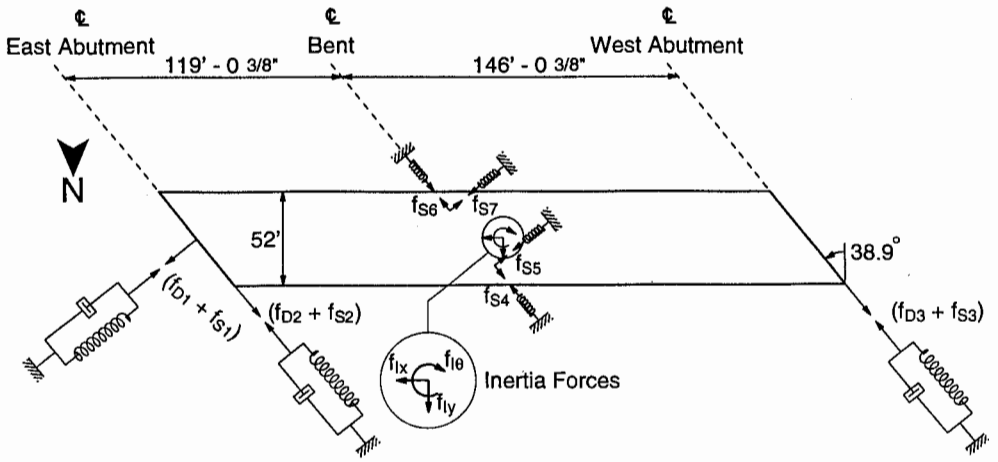


Figure 2. Free-body diagram of an idealized model of US 101/ Painter Street Overpass

**Equations of Equilibrium**

The three equations of dynamic equilibrium for the system of Figure 2 are:

$$f_I + f_D + f_S = 0 \qquad (1)$$

in which $f_I^T = \langle f_{Ix},\ f_{Iy},\ f_{I\theta} \rangle$ is the vector of inertia forces, $f_D$ is the vector of damping forces, and $f_S$ is the vector of spring forces; $f_D$ and $f_S$ are formed by transforming forces at the abutments -- $(f_{D1}+f_{S1})$ , $(f_{D2}+f_{S2})$ , and $(f_{D3}+f_{S3})$ ; and the forces at the columns -- $f_{S4}$, $f_{S5}$, $f_{S6}$, and $f_{S7}$.

**Abutment Forces and Deformations**

The only unknowns in equation (1) are the abutment forces, which are determined by solving the three equations at each instant of time. The three components of the inertia force vector are computed from the mass properties, determined from the structural plans, and recorded accelerations. The force in each column spring is determined from its known stiffness and deformation.

At each time-instant, the deformation in the spring-damper system, modeling the abutment-soil system, or the column spring is obtained by subtracting the free-field motion from the motion at the top of the abutment or the column; the latter can be computed from recorded motions of the road deck.

**Abutment Stiffness**

If the computed abutment force is plotted against its calculated deformation for many time instances, we will obtain hysteresis loops. The abutment stiffness is calculated from these hysteresis loops as described next. The force-deformation hysteresis loops are generated for the selected earthquakes. The stiffness of each of the abutment-soil systems is determined by isolating individual loops. Three such loops -- one for each of the three abutments -- are shown in Figure 3.

The somewhat elliptical shape of the loop for the spring normal to the east abutment (Figure 3a) suggests elastic behavior. From such a loop the spring stiffness is obtained by selecting its slope as shown by the two straight lines; the corresponding values are 29768 and 23500 kips/ft. Although the loop for the spring along the east abutment (Figure 3b) deviates considerably from a

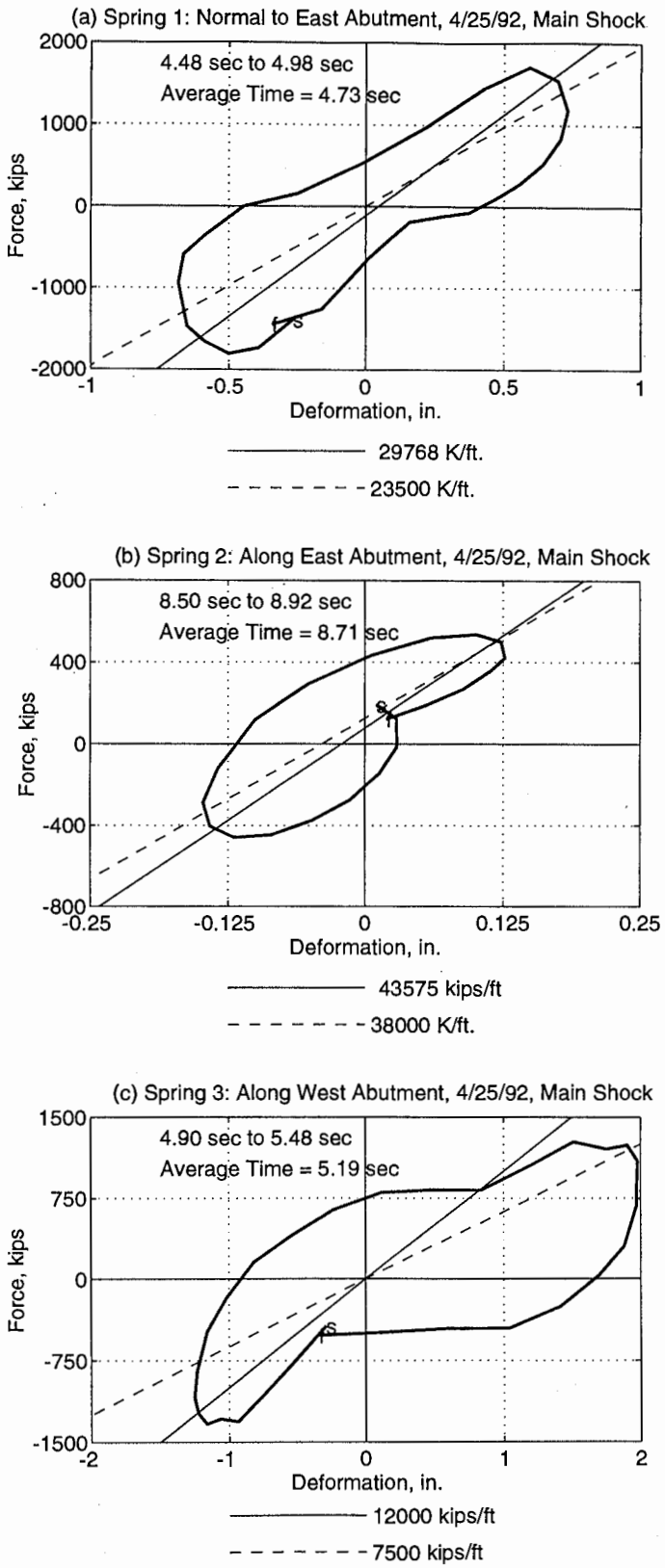


Figure 3. Selected force-deformation hysteresis loops

perfect ellipse, it is still possible to estimate the stiffness value for this spring; the upper and lower bound values in this case are 43575 and 38000 kips/ft.

Unlike the two previous loops, which suggest elastic behavior of the springs, the loop selected for the spring along the west abutment (Figure 3c) exhibits significant non linearity as evident from the elasto-plastic with strain hardening force-deformation behavior. From such loops, the upper and lower bounds of the stiffness are obtained by selecting the secant stiffness values; these values are 7500 and 12000 kips/ft for the positive and negative deformations, respectively.

Such results are used next to investigate variation of the abutment stiffness with its deformation during the earthquake. For this purpose, the time-variation of the stiffness during the larger earthquake is examined first. Subsequently, abutment stiffness values are compared for the two selected earthquakes. Also compared are the transverse stiffness values of the two abutments to explain the torsional motions of the road deck during the large earthquake.

## TIME-VARIATION OF ABUTMENT STIFFNESS

Figure 4 shows the time-variation of stiffness for the three abutments during the main shock of the 1992 Cape Mendocino/ Petrolia earthquake. Since the stiffness value is the average stiffness over the time duration of one loop, it is shown as a discrete point plotted at the middle of this duration. It is clear from these results that the abutment stiffness varies significantly during the same earthquake. This variation is particularly large for the spring normal to the east abutment (Figure 4a). In order to further investigate this behavior of the abutment, plotted on the right vertical axis of Figure 4 is its total deformation, which is the sum of the deformation amplitudes in the positive and negative directions. By examining the deformations along with the stiffnesses, the following general pattern emerges.

- The abutment tends to be stiff for small deformation such as during the build-up phase of the shaking (first set of values in Figures 4a and 4b).
- The abutment stiffness reduces with its increasing deformation as the amplitude of the motion increases during the strong motion phase (values between 5 and 9 sec in Figures 4a to 4c).
- The abutment recovers some of its stiffness with subsequent reduction in its deformation as the motion becomes less intense towards the later part of the shaking (values after 10 sec in Figures 4a and 4c).
- The recovery of abutment stiffness is only partial: the stiffness for a deformation level may not return to the value prior to a large deformation cycle. This recovery is gradual over time and is especially slow after repeated large deformation cycles (Figure 4a).

This abutment behavior indicates that soil enclosed between the wingwalls provides significant resistance to the abutment motion for small deformation levels. For large deformations, however, the soil becomes less effective. The reduction in stiffness for large deformation may also be due to nonlinear behavior of the soil (Figure 3c).

## COMPARISON OF ABUTMENT STIFFNESS DURING TWO EARTHQUAKES

Compared in Figure 5 are the abutment stiffness values during the second event of 1986 Cape Mendocino earthquake and the main shock of 1992 Cape Mendocino/ Petrolia earthquake. Since

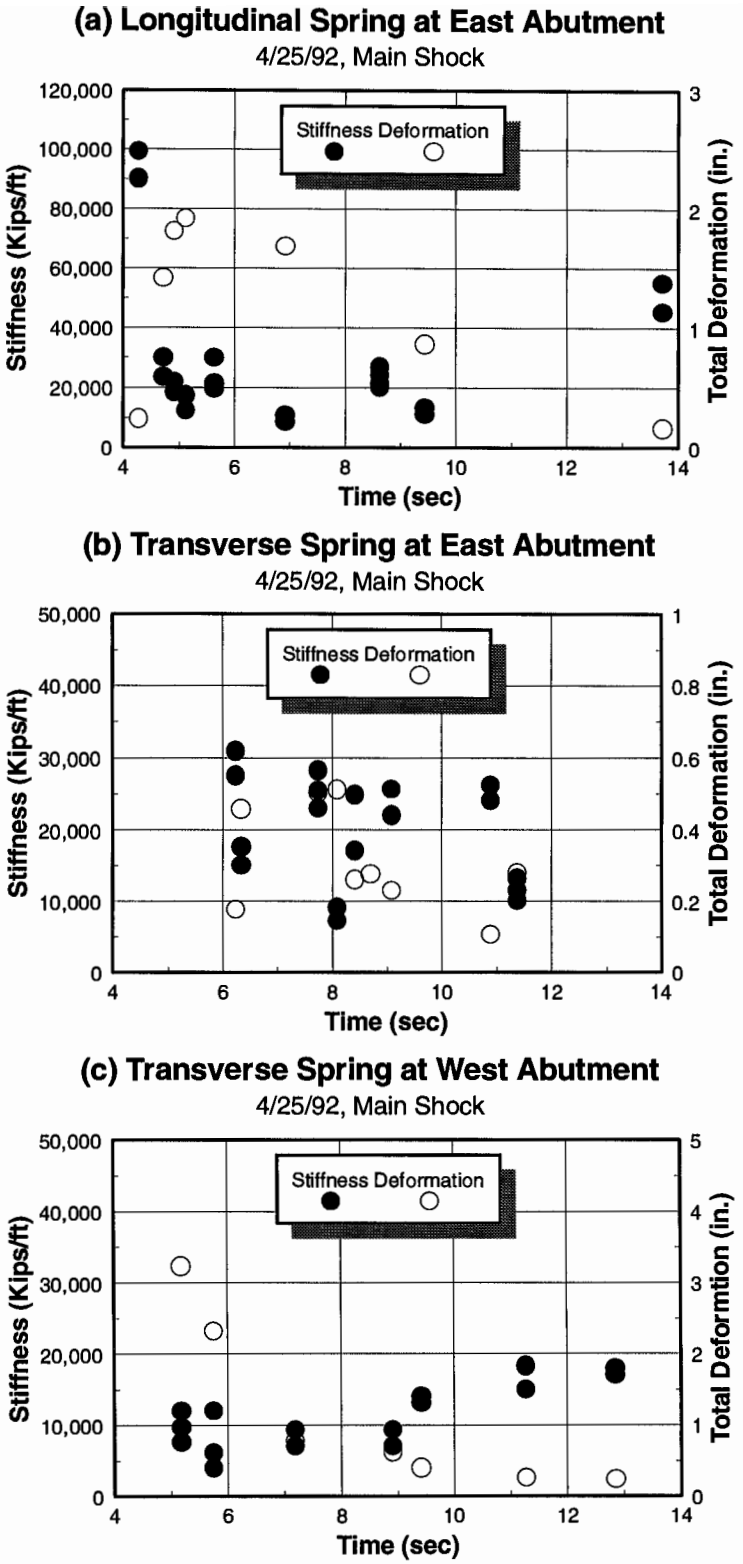


Figure 4. Time-variation of abutment stiffness and deformation

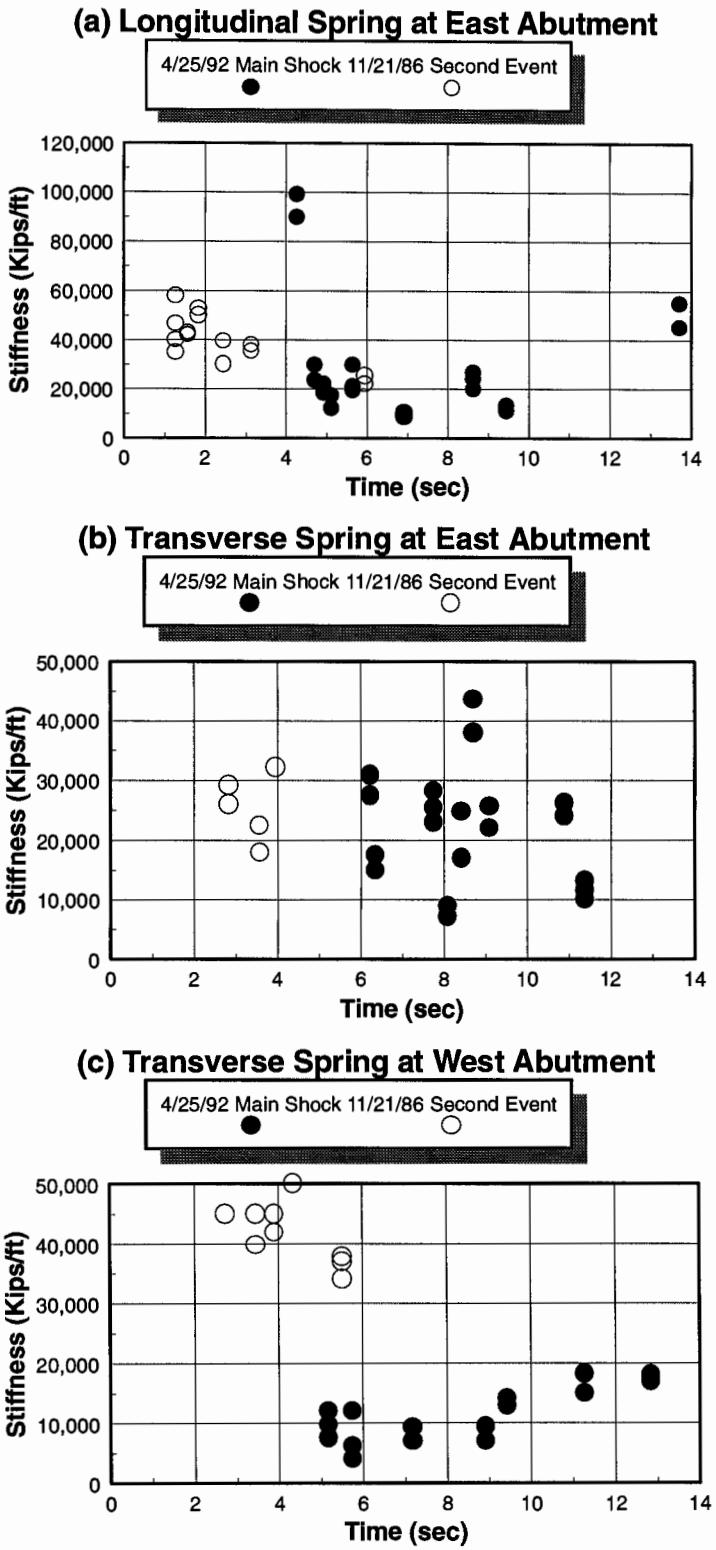


Figure 5. Comparison of stiffness for two earthquakes

the duration of shaking and amplitudes of motion are smaller for former of these two earthquakes, only a few stiffness values during the strong shaking phase are identified; many more stiffness values spread over all the three phases are available for the latter earthquake. These results show that trends in the abutment behavior are consistent with the trends identified in the previous section. The abutment is in general less stiff during the latter of the two earthquakes (Figures 5a and 5c) because of larger abutment deformations resulting from more intense shaking during this earthquake. For the purpose of this comparison, abutment deformations similar to those shown in Figure 4 for the 1992 earthquake were also computed for the 1986 earthquake but are not included here for brevity. This effect is more pronounced for the west abutment because of its larger deformations resulting from torsional motions of the road deck during the 1992 earthquake (Figure 5c). For similar deformations during the two earthquakes, such as those in the transverse direction at the east abutment, the abutment stiffnesses are also similar (Figure 5b).

## TORSIONAL MOTIONS OF THE ROAD DECK

The road deck of the US 101/ Painter Street Overpass experienced significant torsional motions about its vertical axis during the main shock of the 1992 Cape Mendocino/ Petrolia earthquake; peak acceleration at the west end of the road deck was more than one-and-a-half times the value at the east end during this earthquake. In order to investigate the cause of this behavior of the road deck, the transverse stiffnesses of the two abutments (Figures 4b and 4c) are compared in Figure 6. The transverse stiffness of the west abutment is significantly smaller compared to the east abutment because of several reasons. The two abutments are of the same size but the west abutment is taller and hence less stiff. Furthermore, the east abutment is constructed monolithic with the footing while the west abutment is seated on a neoprene bearing to permit thermal movement that introduces additional flexibility at the west abutment. The center of rigidity of the deck would be closer to stiffer of the two abutments, the east abutment, whereas the center of mass would be located close to midway between the two abutments. The resulting eccentricity between the centers of mass and rigidity contributed to the torsional motion of the deck. As shown earlier (Goel and Chopra, 1990), the motion should be larger on the flexible side, the west abutment, and this is consistent with the recorded motions.

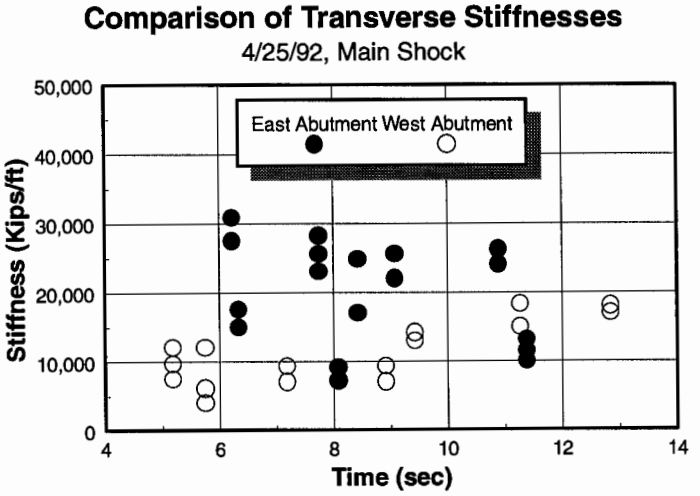


Figure 6. Comparison of transverse stiffnesses of the east and west abutments

## EVALUATION OF CURRENT PROCEDURES

Compared in Figure 7 are the abutment stiffness values determined from recorded motions (Figures 4 to 6) with the values computed by CALTRANS, AASHTO-83, and ATC-6 procedures; the ASSHTO-83 and ATC-6 values are identical. Also included are values determined by Gates and Smith (1982) and Romstad and Maroney (1990). The results presented are for the main shock of the 1992 Cape Mendocino/ Petrolia earthquake.

The stiffness values for the CALTRANS procedure are determined from the abutment capacity (CALTRANS, 1988) in conjunction with the acceptable deformation. Two values of the acceptable deformation are considered: 1 inch and 2.4 inch; the former corresponds to the limit when the soil pressure behind the backwall of the abutment reaches its maximum value of 7.7 ksf, and the latter corresponds to the limiting value for avoiding damage to the abutment (CALTRANS, 1988, 1989). Note that the iterative procedure in which the initial stiffness is computed by assuming the soil stiffness of 200 kips/in per linear foot of the abutment backwall or wingwall (Tsai et al., 1993; CALTRANS, 1990) is not included in this investigation because CALTRANS engineers no longer consider this as a preferred procedure.

Table 2 shows the computed abutment stiffnesses using the above-described procedure. For computing longitudinal stiffness, several possibilities are considered. First two correspond to resistance provided only by one abutment such as before closure of the expansion joint gap or after failure of the shear key at the west abutment. The other two correspond to resistance provided by both the abutments when the shear key is engaged at the west abutment. Two possible failure modes are considered to calculate the backwall capacity: shear failure in the backwall just below the road deck soffit before the piles fail, and the failure of piles before the backwall fails. In each case, the soil depth equal to the road deck is considered for computing the soil resistance (CALTRANS, 1988). The transverse stiffness is based on the shear capacity of one wingwall and foundation capacity; the foundation capacity for the east abutment is selected as the capacity of the piles whereas that for the west abutment it is taken as the capacity of the shear key, which is assumed to be 0.75 times the capacity of the piles.

Figure 7a shows that the longitudinal stiffness computed by the CALTRANS procedure with 2.4 inch deformation matches quite well with values during the strong shaking phase of the earthquake. The exceptions occur during the build-up phase and towards the end of the earthquake where the abutment stiffness may be significantly larger than the CALTRANS values. This occurs because the abutment deformations during these phases of the earthquake are much smaller than 2.4 inch assumed in calculating the CALTRANS values. For obvious reasons, the CALTRANS values for 1 inch abutment deformation are significantly higher compared to values during strong shaking phase of the earthquake.

Since the stiffness computed by the ASSHTO-83/ATC-6 procedure is an initial estimate, it is larger than the values during the earthquake; it is expected that the final value obtained by the iterative procedure would be closer to the values during the earthquake. The stiffness determined by Gates and Smith is significantly higher because this value is determined for lower deformation levels (ambient vibration). Since Romstad and Maroney suggested that the abutment is rigid (infinitely stiff) in this direction, their value is not included.

Results for the transverse stiffness show that the east abutment in general remained much stiffer during the earthquake compared to the CALTRANS values for both deformation levels -- 1 inch and 2.4 inch -- and ASSHTO-83/ATC-6 value (Figure 7b). This difference can be explained

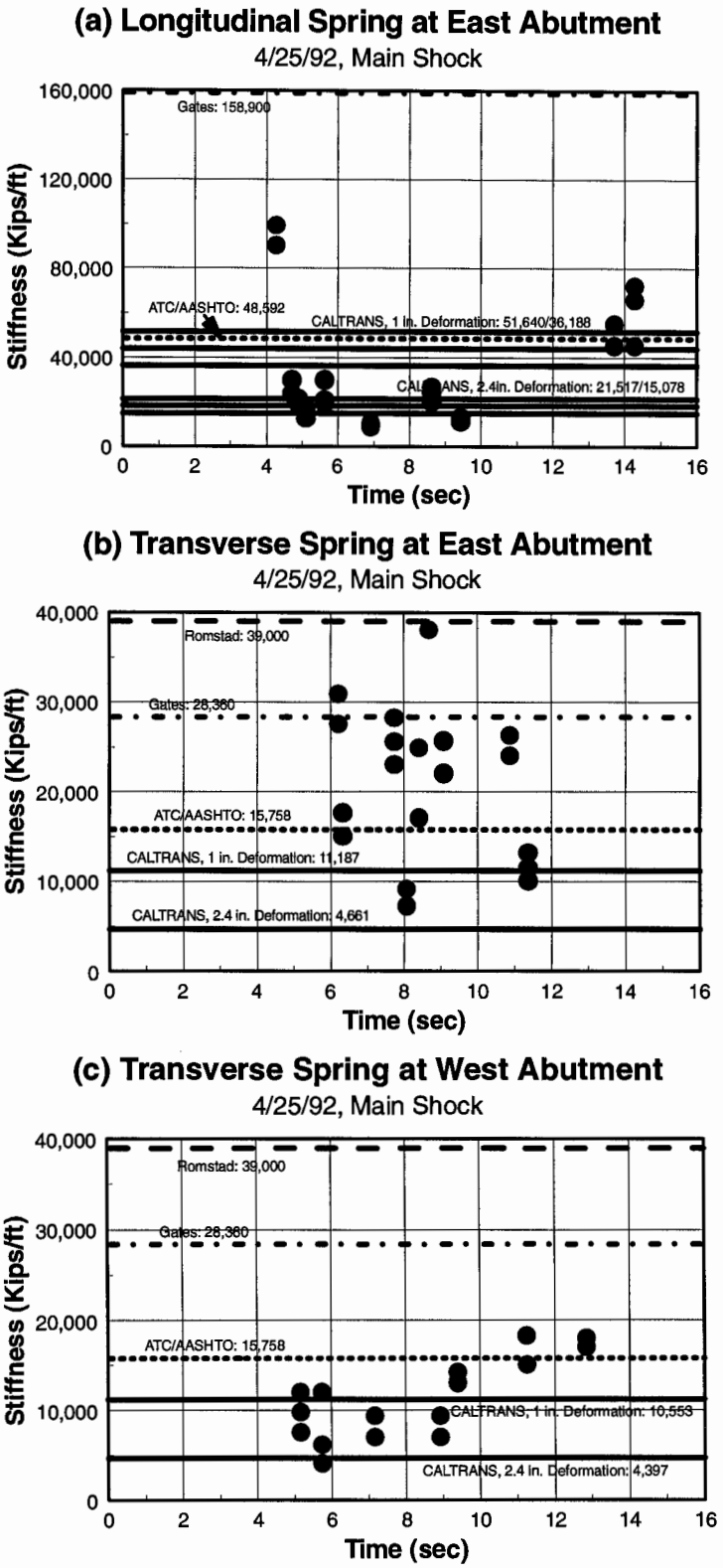


Figure 7. Comparison of abutment stiffness values determined from recorded motions with the values computed using the current procedures

Table 2. Abutment stiffness from CALTRANS procedures

| Direction | Stiffness (kips/ft) | Assumptions |
|---|---|---|
| Longitudinal | 43,960 | $EQ_L = R_{SOIL} + V_{DIAPHRAGM}$, Deformation ≤ 1 inch. |
| | 36,188 | $EQ_L = R_{SOIL} + R_{PILES,\ ONE\ ABUT.}$, Deformation ≤ 1 inch. |
| | 51,640 | $EQ_L = R_{SOIL} + V_{DIAPHRAGM} + R_{PILES,\ ONE\ ABUT.}$, Deformation ≤ 1 inch. |
| | 43,868 | $EQ_L = R_{SOIL} + R_{PILES,\ BOTH\ ABUT.}$, Deformation ≤ 1 inch. |
| | 18,317 | $EQ_L = R_{SOIL} + V_{DIAPHRAGM}$, Deformation = 2.4 inch. |
| | 15,078 | $EQ_L = R_{SOIL} + R_{PILES,\ ONE\ ABUT.}$, Deformation = 2.4 inch. |
| | 21,517 | $EQ_L = R_{SOIL} + V_{DIAPHRAGM} + R_{PILES,\ ONE\ ABUT.}$, Deformation = 2.4 inch. |
| | 18,278 | $EQ_L = R_{SOIL} + R_{PILES,\ BOTH\ ABUT.}$, Deformation = 2.4 inch. |
| Transverse East | 11,187 | $EQ_T = V_{WW} + R_{PILES}$, Deformation ≤ 1 inch. |
| | 4,661 | $EQ_T = V_{WW} + R_{PILES}$, Deformation = 2.4 inch. |
| Transverse West | 10,553 | $EQ_T = V_{WW} + 0.75 R_{PILES}$, Deformation ≤ 1 inch. |
| | 4,397 | $EQ_T = V_{WW} + 0.75 R_{PILES}$, Deformation = 2.4 inch. |

by noting that the earthquake-induced deformations are significantly smaller compared to those assumed in calculating the code values. The stiffness tends to be close to the value determined by Gates and Smith from low-level vibration but smaller than the value suggested by Romstad and Maroney based on smaller earthquakes. For the west abutment, the CALTRANS values for the two deformation levels form the upper and lower bounds of its stiffness during strong shaking phase (Figure 7c). Since the deformations of this abutment during the strong shaking phase of the earthquake are in the range of 1 to 2.4 inch, it appears that the CALTRANS procedure leads to good estimate of the abutment stiffness. During the decaying phase, however, the stiffness values may be higher than both the CALTRANS values because of much smaller deformation of the abutment. The ASSHTO-83/ATC-6 value tends to be higher than the earthquake value. Since the values determined by Gates and Smith (1982) and Romstad and Maroney (1990) are both for smaller deformation levels, these values tend to be much higher than the values during the earthquake.

## CONCLUSIONS

In this investigation, abutment stiffnesses are determined directly from the recorded earthquake motions of the US 101/ Painter Street Overpass using a simple equilibrium-based approach without finite-element modeling of the structure or the abutment-soil systems. The values determined in this manner include the effects of soil-structure interaction and nonlinear behavior of the soil. Using these values, this investigation on variation of the abutment stiffness with its deformation during the earthquake and torsional motions of the road deck of this structure has led to the following conclusions. The abutment stiffness may be significantly

different during different phases of the shaking and depends on its deformation: larger is the deformation, smaller is the stiffness. The road deck of this structure experienced significant torsional motions in part because of eccentricity created by different transverse stiffnesses at the two abutments. Evaluation of the current modeling procedures for abutment stiffness indicates that the CALTRANS procedure leads to good estimate of the abutment stiffness provided the deformation assumed in computing the stiffness is close to actual deformation during the earthquake, and ASSHTO-83 and ATC-6 result in stiffer initial estimate of abutment stiffness.

## ACKNOWLEDGMENTS

This investigation is supported by the Strong Motion Instrumentation Program, California Division of Mines and Geology. The authors are grateful for this support. The authors are also grateful to Bob Darragh, Moh-Jiann Huang, Praveen Malhotra, and Anthony Shakal for providing structural plans and earthquake records and Pat Hipley for assisting with implementation of the CALTRANS procedure for computing abutment stiffness. Any opinion, discussion, and conclusions are those of the authors and do not necessarily reflect the views of the sponsor.

## REFERENCES

AASHTO-83. (1988). *Guide Specifications for Seismic Design of Highway Bridges,* American Association of State Highway and Transportation Officials, Washington, D.C.

ATC-6. (1981). *Seismic Design Guidelines for Highway Bridges*, Applied Technology Council, Berkeley, CA, October.

CALTRANS. (1990). *Bridge Design Specifications,* California Department of Transportation, Sacramento, CA, June.

CALTRANS. (1989). *Bridge Design Aids 14-1*, California Department of Transportation, Sacramento, CA, October.

CALTRANS. (1988). *Memo to Designers 5-1,* California Department of Transportation, Division of Structures, Sacramento, CA, September.

Gates, J. H. and Smith, M. J. (1982). *Verification of Dynamic Modeling Method by Prototype Excitation,* FHWA/CA/SD-82/07, California Department of Transportation, Office of Structures Design, Sacramento, California, November.

Goel, R. K. and Chopra, A. K. (1990). *Inelastic Seismic Response of One-Story, Asymmetric-Plan Systems,* Report No. UCB/EERC-90/14, Earthquake Engineering Research Center, University of California, Berkeley, California, October.

Jennings, P. C. and Wood, J. H. (1971). "Earthquake Damage to Freeway Structures," *Engineering Features of the San Fernando Earthquake*, Report No. EERL 71-02, Earthquake Engineering Research Laboratory, California Institute of Technology, Pasadena, CA.

Romstad, K. and Maroney, B. (1990). *Interpretation of Painter Street Overcrossing Records to Define Input Motions to the Bridge Superstructure*, Final Report to Department of Conservation, Division of Mines and Geology, Office of Strong Motion Studies, October.

Shakal, A. F., et al. (1992). *CSMIP Strong-Motion Records from the Petrolia, California Earthquakes of April 25-26, 1992*, Report No. OSMS 92-05, California Department of Conservation, Division of Mines and Geology, Office of Strong Motion Studies, May 20.

Sweet, J. and Morrill, K. B. (1993). "Nonlinear Soil-Structure Interaction Simulation of the Painter Street Overcrossing," *Proceedings of the Second Annual Caltrans Seismic research Workshop*, Sacramento, CA, March 16-18.

Tsai, N. C. et al. (1993). *Application of CALTRANS' Current Seismic Evaluation Procedures to Selected Short Bridge Overcrossing Structures,* Technical Report, Dames and Moore, Oakland, CA, June.

# UTILIZATION OF CSMIP STRONG-MOTION RECORDS TO RATIONALIZE HORIZONTAL FORCE FACTORS ($C_p$)

R.M. Czarnecki[1], D.N. Rentzis[1], M.A. Bello[2], D.M. Bergman[3]

## ABSTRACT

The California Strong Motion Instrumentation Program (CSMIP) of the Department of Mines and Geology has obtained and processed a number of significant building response records from its network of seismographs in California. This study was conducted using strong motion data to investigate the performance of nonstructural elements and building components under actual earthquake loadings and to improve the seismic provisions of the building codes. The study includes the analysis of building response records obtained primarily from the Loma Prieta earthquake of 1989.

## INTRODUCTION

The seismic design of elements of structures and nonstructural components supported by structures is governed by the Uniform Building Code (UBC) and by the California Building Code, Title 24, Part 2 (CBC) for public school and hospital construction. The lateral design force, $F_p$, is determined by the product of Seismic Zone (Z), Importance Factor (I), the Horizontal Force Factor ($C_p$) and the weight ($W_p$). The current seismic demand values ($C_p$) are presented in Table No. 23-P of the 1991 edition of the Uniform Building Code (UBC-91).

In the current code formulation, the value of $C_p$ is intended to account for several phenomena including:

- The response characteristics of equipment and components
- The frequency content of the input ground motion (for ground mounted items) or building motion (for items located above ground)
- The ductility and redundancy of equipment and components.

By relying on a simple factor ($C_p$) to account for these complex phenomena, the code approach makes broad assumptions on the behavior and response of elements and components. Furthermore, the code assigns a single value of $C_p = 0.75$ for seismic design of a wide variety of different items that may have significantly different response characteristics.

1 URS/John A. Blume & Associates, Engineers, San Francisco, CA
2 Marguerite A. Bello, Structural Engineer, Oakland, CA
3 Consulting Civil Engineer, San Francisco, CA

The $C_p$ values in Table 23-P have been selected based upon the judgement of experienced engineers. While there is no evidence to suggest that the current code approach is inadequate, a comprehensive technical rationale for this approach is lacking. Thus, the current code approach may be overly conservative in some cases and not conservative in others.

The purpose of this study is to examine the current code approach in light of actual strong motion data (building response and ground response) collected by CSMIP and the U.S. Geological Survey (USGS) during the Loma Prieta and Landers California earthquakes. These recorded motions will be used to determine the actual seismic demand on nonstructural components and equipment, both ground mounted and building mounted. The actual seismic demand determined in this manner will then be compared with the applicable code required demand. The study will identify variables which have an influence on the actual seismic demand and establish trends with these variables.

The study will also address the capacity, redundancy and ductility of nonstructural components and equipment. Since these are broad topics which require extensive work beyond the scope of this study, the objective here will be to quantify these phenomena to the extent possible using available data and information from post-earthquake damage reports made available to CSMIP.

The most important objective of the study is to combine experience data on seismic demand and capacity in order to propose an improved, rational approach for the seismic design of nonstructural components and equipment. Specifically, the objectives are to develop a new code format and to establish design parameters on a preliminary basis. These parameters would be subject to refinement and revision in the future as more strong motion data and other information becomes available on the seismic demand and capacity of nonstructural components and elements.

## PROPOSED DESIGN FORMULATION

In general, a rational approach for the seismic design of nonstructural elements and building components may be expressed as follows:

$$F_p = \frac{S_a \cdot W_p}{R_c}$$

where

$F_p$ = the total lateral force requirement

$S_a$ = the first mode spectral acceleration of the item under consideration obtained from the design response spectrum

$W_p$ = the weight of the item under consideration

$R_c$ = a performance factor which reduces the actual seismic demand to a level compatible with elastic design methods.

In this general formulation, $S_a$ would be obtained from a ground response spectrum for ground mounted items and from a floor response spectrum for floor mounted items. Within the context of UBC and CBC design methodology, the disadvantage of this general formulation is that neither ground response nor floor response spectra are typically available as part of the code design process. However, this problem can be overcome by defining a new seismic demand coefficient $C_p'$ as follows:

$$S_a = PGA \cdot C_p'$$

where

PGA = the site peak ground acceleration (represented by the product $Z \cdot I$ for code design)

$C_p'$ = seismic demand coefficient.

As suggested in the paper, values of $C_p'$ can be obtained from interpretation of strong motion data. Given these definitions, the proposed formulation for design of nonstructural components and elements is as follows:

$$F_p = \frac{PGA \cdot C_p' \cdot W_p}{R_c}$$

or

$$F_p = \frac{Z \cdot I \cdot C_p' \cdot W_p}{R_c}$$

The primary purpose of this paper is to use strong motion data to determine typical values of $C_p'$ and $R_c$.

## DESCRIPTION OF STRONG MOTION DATA

The strong motion data used to accomplish the goals of this study consists primarily of ground response and building response records obtained and processed by CSMIP during the Loma Prieta earthquake of October 17, 1989 [1,2]. Two additional sets of response records obtained by CSMIP during the Landers earthquake of June 28, 1992 and one set of building response records obtained by USGS during the Loma Prieta earthquake were also used. A summary of this data is provided in Table 1.

The data used in the study consisted of corrected time histories and corresponding response spectra for 0%, 2%, 5%, 10%, and 20% of critical damping. In general, the records from each recording station includes 3 orthogonal components of ground motion at the basement or

first floor level and horizontal components of building motion at intermediate floor levels above grade.

## DETERMINING VALUES OF $C_p'$ FROM STRONG MOTION DATA

The floor and ground response spectra described in the previous section may be used to determine values of $C_p'$. This can be accomplished recalling the previously defined relationship between $S_a$ and $C_p'$ and expressing these values as functions of equipment period, t:

$$S_a(t) = PGA \cdot C_p'(t)$$

or $$C_p'(t) = \frac{S_a(t)}{PGA}$$

Thus, $C_p'(t)$ may be thought of as a nondimensional spectral shape or transfer function which, when multiplied by the PGA, gives the spectral ordinate as a function of period, $S_a(t)$.

In determining $C_p'(t)$ from strong motion data, it is important to consider 4 different circumstances: ground mounted items, floor mounted items, rigid items, and flexible items.

For ground mounted items, $C_p'(t)$ is appropriately determined using ground response spectra (GRS). In this case, $C_p'(t)$ strictly represents the dynamic amplification characteristics inherent in ground motion and depends primarily on earthquake magnitude, distance from fault, soil type, and period and damping of equipment.

For floor mounted items, $C_p'(t)$ is obtained from floor response spectra (FRS). In addition to the factors mentioned in the previous paragraph, $C_p'(t)$ for floor mounted items depend on the dynamic properties of the building in which the items are mounted, the location of the item within the building, and the period and damping of the item.

For design purposes, it is convenient to further simplify the formulation $C_p'(t)$ to eliminate the period dependence, the fundamental mode period of the nonstructural element or component under consideration. In general, designers will be unable to precisely define the periods of such items, so it makes little sense to develop a design procedure that is period dependent. A more simplistic approach is to define $C_p'$ separately for rigid equipment and flexible equipment.

$C_p'$ values for rigid equipment are determined from recorded response spectra by taking the maximum value of $C_p'(t)$ for $t \leq 0.06$ second.

To determine $C_p'$ values for flexible equipment or component items mounted above grade within buildings it is necessary to consider the period of the item under consideration and the fundamental mode period of the building within which the strong motion data was recorded. The maximum values of $C_p'$ would typically but not always occur when these periods are close or equal to each other. For the purpose of establishing simple and conservative design rules it

is necessary to make an assumption about the relationship between the periods of equipment or components and the periods of the buildings within which these items are located. In this study it has been assumed all items that are considered "flexible" (i.e., nonrigid) have periods that correspond to the period range of the fundamental mode of the building. Specifically, it has been assumed that the period range of flexible equipment or components will be in the range of 0.6T to 1.4T where T is the fundamental mode period of the building. Using this period range is consistent with the 1991 NEHRP provisions [3].

To determine a single value for $C_p'$ for flexible items, the values of the function $C_p'(t)$ was examined in the range $0.6T \leq t \leq 1.4T$. Within this range, the mean value and standard deviation of the function $C_p'(t)$ were identified, and the single value of $C_p'$ were calculated as follows:

$$C_p' = \text{Mean } C_p'(t) + \text{One Standard Deviation of } C_p'(t).$$

$C_p'$ computed as shown above was used in this study for flexible equipment located at roof level in buildings. For simplification of the $C_p'$ derivation, a damping value of 5% of critical was used because it is approximately equal to the average of 2%, 5% and 10% which represents the dynamic characteristics of the majority of equipment and nonstructural components.

In order to determine the $C_p'$ factor from measured records, the response period of the building within which the records were obtained must be ascertained. These periods were determined primarily from the 1992 CSMIP sponsored study where Cole, et al. [4] compared the building periods measured from earthquake recorded response to the UBC period formulation for the different types of buildings. Most of the buildings included in this study were also in Cole's work. Where the periods were not available from Cole or where other than the fundamental mode produced the largest $C_p'$ value, the building periods were estimated for this study from CSMIP recordings. As part of this study it was acknowledged that for the long period buildings, the peak of the spectral value (and maximum $C_p'$) may occur in higher modes, depending on the ground motion characteristics.

## DETERMINING VALUES OF $R_c$ FROM STRONG MOTION DATA

As previously defined, $R_c$ for equipment and component items is a performance factor which reduces the actual earthquake demand to a level that is compatible with elastic design methods. $R_c$ is similar to $R_w$ used in the UBC formulation for seismic base shear in that $R_c$ is intended to reflect the ability of equipment and components to adequately perform at levels of seismic demand that exceed their elastic design capacity. More specifically, $R_c$ may be considered as the ratio between the ultimate or failure load capacity to the elastic design capacity as follows:

$$R_c = \frac{\text{Failure Load Capacity}}{\text{Elastic Design Capacity.}}$$

One way to establish $R_c$ is by testing and analysis of equipment and components to establish the numerator and denominator of this ratio. If the code approach suggested in this paper is

adopted, the manufacturers and suppliers of these items will eventually be encouraged to provide the necessary data for their products to establish these values. Until this is accomplished, it is possible to obtain a first estimate of $R_c$ by considering the performance of equipment and components in buildings that were instrumented and subjected to strong earthquake motion (i.e., the buildings listed in Table 1).

If the post-earthquake investigation of such items revealed that an element or component was not damaged due to the strong motion recorded during the earthquake, one can conclude that the failure capacity equalled or exceeded recorded demand. If the post-earthquake investigation revealed that an element or component was damaged, it would indicate that the failure capacity was less than the recorded demand. Under this condition, the actual failure capacity must be determined based on the strength and dynamic properties of the item in question.

Although the damage from the Loma Prieta earthquake was extensive at many locations, damage to the nonstructural elements in those structures that were instrumented by the CSMIP strong motion instruments did not appear to be severe. From the post-earthquake investigation reports that were made available, the nonstructural components and equipment in the buildings that were instrumented by the strong motion recorders fared quite well and the damage to components and elements was quite limited. If it is assumed that the equipment was undamaged, this leads to the conclusion that the failure capacity of the equipment was equal to or greater than the earthquake demand. For the purpose of this study, it was assumed that the nonstructural items in the instrumented buildings were on the verge of failure during the earthquake motion for which the building response was recorded. This implies that the actual demand experienced by these items during the earthquake was equal to the failure capacity of these items. This is recognized as a potentially conservative assumption. If the actual failure capacity is much greater than the demand experienced during the recorded earthquake, this will lead to an underestimate of $R_c$.

To complete the determination of $R_c$ it is necessary to quantify the elastic design capacity of the nonstructural items in the instrumented buildings. For this study it was assumed that the elastic design capacity was equal to the code design requirement (i.e., $ZIC_p$) that was applicable at the time the item was designed or installed. If one accepts the premise that the code is a minimum requirement, this assumption is potentially unconservative to the extent that the actual design capacity may have exceeded the code required strength.

Given these assumptions, the formulation of $R_c$ from strong motion data may be expressed as follows:

$$R_c = \frac{\text{Failure Load Capacity}}{\text{Elastic Design Capacity}} = \frac{\text{Recorded Earthquake Demand}}{\text{Code Design Requirement}} = \frac{PGA \cdot C_p'}{Z \cdot I \cdot C_p}$$

where PGA and $C_p'$ are as previously defined and are specific to each instrumented building record.

It is recognized that the formulation of $R_c$ in this manner involves rather board assumptions, and there is no basis to believe that for any given component the conservative and unconser-

vative aspects of the formulation will be self-canceling. However, it is reasonable to expect that the central trend of $R_c$ can be established by examining and interpreting $R_c$ as determined above from a large body of data. Nevertheless, $R_c$ as indicated above was calculated and tabulated as part of this study.

## INTERPRETATION OF DATA

Based on the above formulations, the $C_p'$ and $R_c$ factors were obtained using strong motion data from the instrumented buildings (Table 1) and the respective seismic design coefficients (Table 2). For the purpose of comparison, the largest values of $C_p'$ and $R_c$ for rigid and flexible items determined for each building are listed in Table 3. The values thus derived were essentially all from the motions at the roof.

For rigid items, the value of $C_p'$ ranges from 1.72 to 4.63 with an average value of 2.90. It should be noted that these values approximately represent the amplification factor between the peak ground acceleration and the maximum floor (roof) acceleration. Both the range of values and the average is consistent with expectations and observations from previous earthquakes.

For flexible items, the value of $C_p'$ ranges from 5.28 to 23.56 with an average of 11.58. These values indicate the potential for large response amplification if the component period coincides with the building period. The largest value has resulted from a response of one of the higher modes of a long period building. This points to the need for considering the contribution of higher mode response in the design of components and elements.

A revealing comparison is the $C_p'$ ratio of flexible and rigid components which were observed from the analysis of these records. This ratio can be compared with the multiplier of 2 or 4 currently in the CBC for flexible items. Although the use of the factors is not based solely on the amplification alone, it is of value to look at the amplification that takes place in the buildings. The result is shown in Column 8 of Table 3. The ratios range from a low of 2.56 (Station 23) to a high of 6.32 (Station No. 17) with an average value of 3.90. A closer examination indicates that those stations with high ratios appeared to result on taller (long period) buildings where the largest $C_p'$ for the building resulted from the response of higher modes, again pointing to the need to consider higher modes.

The $R_c$ values in Table 3 are obtained by multiplying the $C_p'$ by the PGA and dividing it by $ZIC_p$. For an initial comparison, the seismic design coefficients were all taken as equal with $ZC_p = 0.2$ and $I = 1$. For a comparison of the performance factor, the $R_c$ for the rigid items ranges from a low of 0.69 to a high of 6.01 with an average value of 1.89. For the flexible items, $R_c$ ranges from 2.05 to 18.75 with an average value of 7.10. These values may be somewhat misleading because not all of the components and elements were designed for the same seismic coefficients (i.e., $ZIC_p = 0.2$) and because the motion level for most of the buildings was not large enough to test the limit of the $R_c$ value.

Upon closer examination of the data, only those buildings where the PGA was greater than 0.2g and the PFA was greater than 0.5g were studied (Table 4). For the rigid item condition,

the $R_c$ values range from 2.0 and 6.01 with an average of 3.21. For the flexible condition, $R_c$ ranges from 6.15 to 18.75 with an average of 10.87. These values were calculated based on the seismic design coefficient, $ZIC_p = 0.2$.

To further refine these values, the seismic design coefficient used in the original design or for upgrade of a respective site was considered. The numerical value of the specific design or upgrade was available for some, others were more qualitative in nature. Therefore, the performance factor is discussed more in quantitative terms.

- Station 1: $R_c = 6.01$ and 18.75 for rigid and flexible items, respectively. The owner apparently performed a major upgrade of the facility several years before the Loma Prieta earthquake to comply with seismic requirements which were much higher than that required by the code, even for an essential facility. Based on discussions with the facility representative and assuming that the seismic design coefficient might have been greater than 1.0g, the revised $R_c$ values would be 1.20 and 3.75 for rigid and flexible items, respectively. There was no apparent damage at this location. Equipment racks displaced more than a foot, but the function of the facility was not disrupted.

- Station 33: $R_c = 4.77$ and 15.90 for rigid and flexible items, respectively. Here also, the owner upgraded the equipment support in this facility before the Loma Prieta earthquake. The facility was upgraded for a seismic coefficient ($ZIC_p$) of 0.5g. The $R_c$ values based on the actual design would be 1.91 and 6.36 for rigid and flexible, respectively. There were reports of limited minor damage at this facility (e.g., an expansion anchor failure due to an inadequate edge distance), but this was not in the building that was instrumented by the CSMIP.

- Station 14: $R_c = 3.18$ and 14.05 for rigid and flexible items, respectively. The building was designed and built after the San Fernando earthquake of 1971, but prior to the incorporation of new provisions for essential facilities into the code. However, special consideration was apparently taken into account in the form of additional bracing for equipment. Consequently, an importance factor of 1.5 was assumed. This results in the revised seismic design coefficient, $ZIC_p = 0.3$g, which reduces the $R_c$ factors to 2.12 and 9.37 for rigid and flexible items, respectively. The reported damage included a fan unit pipe support, partition cracking, and a fallen suspended ceiling.

- Stations 2, 4 and 18: The buildings and their contents for these two stations were built a using seismic design coefficient ($ZC_p$) = 0.3; I is assumed to be 1.0 since the structures are not classified as essential facilities.

Taking these increased seismic design coefficients into consideration, the threshold level of performance factors were adjusted as shown on Table 4. These values range from 1.20 to 3.02 with an average value of 2.06 for rigid items and 3.75 to 9.85 with an average of 6.86 for flexible items.

The fourth column of Table 4 presents an amplification factor entitled Flex/Rigid. This amplification ratio ranges from 2.56 to 4.42 with mean value of 3.37. This amplification can

be interpreted as a factor which relates the seismic demand for flexible items to the demand for rigid items mounted at the roof level. This amplification factor is somewhat comparable to $C_p$ found in the codes for flexible versus rigid items. In the UBC this amplification is 2 whereas in the CBC the amplification is 4. The range of the data in Table 4 approximately covers the range of requirements between the UBC and CBC.

The factors derived in this study ($C_p'$ and $R_c$ for rigid and flexible items) will need considerable refinement and further research before they can be adopted into a new code requirement for design of components and elements. Nevertheless, it is of value to examine the proposed code format in light of the factors $C_p'$ and $R_c$ obtained by this study and to compare the resulting design requirement to current Code. For this purpose, the average values of $C_p'$ and $R_c$ obtained in this study are used:

| | Flexible Items | Rigid Items |
|---|---|---|
| $C_p'$ | 11.58 | 2.90 |
| $R_c$ | 6.78 | 2.06 |
| $C_p'/R_c$ | $1.71 \approx 1.75$ | $1.41 \approx 1.5$ |

A comparison of the new proposed code format with UBC and CBC for items located above grade in a structure is presented below.

Proposed formulation:

Rigid Items: $F_p = \frac{ZIC_p'W_p}{R_c} \approx 1.5ZIW_p$

Flexible Items: $F_p = \frac{ZIC_p'W_p}{R_c} \approx 1.75ZIW_p$

Current Code Formulation:

Rigid Items: $F_p = ZIC_pW_p = 0.75ZIW_p$

Flexible Items: $F_p = 2ZIC_pW_p = 1.5ZIW_p$
(UBC)

Flexible Items: $F_p = 2ZIC_pW_p = 1.5ZIW_p$
(CBC - resonance prevented)

Flexible Items: $F_p = 4ZIC_pW_p = 3.0ZIW_p$
(CBC - resonance possible)

For rigid items, $C_p'/R_c$ is 1.5, twice the applicable coefficient of 0.75 found in both codes. For flexible items, $C_p'/R_c$ is comparable to the requirements of the UBC ($2C_p = 1.50 \leq 2.0$) and CBC (for flexible but restrained items). However, $C_p'/R_c = 2.0$ is less than the CBC

requirements for flexible, unrestrained items ($4C_p \leq 3.0$) In this case, one may interpret the code to underestimate the seismic demand on flexible items install in public schools or hospitals.

However, $R_c$ was based on the assumption that all the equipment anchorage in this study had reached the threshold of damage. Consequently, $R_c$ was a lower bound. The method proposed herein is rational because it utilizes earthquake experience data to formulate an equivalent elastic seismic design coefficient, $C_p'/R_c$. However, because the ratio $C_p'/R_c$ is highly sensitive to uncertainties in $R_c$, and due to the lack of abundant damage data, the result is considered inconclusive. Also, the formulation based primarily on the Loma Prieta data does not provide definitive conclusion to justify change of the current code formulation. The formulation for flexible items with several variables that influence the outcome requires closer examination. Based on the above results, it is recommended to view the conclusions herein as preliminary and the need for further research as imperative.

## SUPPLEMENTAL PARAMETRIC STUDIES

Several other parameters were examined as part of this study in order to determine factors which influence $C_p$. The results of the studies are summarized below:

AMPLIFICATION AT VARIOUS FLOOR LEVELS: In addition to the amplification observed at the roof level in conjunction with the determination of $C_p'$ and $R_c$, the amplification that takes place at other floors was studied. The result for rigid items is shown in Table 5A. There is a trend for an increase in amplification with height. The result is similar to the study by Drake and Gillengerten [5] performed on a larger sample of buildings and earthquakes, including some of the buildings considered in this study. A result from the study of flexible items is shown in Table 5B. A similar but larger amplification at essentially all levels was observed.

INFLUENCE OF STRUCTURE TYPE: Another set of parameters investigated include the characteristics of the buildings such as building height, lateral force resisting system, and construction materials. The amplification factors and the performance factors reported herein were correlated with the lateral force resisting system type and height of the buildings, as discussed below.

The buildings were grouped into two structural system types, namely moment resisting frames and shearwall structures. There were ten steel frame and one concrete frame buildings in the data set. For the shearwall buildings, there were twelve without frames and eight with frames. All of the buildings were evaluated in terms of the lateral force resisting system and building height. The results from this study showed very little correlation between the performance factors and the building classification.

INFLUENCE OF SOIL In addition to the soils information provided by CSMIP in association with its strong motion earthquake data, additional soils information was obtained by Geotechnical Consultants, Inc. [6]. The parameters studied were site geology, foundation type and

soil profile. An attempt to correlate amplification and performance values with these foundation and soil data was not successful. Additional data from other earthquakes and additional data from free field station near the buildings may produce a better correlation.

## CONCLUSIONS AND RECOMMENDATIONS

Based on the analyses of the structural response records from the Loma Prieta earthquake provided by CSMIP to rationalize horizontal force factors, the following conclusions and recommendations are made:

(1) The performance factors for the rigidly mounted elements and equipment appear to range between 2 and 4. For the flexible items, the factors range between from 6 to 12.

(2) The level of motion from the Loma Prieta earthquake for the buildings studied does not appear to be large enough to adequately test the appropriateness of the reported performance factors in the proposed code formulation. It would be of great value to apply this methodology to the Northridge earthquake experience records when the data becomes available. (Just prior to the submittal of this paper, strong motion records from the Sylmar hospital was made available. They are currently being studied for presentation at the SMIP94 seminar.)

(3) The amplification factors increase with building height. The amplification, using all of the data from this study, ranged from 1.17 to 4.63 with an average of 2.70 for the rigid condition and from 1.36 to 7.51 with an average of 3.94 for the flexible condition.

(4) The ratio of $C_p'/R_c$ for rigid items was found to be twice the applicable $C_p$ found in the codes (1.5 versus 0.75), implying that the code requirements for rigid items may be too low. On the other hand, $C_p'/R_c$ for flexible items was found to be less than 2, compared to flexible, unrestrained items with $C_p \leq 3.0$ for CBC. However, the lack of abundant damage data suggests that additional data is necessary to reach a more definitive conclusion.

(5) The correlation was poor between the performance factors and the structure type and local geology.

## ACKNOWLEDGEMENTS

The principle funding for this study was provided by the Office of Statewide Health Planning and Development and administered by the California Strong Motion Instrumentation Program, California Department of Conservation, Division of Mines and Geology, Office of Strong Motion Studies. Additional funding was provided by the management of URS/John A. Blume & Associates, Engineers. These sponsors are gratefully acknowledged. The authors wish to thank Moh Huang, Anthony Shakal and their staff at CSMIP for their assistance in collecting and providing the strong motion records and the available walk-down reports used herein. The

authors also wish to thank the review committee members; Chris Poland, Don Jephcott, Jack Meehan and Moh Huang, for their suggestions and guidance during the course of this study.

## REFERENCES

1 *CSMIP Strong-Motion Records from the Santa Cruz Mountains (Loma Prieta) Earthquake of 17 October 1989*, California Department of Conservation, Division of Mines and Geology, Office of strong Motion Studies, Report OSMS 89-06.

2 Data Set: LOMA PRIETA 89-IL, -L: *The Processed Strong-Motion Data from 30 Instrumented Buildings from the 1989 Loma Prieta Earthquake*, Report OSMS 91-07.

3 Federal Emergency Management Agency (FEMA), *NEHRP Recommended Provisions for the Development of Seismic Regulations for New Buildings*, FEMA 222, 1992.

4 Cole, E.E., et al, Analysis of Recorded Building Data to Verify or Improve 1991 Uniform Building Code (UBC) Period of Vibration Formulas, Seminar on Seismological and Engineering Implications of Recent Strong-Motion Data, Proceedings of SMIP92.

5 Drake, R.M. and J.D. Gillengerten, Examination of CDMG Ground Motion Data in Support of the 1994 NEHRP Provisions, Preprint Copy, October 12, 1993.

6 Letter Report from Geotechnical Consultants, Inc. to URS Consultants, Inc. on the subject: The Use of CSMIP Strong-Motion Records to Rationalize Horizontal Force Factors ($C_p$).

## TABLE 1 - STRONG MOTION STATION INFORMATION
(CSMIP Loma Prieta Data, Unless Otherwise Noted)

| Sta. No. | Building Name | Stories Above/Below | Structure Type | Distance (km) | Peak Horizontal Acceleration (g) | |
|---|---|---|---|---|---|---|
| | | | | | Ground | Bldg |
| 1 | Watsonville Commercial | 4/0 | RC-SW | 18 | 0.36 | 1.20 |
| 2 | Hollister Warehouse | 1/0 | Tilt-Up | 48 | 0.36 | 0.50 |
| 3 | Gilroy Commercial | 2/0 | URM-BW | 28 | 0.29 | 0.60 |
| 4 | San Jose Office | 3/0 | Stl-MRF | 21 | 0.20 | 0.58 |
| 5 | Saratoga Gymnasium | 1/0 | RC-SW | 27 | 0.35 | 0.59 |
| 6 | San Jose Residential | 10/0 | RC-SW | 33 | 0.11 | 0.37 |
| 7 | San Jose Commercial | 10/0 | RC-SW+MF | 33 | 0.10 | 0.33 |
| 8 | San Jose Govt Office | 13/0 | Stl-MRF | 35 | 0.10 | 0.33 |
| 9 | Palo Alto Office | 2/0 | RM-SW | 50 | 0.21 | 0.40 |
| 10 | Redwood City Office | 3/0 | RC-SW+MF | 57 | 0.05 | 0.18 |
| 11 | Belmont Office | 2/1 | RC-SW | 65 | 0.11 | 0.19 |
| 12 | San Bruno Office | 9/0 | RC-SW | 81 | 0.11 | 0.32 |
| 13 | San Bruno Office | 6/0 | RC-MRF | 81 | 0.14 | 0.38 |
| 14 | So. San Francisco Hospital | 4/0 | Stl-MRF | 85 | 0.16 | 0.64 |
| 15 | San Francisco School | 6/0 | RC-SW+MF | 95 | 0.09 | 0.28 |
| 16 | San Francisco Commercial | 18/1 | Stl-MRF | 95 | 0.16 | 0.28 |
| 17 | San Francisco Office | 47/2 | Stl-BF | 96 | 0.16 | 0.46 |
| 18 | Milpitas Industrial | 2/0 | Tilt-up | 43 | 0.14 | 0.58 |
| 19 | Hayward Office | 6/1 | RC-SW+MF | 69 | 0.11 | 0.33 |
| 20 | Hayward Office | 13/0 | Stl-MRF | 70 | 0.08 | 0.24 |
| 21 | Hayward School | 4/0 | RC-SW | 70 | 0.05 | 0.13 |
| 22 | Oakland Residential | 24/0 | RC-SW+MF | 91 | 0.18 | 0.37 |
| 23 | Oakland Office | 2/0 | RM-SW+MF | 92 | 0.25 | 0.52 |
| 24 | Piedmont School | 3/0 | RC-SW | 93 | 0.07 | 0.15 |
| 25 | Berkeley Hospital | 2/1 | StL-BF | 97 | 0.12 | 0.28 |
| 26 | Richmond Govt Office | 3/1 | RC-SW+MF | 108 | 0.11 | 0.23 |
| 27 | Richmond Office | 3/0 | Stl-MRF | 112 | 0.11 | 0.31 |
| 28 | Walnut Creek Commercial | 10/0 | RC-SW+MF | 98 | 0.10 | 0.22 |
| 29 | Pleasant Hill - Commercial | 3/0 | RC-SW | 102 | 0.12 | 0.18 |
| 30 | Concord - Residential | 8/0 | RM-SW | 105 | 0.06 | 0.23 |
| 31 | Palm Springs - Hospital* | 4/1 | Stl-MRF | 43 | 0.07 | 0.21 |
| 32 | San Bernardino - Hospital* | 5/0 | Stl-MRF | 82 | 0.08 | 0.32 |
| 33 | Palo Alto - Hospital** | 7/1 | RC-SW+MF | 47 | 0.36 | 1.10 |

*-Landers Earthquake, **-USGS station, RC-Reinforced Concrete, Stl-Steel, SW-Shear Wall, URM-Unreinforced Masonry, BW-Bearing Wall, MF-Moment Frame, MRF-Moment Resisting Frame

## TABLE 2 - SUMMARY OF SEISMIC DESIGN COEFFICIENTS

| SUMMARY OF Z, I and Cp FACTORS | | | | | | | Partitions, ext. walls above ground, Masonry/conc. fences, Storage racks,cabinets,book stacks Suspended ceilings, access floors, Tanks and vessels, Mech/elec equipment | | Cantilievered parapets, Ornamentations, appendages Chimneys, stacks, towers, tanks on legs, above roof Signs, billboards | |
|---|---|---|---|---|---|---|---|---|---|---|
| No. | Building | Stories | Building Type | Design Date | I | Z | C or Cp | ZC, ZCp or ZICp | C or Cp | ZC, ZCp or ZICp |
| 1 | Watsonville | 4 | Commercial | 1948 | | 4 | 0.05 | 0.2 | 0.25 | 1 |
| 2 | Hollister | 1 | Warehouse | 1979 | 1 | 1 | 0.3 | 0.3 | 0.8 | 0.8 |
| 3 | Gilroy | 2 | Commercial | 1916 | | 4 | 0.05 | 0.2 | 0.25 | 1 |
| 4 | San Jose | 3 | Office | 1983 | 1 | 1 | 0.3 | 0.3 | 0.8 | 0.8 |
| 5 | Saratoga | 1 | Gymnasium | 1971 | | 1 | 0.2 | 0.2 | 1 | 1 |
| 6 | San Jose | 10 | Residential | 1971 | | 1 | 0.2 | 0.2 | 1 | 1 |
| 7 | San Jose | 10 | Commercial | 1964 | | 1 | 0.2 | 0.2 | 1 | 1 |
| 8 | San Jose | 13 | Office | 1972 | | 1 | 0.2 | 0.2 | 1 | 1 |
| 9 | Palo Alto | 2 | Office | 1973 | | 1 | 0.2 | 0.2 | 1 | 1 |
| 10 | Redwood City | 3 | Office | 1967 | | 1 | 0.2 | 0.2 | 1 | 1 |
| 11 | Belmont | 2 | Office | 1973 | | 1 | 0.2 | 0.2 | 1 | 1 |
| 12 | San Bruno | 9 | Office | 1972 | | 1 | 0.2 | 0.2 | 1 | 1 |
| 13 | San Bruno | 6 | Office | 1977 | 1 | 1 | 0.3 | 0.3 | 0.8 | 0.8 |
| 14 | So. San Francisco | 4 | Hospital | 1972 | | 1 | 0.2 | 0.2 | 1 | 1 |
| 15 | San Francisco | 6 | School | 1968 | | 1 | 0.2 | 0.2 | 1 | 1 |
| 16 | San Francisco | 18 | Commercial | 1964 | | 1 | 0.2 | 0.2 | 1 | 1 |
| 17 | San Francisco | 47 | Office | 1978 | 1 | 1 | 0.3 | 0.3 | 0.8 | 0.8 |
| 18 | Milpitas | 2 | Industrial | 1984 | 1 | 1 | 0.3 | 0.3 | 0.8 | 0.8 |
| 19 | Hayward | 6 | Office | 1966 | | 1 | 0.2 | 0.2 | 1 | 1 |
| 20 | Hayward | 13 | Office | 1969 | | 1 | 0.2 | 0.2 | 1 | 1 |
| 21 | Hayward | 4 | School | 1961 | | 1 | 0.2 | 0.2 | 1 | 1 |
| 22 | Oakland | 24 | Residential | 1964 | | 1 | 0.2 | 0.2 | 1 | 1 |
| 23 | Oakland | 2 | Office | 1964 | | 1 | 0.2 | 0.2 | 1 | 1 |
| 24 | Piedmont | 3 | School | 1973 | | 1 | 0.2 | 0.2 | 1 | 1 |
| 25 | Berkeley | 2 | Hospital | 1964 | | 1 | 0.2 | 0.2 | 1 | 1 |
| 26 | Richmond | 3 | Office | 1948 | | 4 | 0.05 | 0.2 | 0.25 | 1 |
| 27 | Richmond | 3 | Office | 1984 | 1 | 1 | 0.3 | 0.3 | 0.8 | 0.8 |
| 28 | Walnut Creek | 10 | Commercial | 1970 | | 1 | 0.2 | 0.2 | 1 | 1 |
| 29 | Pleasant Hill | 3 | Commercial | 1972 | | 1 | 0.2 | 0.2 | 1 | 1 |
| 30 | Concord | 8 | Residential | 1974 | | 1 | 0.2 | 0.2 | 1 | 1 |
| 31 | Palm Springs | 4 | Hospital | 1967 | | 1 | 0.2 | 0.2 | 1 | 1 |
| 32 | San Bernardino | 5 | Hospital | 1986 | 1.5 | 1 | 0.3 | 0.45 | 0.8 | 1.2 |
| 33 | Palo Alto | 7 | Hospital (Bldg. E) | 1968 | | 1 | 0.2 | 0.2 | 1 | 1 |

TABLE 3 - AMPLIFICATION AND PERFORMANCE FACTORS

| Sta No. | Name | T (sec) | PGA | PFA | $C_p'$ (Rigid) | $C_p'$ (Flex) | Flex/ Rigid | $R_c$** (Rigid) | $R_c$** (Flex) |
|---|---|---|---|---|---|---|---|---|---|
| 1 | Watsonville | 0.35 | 0.36 | 1.20 | 3.34 | 10.43 | 3.12 | 6.01 | 18.75 |
| 2 | Hollister | 0.80 | 0.25 | 0.50 | 2.04 | 6.63 | 3.25 | 2.55 | 8.30 |
| 3 | Gilroy | 0.40 | 0.29 | 0.60 | 2.08 | 6.78 | 3.26 | 3.02 | 9.85 |
| 4 | San Jose | 0.69 | 0.18 | 0.55 | 3.09 | 11.88 | 3.84 | 2.78 | 10.70 |
| 5 | Saratoga | 0.18 | 0.24 | 0.46 | 1.93 | 5.47 | 2.83 | 2.32 | 6.55 |
| 6 | San Jose | 0.70 | 0.09 | 0.37 | 3.92 | 16.89 | 4.31 | 1.76 | 7.60 |
| 7 | San Jose | 0.8 | 0.10 | 0.33 | 3.28 | 14.81 | 4.52 | 1.64 | 7.40 |
| 8 | San Jose | 2.23 | 0.09 | 0.32 | 3.77 | 14.42 | 3.82 | 1.70 | 6.50 |
| 9 | Palo Alto | 0.34 | 0.21 | 0.40 | 1.90 | 5.88 | 3.09 | 2.00 | 6.15 |
| 10 | Redwood City | 0.17 | 0.05 | 0.18 | 3.56 | 14.89 | 4.18 | 0.89 | 3.70 |
| 11 | Belmont | 0.18 | 0.11 | 0.19 | 1.75 | 5.44 | 3.11 | 0.96 | 3.00 |
| 12 | San Bruno | 1.20 | 0.11 | 0.32 | 2.88 | 10.44 | 3.63 | 1.58 | 5.75 |
| 13 | San Bruno | 1.10 | 0.11 | 0.38 | 3.37 | 14.52 | 4.31 | 1.85 | 8.00 |
| 14 | S. San Francisco | 0.71 | 0.16 | 0.64 | 3.98 | 17.59 | 4.42 | 3.18 | 14.05 |
| 15 | San Francisco | 0.74 | 0.09 | 0.28 | 2.95 | 12.51 | 4.24 | 1.33 | 5.65 |
| 16 | San Francisco | 0.75 | 0.16 | 0.28 | 1.75 | 5.37 | 3.07 | 1.40 | 4.30 |
| 17 | San Francisco | 1.00* | 0.10 | 0.46 | 3.73 | 23.56 | 6.32 | 1.87 | 11.80 |
| 18 | Milpitas | 0.20 | 0.14 | 0.58 | 4.13 | 16.86 | 4.08 | 2.89 | 11.80 |
| 19 | Hayward | 0.67 | 0.11 | 0.33 | 3.34 | 10.68 | 3.20 | 1.84 | 5.85 |
| 20 | Hayward | 0.43* | 0.08 | 0.24 | 1.96 | 11.19 | 5.71 | 0.78 | 4.50 |
| 21 | Hayward | 0.22 | 0.05 | 0.13 | 2.57 | 12.38 | 4.82 | 0.64 | 3.10 |
| 22 | Oakland | 0.55* | 0.18 | 0.37 | 2.12 | 6.16 | 2.91 | 1.91 | 5.55 |
| 23 | Oakland | 0.50 | 0.25 | 0.52 | 2.06 | 5.28 | 2.56 | 2.58 | 6.60 |
| 24 | Piedmont | 0.18 | 0.07 | 0.15 | 2.06 | 5.91 | 2.87 | 0.72 | 2.05 |
| 25 | Berkeley | 0.33 | 0.10 | 0.28 | 2.74 | 12.66 | 4.62 | 1.37 | 6.35 |
| 26 | Richmond | 0.33 | 0.11 | 0.23 | 1.82 | 6.86 | 3.77 | 1.00 | 3.75 |
| 27 | Richmond | 0.60 | 0.08 | 0.31 | 3.75 | 15.83 | 4.22 | 1.50 | 6.35 |
| 28 | Walnut Creek | 0.80 | 0.05 | 0.22 | 4.63 | 18.62 | 4.02 | 1.16 | 4.65 |
| 29 | Pleasant Hill | 0.38 | 0.08 | 0.13 | 1.72 | 6.57 | 4.82 | 0.69 | 2.65 |
| 30 | Concord | 0.74 | 0.06 | 0.23 | 3.94 | 18.24 | 4.63 | 1.18 | 5.45 |
| 31 | Palm Springs | 0.71 | 0.07 | 0.21 | 3.02 | 13.81 | 4.57 | 1.06 | 4.85 |
| 32 | San Bernardino | 0.50 | 0.08 | 0.32 | 3.95 | 16.86 | 4.27 | 1.58 | 6.75 |
| 33 | Palo Alto | 0.35 | 0.36 | 1.10 | 2.65 | 8.83 | 3.33 | 4.77 | 15.90 |

(*) - higher mode period, (**) - For $ZC_P = 0.2$

## TABLE 4 - AMPLIFICATION AND PERFORMANCE FACTORS

| Sta. No. | Name | T (sec) | Flex/ Rigid | $R_p$** (Rigid) | $R_p$** (Flex) | Adjusted $ZIC_p$ | Adjusted $R_p$ (Rigid) | Adjusted $R_p$ (Flex) |
|---|---|---|---|---|---|---|---|---|
| 1 | Watsonville | 0.35 | 3.12 | 6.01 | 18.75 | 1.0 | 1.20 | 3.75 |
| 2 | Hollister | 0.80 | 3.25 | 2.55 | 8.30 | 0.3 | 1.70 | 5.53 |
| 3 | Gilroy | 0.40 | 3.26 | 3.02 | 9.85 | 0.2 | 3.02 | 9.85 |
| 4 | San Jose | 0.69 | 3.84 | 2.78 | 10.70 | 0.3 | 1.85 | 7.13 |
| 5 | Saratoga | 0.18 | 2.83 | 2.32 | 6.55 | 0.2 | 2.32 | 6.55 |
| 9 | Palo Alto | 0.34 | 3.09 | 2.00 | 6.15 | 0.2 | 2.00 | 6.15 |
| 14 | S. San Francisco | 0.71 | 4.42 | 3.18 | 14.05 | 0.3 | 2.12 | 9.37 |
| 18 | Milpitas | 0.20 | 4.08 | 2.89 | 11.80 | 0.3 | 1.93 | 7.33 |
| 23 | Oakland | 0.50 | 2.56 | 2.58 | 6.60 | 0.3 | 2.58 | 6.60 |
| 33 | Palo Alto | 0.35 | 3.33 | 4.77 | 15.90 | 0.5 | 1.91 | 6.36 |

(**) - For $ZC_p = 0.2$

## TABLE 5 - AMPLIFICATION AT VARIOUS LEVELS

### (A: RIGID ITEMS)

| | BASE | 0.25H | 0.50H | 0.75H | H |
|---|---|---|---|---|---|
| AVERAGE VALUES | 1.0 | 1.38 | 1.68 | 1.85 | 2.70 |
| MAXIMUM VALUES | 1.0 | 2.17 | 2.97 | 3.74 | 4.63 |
| MINIMUM VALUES | 1.0 | 0.87 | 1.01 | 1.03 | 1.17 |

H = Height of building.

### (B: FLEXIBLE ITEMS)

| | BASE | 0.25H | 0.50H | 0.75H | H |
|---|---|---|---|---|---|
| AVERAGE VALUES | 1.0 | 1.55 | 2.25 | 2.79 | 3.94 |
| MAXIMUM VALUES | 1.0 | 2.95 | 5.02 | 6.01 | 7.51 |
| MINIMUM VALUES | 1.0 | 0.86 | 1.01 | 1.00 | 1.36 |

H = Height of building.

# EVALUATION OF OVERTURNING FORCES ON SHEAR WALL BUILDINGS

William E. Gates[1], Gary S. Hart[2], Sunil Gupta[3], Mukund Srinivasan[2]

## ABSTRACT

The strong motion instrumentation program (SMIP) of the California Division of Mines & Geology (CDMG) has been designed to instrument specific building types in specific areas of California where strong ground motion records may be readily obtained from active seismic sources. The records are intended for use by structural engineers and researchers in developing analytical and design procedures that more accurately represent the building's behavior in earthquakes. Recent California earthquakes have provided significant data on a series of instrumented shear wall buildings along with observable data on their earthquake performance.

This paper presents a detailed investigation of three high-rise shear wall buildings in the nine- to ten-story range with three different shear wall configurations: perimeter walls, core walls and distributed walls. The dynamic earthquake response of these buildings is assessed to evaluate overturning forces in the shear walls under three recent northern California earthquakes: 1984 Morgan Hill; 1986 Mt. Lewis; and 1989 Loma Prieta. Two methods of data reduction and analysis are employed in the investigation to assess the significance of soil-structure interaction on building overturning forces. These include: simplified data analysis procedures using recorded motions, mode shapes and building weights to assess dynamic performance and three-dimensional linear elastic dynamic analyses using soil-structure models for the shear walls and foundation systems.

Realistic three-dimensional models of the structures refined through system identification techniques are used to study the response to the three earthquakes. These analyses indicated that under the larger earthquakes structural softening occurred that was associated both with soil strain levels as well as shear wall cracking. The analytical results are compared with code procedures for predicting the periods of the structures as well as the distribution of overturning forces.

## INTRODUCTION

The interaction between shear wall structures and their foundation system under lateral loads that induce overturning forces in the walls, has normally been neglected in conventional building code seismic design practice. Prior to the SMIP program of instrumentation, shear wall structures were not instrumented to record the rocking component of motion induced by earthquake. It has only been within the last ten years that adequate instrumentation of shear wall structures along with the occurrence of earthquakes in the vicinity of the instrumented buildings has provided data for use in analytical investigation and verification of design procedures for seismic overturning.

The scope of this investigation was to evaluate the overturning forces in three separate buildings with three different types of shear wall systems, two types of foundation systems, and recorded motions from three separate events in two of the buildings and one common event in all three buildings. Three-dimensional linear elastic soil-structure models were formulated using conventional computer codes (SAP90 and ETABS) to evaluate the influence of overturning forces in the shear walls of the buildings. System identification techniques along with conventional structural modeling procedures were used to define and refine the models and to identify the contributions from soil and structural deformation in the recorded response. Recorded motions at the base of the structures were input to the models and computed at the roof for comparison with the recorded motions as a confirmation of the basic structural model. The computed forces in the walls of the structure were investigated in terms of overturning effects.

---

1. William E. Gates - Dames & Moore
2. Gary S. Hart and Mukund Srinivasan - Hart Consultant Group
3. Sunil Gupta - EQTECH Consultants

The buildings, their California Strong Motion Instrumentation Program (CSMIP) number, location, shear wall type, and recorded earthquakes are listed in Table 1.

**TABLE 1 - BUILDING CHARACTERISTICS AND RECORDED EARTHQUAKES**

| Building Identification | Description of Structure | Recorded Earthquakes |
|---|---|---|
| Bldg. 1 CSMIP Station 57355<br>San Jose, CA | 10-story commercial<br>building<br>perimeter shear walls<br>and frames<br>mat foundation | 1984 Morgan Hill<br>1986 Mt. Lewis<br>1989 Loma Prieta |
| Bldg. 2 CSMIP Station 57356<br>San Jose, CA | 10-story residential<br>building<br>distributed bearing/<br>shear walls<br>pile foundation | 1984 Morgan Hill<br>1986 Mt. Lewis<br>1989 Loma Prieta |
| Bldg. 3 CSMIP Station 58394<br>San Bruno, CA | nine-story government<br>office building<br>central core walls<br>mat foundation | 1989 Loma Prieta |

Buildings 1 and 2, are located about a 1/4 mile apart (three city blocks) in the central part of San Jose. As shown in Figure 1, the San Jose buildings are located about 18 miles north of the epicenter for the Loma Prieta earthquake, 12 miles east of the epicenter for the Morgan Hill earthquake, and 15 miles southwest of the Mt. Lewis earthquake epicenter. Building 3 in San Bruno is located about 56 miles north by northwest of the Loma Prieta epicenter.

## DESCRIPTION OF BUILDINGS

### No. 1 - Ten-story Commercial Building - San Jose

The ten-story commercial office building shown in Figure 2 has plan dimensions of 190 feet x 82 feet. It's total height above the ground surface is 124 feet and it has a single basement that extends 17 feet below ground. The building is constructed of reinforced concrete with exterior shear walls and interior moment frames as the lateral force resisting system in the transverse (east-west) direction. In the longitudinal (north-south) direction the lateral loads are resisted by two exterior and two interior reinforced concrete moment frames. The floor and roof diaphragms are composed of a one-way slab and joist system. The building's foundation consists of a five foot thick reinforced concrete mat. All of the reinforced concrete elements of the building above ground floor level are constructed of light weight concrete. The remaining grade level and below construction consists of normal weight (hard rock) concrete. Although the building was designed in 1965 in accordance with the provisions of the 1964 UBC, careful consideration was given to detailing the moment frames so as to ensure ductile behavior during earthquakes.

The CDMG strong motion instrumentation of Building 1 is shown in Figure 2. Thirteen accelerometers have been installed on the building to record both translational and torsional effects in the floor slabs as well as vertical rocking motions in one of the shear walls.

**No. 2 - Ten-story Residential Building - San Jose**

The ten-story residential building in San Jose shown in Figure 3 is a reinforced concrete structure with one-way post-tensioned floor slabs. The overall plan dimension of the building is 209.5 feet by 63.5 feet. The height of the building above ground surface is 94 feet. The building's transverse (east-west) wall system is designed as a combination bearing wall for vertical loads and shear wall for lateral loads. In the longitudinal direction (north-south) the lateral force resisting system consists of a series of intermittently spaced shear walls along both sides of the interior central corridor. Two of the longitudinal interior shear walls are terminated at the sixth floor level. The lateral stiffness in the longitudinal direction is significantly lower than the stiffness in the transverse direction. The building is founded at grade level on precast-prestressed concrete piles that are placed directly below the bearing/shear walls. All of the shear walls in the building are constructed of normal weight (hard rock) concrete while the elevated post-tensioned floor slabs are constructed of light weight concrete. The piles, pile caps, and grade slab are all constructed of normal weight concrete.

The building was designed in 1970 and 1971 according to the provisions of the 1970 UBC. The 1971 San Fernando earthquake occurred while the structure was under design. The designers made a point of incorporating lessons learned from the performance of similar shear wall structures in the San Fernando earthquake. Additional steel was added to the shear walls of the building beyond that called for in the 1970 UBC to enhance the building's earthquake resistance. Construction of Building 2 was completed in 1972.

A total of 13 strong motion accelerometers have been deployed in Building 2 under the CDMG Strong Motion Instrumentation Program. This array of accelerometers is designed to measure horizontal building motions at the roof, sixth floor and ground floor as well as vertical building motions, rocking of a major transverse shear wall, and transverse flexural deformations in the long narrow roof diaphragm.

**No. 3 - Nine-story Government Office Building - San Bruno**

Figure 4 illustrates the nine-story government office building in San Bruno, California. The building's plan dimensions are 192 feet by 84 feet and its roof height is 104 feet above the first floor. The structural lateral load resisting system consists of a central elevator/stair core constructed of reinforced concrete. The vertical load carrying system consists of post-tensioned flat slabs without drop panels that are supported on concrete columns. The foundation system consists of a ribbed mat composed of a thick floor slab supported on deep reinforced concrete grade beams. The building was constructed in 1972.

The CDMG strong motion instrumentation of the building consists of 16 accelerometers as shown in Figure 4. The accelerometer locations have been chosen to provide data on the flexibility of the roof diaphragm, lateral transnational performance of the building, and rocking of the core wall in the transverse (north-south) direction.

## SOIL PROPERTIES

Soil reports for the design of Buildings 1 and 2 in San Jose were located through the assistance of the design engineers. These provided information on the soil profiles and in the case of Building 2 the relative stiffness of each soil layer based on actual sampling blow counts. From this information the shear modulus, poissons ratio and density of the soil materials were estimated at in situ strain conditions as well as large strain conditions associated with earthquake. These properties were used in modeling the soil foundation stiffness characteristics under the mat and pile foundation for Buildings 1 and 2, respectively.

For Building 3, no soil report was obtainable. Instead, system identification techniques were employed along with best estimate soil properties for the area to arrive at an approximate soil-spring stiffness for building rocking.

## RECORDED MOTIONS

Strong motion records from each of the three buildings have been published by CDMG along with fourier spectra and response spectra. Table 2 summarizes the recorded peak accelerations in each of the three buildings for the various earthquakes. It is evident from this table that the two buildings in San Jose experienced significantly higher levels of ground shaking from the Loma Prieta earthquake than either the Morgan Hill or Mt. Lewis events.

**TABLE 2 - SUMMARY OF RECORDED PEAK ACCELERATIONS IN G's**

| Bldg. | Earthquake | Longitudinal Direction | | Transverse Direction | |
|---|---|---|---|---|---|
| | | Base | Roof | Base | Roof |
| 1 | 1984 Morgan Hill | .058 | .180 | .061 | .220 |
| | 1986 Mt. Lewis | .029 | .078 | .034 | .077 |
| | 1989 Loma Prieta | .092 | .254 | .105 | .375 |
| 2 | 1984 Morgan Hill | 0.056 | 0.216 | 0.061 | 0.133 |
| | 1986 Mt. Lewis | 0.030 | 0.119 | 0.036 | 0.082 |
| | 1989 Loma Prieta | 0.094 | 0.371 | 0.127 | 0.242 |
| 3 | 1989 Loma Prieta | 0.114 | 0.320 | 0.158 | 0.372 |

## INTERPRETATION OF BUILDING RESPONSE FROM RECORDED MOTIONS

Strong motion records for the buildings have been analyzed using the raw data provided in digital form by CDMG to assess the mode shapes, periods of vibration, damping, base shears and overturning moments. These findings have been corroborated by previous studies. Table 3 summarizes the fundamental translational or torsional modes of vibration for each of the three buildings and for each of the three earthquakes recorded in Buildings 1 and 2 in San Jose.

**TABLE 3**
**PERIODS IN SECONDS**

MH - Morgan Hill
ML - Mt. Lewis
LP - Loma Prieta

Building 1

| Bldg. No. | Mode | Periods from Recorded Motions MH (1984) | ML (1986) | LP (1989) | Computer Model |
|---|---|---|---|---|---|
| 1 | 1 | 0.91 (N-S) | 0.91 (N-S) | 1.01 (N-S) | 1.03 (N-S) |
| | 2 | 0.61 (E-W) | 0.61 (E-W) | 0.75 (E-W) | 0.77 (E-W) |
| | 3 | 0.37 (TOR) | 0.39 (TOR) | 0.44 (TOR) | 0.44 (TOR) |
| 2 | 1 | 0.65 (N-S) | 0.63 (N-S) | 0.73 (N-S) | 0.59 (N-S) |
| | 2 | 0.43 (E-W) | 0.41 (E-W) | 0.43 (E-W) | 0.43 (E-W) |
| | 3* | -- | -- | -- | 0.38 (TOR) |
| | 4 | 0.18 (N-S) | 0.18 (N-S) | 0.19 (N-S) | 0.17 (N-S) |
| 3 | 1 | -- | -- | 1.45 (N-S) | 1.80 (N-S) |
| | 2 | -- | -- | 1.38 (TOR) | 1.42 (TOR) |
| | 3 | -- | -- | 1.00 (E-W) | 1.15 (E-W) |

* Mode 3 is a torsional mode in the computer model at T = 0.38 seconds.

It is evident from Table 3 that the fundamental period of vibration during the Loma Prieta earthquake is longer for the two translation and torsional components of motion in Building 1 and the longitudinal (north-south) component of motion in Building 2. This is due in part to the strain dependent softening of the supporting foundations and in part to the cracking and softening of the shear walls under the larger motions produced by the Loma Prieta event.

## COMPUTER MODELS OF BUILDINGS

Figures 5, 6 and 7 present the three-dimensional elastic finite element models for Buildings 1, 2 and 3, respectively. All three buildings were found to have rigid floor diaphgrams based on the recorded accelerations and displacements. Thus Buildings 1 and 2 have been modeled using the ETABS program and Building 3 was modeled using the SAP90 computer program. An additional level has been added to the models to incorporate soil rocking stiffness characteristics. The models for Buildings 2 and 3 represent fixed base solutions with structural properties based on gross section properties.

## ANALYTICAL RESULTS

### Periods and Mode Shapes of Vibrations

Table 3 summarizes the computed frequencies for each of the three models shown in Figures 5, 6, and 7. Mode shapes associated with these periods of vibration are shown in the same figures as the models.

The periods computed for Building 1 are from the computer model developed specifically to approximate the conditions with the Loma Prieta earthquake. This model includes soil springs to simulate rocking at the base. Also, cracked section properties were assumed for the moment frames at 80 percent of gross section properties and for the shear walls at 50 percent of the gross section properties as suggested by Wallace, et.al. (1990). This reduction in structural stiffness produced excellent correlations with the Loma Prieta records for the north-south and east-west directions.

### Time History Analyses

Figure 8 presents the plot of time history motion recorded parallel to the transverse (east-west) shear walls of Building 1 as recorded at the roof level and as computed with the analytical model for the Loma Prieta earthquake. The solid line represents the recorded earthquake and the dotted line represents the computed response using as input motion the record from the base of the structure. In general the correlation between computed and recorded roof motions is reasonably close.

The lower half of Figure 8 represents the response spectra computed from the recorded motions at the roof versus the response spectra of computed motions using the analytical model shown in Figure 5. The response spectra comparison also shows good correlation.

Figure 9 presents the comparison of roof motions for Building 2 under the Morgan Hill earthquake recorded in the longitudinal and transverse directions versus the computed response. The correlation in this case is good considering the model has a fixed base.

## CONCLUSIONS

The following are conclusions from the investigation of the three shear wall buildings:

1. The earthquake records provided ample evidence that foundation/shear wall rocking occurs under small to moderate size earthquakes in these structures.

2. Lengthening in building period occurs both due to structural rocking and due to inelastic behavior (cracking) of the shear walls.

3. The records provided ample evidence that the reinforced and prestressed concrete floor diaphragms in all three buildings were rigid relative to other building deformations.

4. Rocking of the shear wall/foundation system can be modeled with the appropriate soil properties or through system identification using the records in the building as a basis for correlation.

5. The geometry of Building 2 resulted in more walls in the transverse direction than the longitudinal direction. This may explain why no cracking was reported or observed in the transverse walls while the longitudinal walls were reported to have cracked under the Loma Prieta earthquake. It also explains why the building is stiffer and has shorter periods in the transverse direction than the longitudinal direction.

6. In the transverse direction of Building 1 and the longitudinal direction of Building 2 lengthening of structural periods under the Loma Prieta earthquake relative to the periods computed under the Morgan Hill and Mt. Lewis events was probably due to cracking in the walls.

## ACKNOWLEDGEMENT

This research project was sponsored by the California Department of Conservation, Division of Mines & Geology, Office of Strong Motion Studies. The authors wish to thank Moh Huang, Anthony Shakal, and Robert Darragh at CSMIP for their assistance in collecting the strong motion records and building drawings required for the project, and the assistance of the design engineers on Buildings 1 and 2 in providing background information and geotechnical reports used in modeling soil properties at the sites in San Jose.

## REFERENCES

**STRONG MOTION RECORDS**

CDMG, 1984, CSMIP Strong Motion Records from the Morgan Hill, CA Earthquake of 24 April 1984.

CDMG, 1986, CSMIP Strong Motion Records from the Mt. Lewis, CA Earthquake of 31 March 1986.

CDMG, 1989, CSMIP Strong Motion from the Santa Cruz Mountains (Loma Prieta), CA Earthquake of 17 October 1989.

**CSMIP BUILDINGS SN 355, SN 356 and SN 394**

Moehle, J. P., J. W. Wallace and J. M. Cruzado, 1990, Implications of Strong Motion Data for the Design of Reinforced Concrete Bearing Wall Buildings, Final Report to CDMG, June 1.

Naaseh, S., 1985, The Morgan Hill Earthquake of April 24, 1984 - Performance of Three Engineered Structures, EERI Spectra, Vol. 1, No. 3, pp 579-593.

SEAOC, 1991, Reflections on the Loma Prieta Earthquake, pp 43-53, April.

Sedarat, H. and S. Gupta, 1992, Torsional Response Characteristics of Regular Buildings under Different Seismic Excitation Levels, Proc. 10th World Conference Earthquake Engineering, July.

Wallace, J. W., J. P. Moehle and J. M. Cruzado, 1990, Implications for the Design of Shear Wall Buildings Using Data From Recent Earthquakes, Proceedings 4th US National Conference Earthquake Engineering May 20-24.

Werner, S. D. and A. Nisar, 1992, Use of Strong Motion Records in Buildings to Evaluate 1991 NEHRP Seismic Design Provisions, for BSSC, December.

**SOIL STRUCTURE INTERACTION**

Luco, J. E., et. al., 1987, On the Apparent Change in Dynamic Behavior of a Nine Story Reinforced Concrete Building, Bulletin, Seismological Society of America, Vol. 77, No. 6, pp. 1961-1983, December.

Papageorgiou, A. S., B-C. Lin, 1991, Analysis of Recorded Earthquake Response and Identification of a Multi-story Structure Accounting for Foundation Interaction Effects, Journal Soil Dynamics and Earthquake Engineering, Vol. 10, No. 1, pp 55-64, January.

**SEISMIC DESIGN OF SHEAR WALLS**

Derecho, A. T., et. al., 1979, Strength, Stiffness and Ductility Requirements in Reinforced Concrete Structural Walls for Earthquake Resistance, Journal, American Concrete Institute, Vol. 76, pp 875-895, August.

Fintel, M. 1974, Ductile Shear Walls in Earthquake Resistance Multi-story Buildings, Journal American Concrete Institute Vol, 71, No. 6, pp 296-365, June.

Wallace, J. W., and J. P. Moehle, 1992, Ductility and Detailing Requirements of Bearing Wall Buildings, ASCE Journal of Structural Engineering, Vol. 118, No. 6, pp 1625-1644, June.

Wallace, J. W., 1994, New Methodology for Seismic Design of RC Shear Walls, ASCE Journal of Structural Engineering, Vol. 120, No. 3, pp 863-884, March.

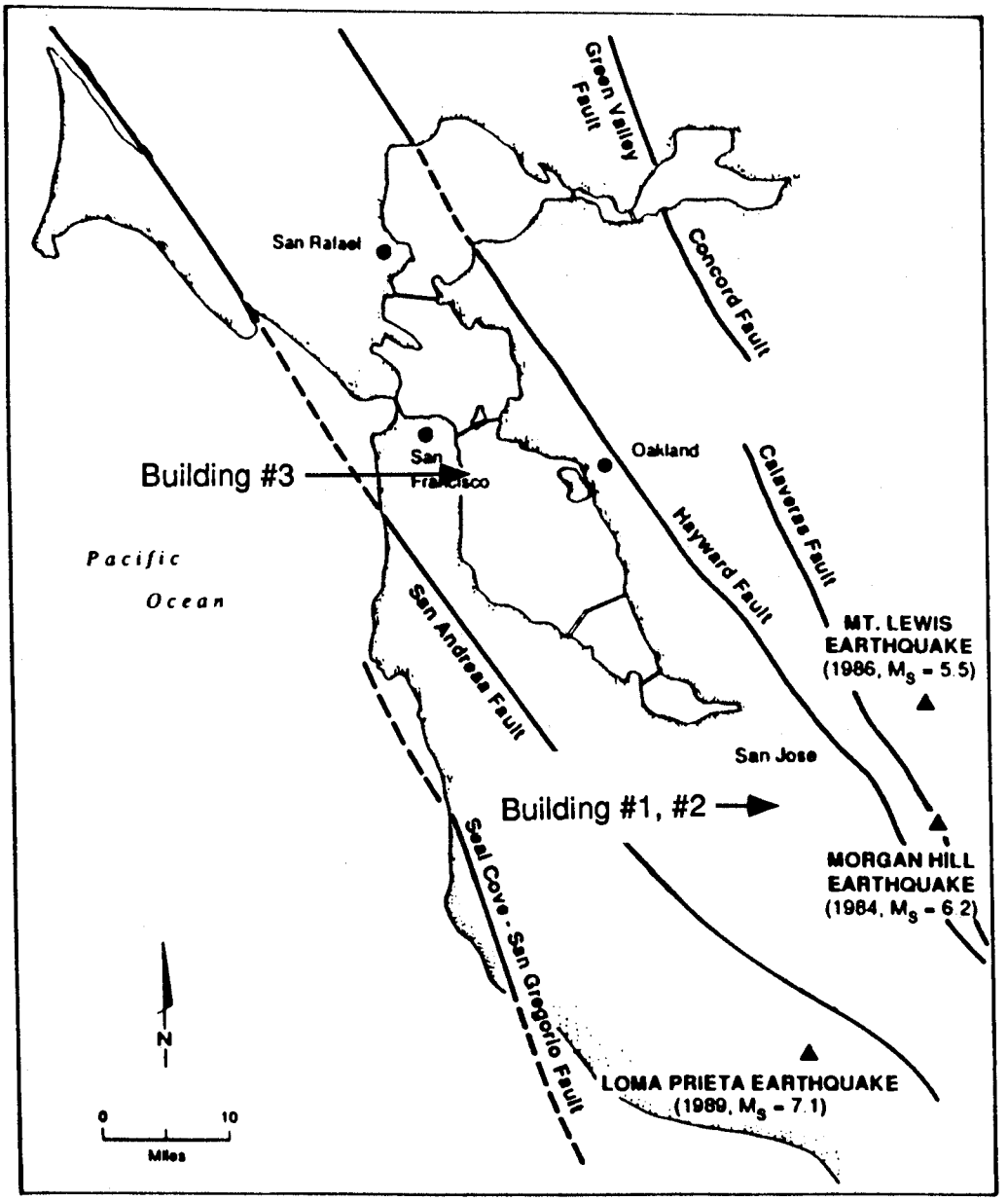


Figure 1. Proximity of Major Faults and Earthquake Epicenters to Building Locations

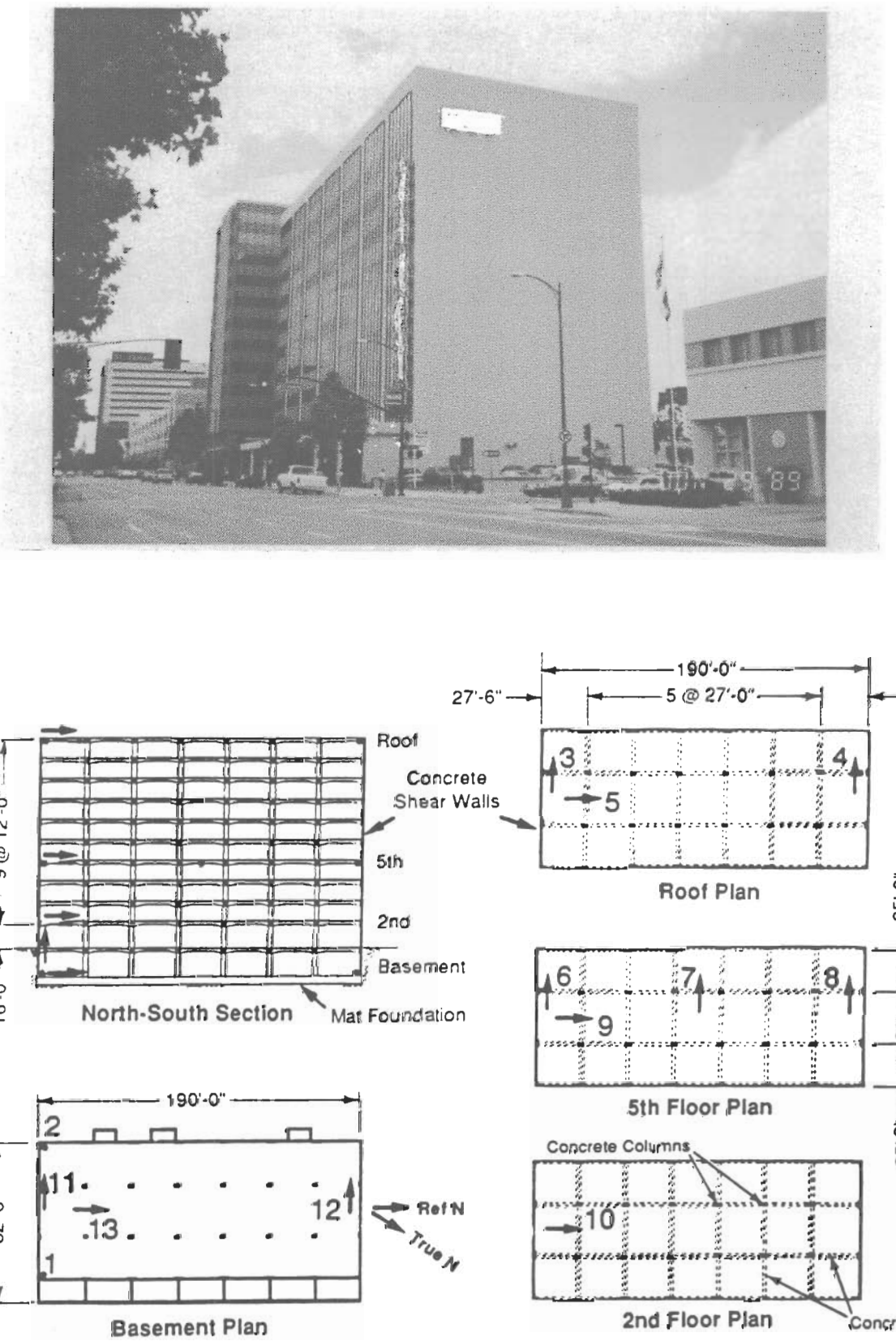


Figure 2. Building #1 - 10 Story Commercial Building, San Jose

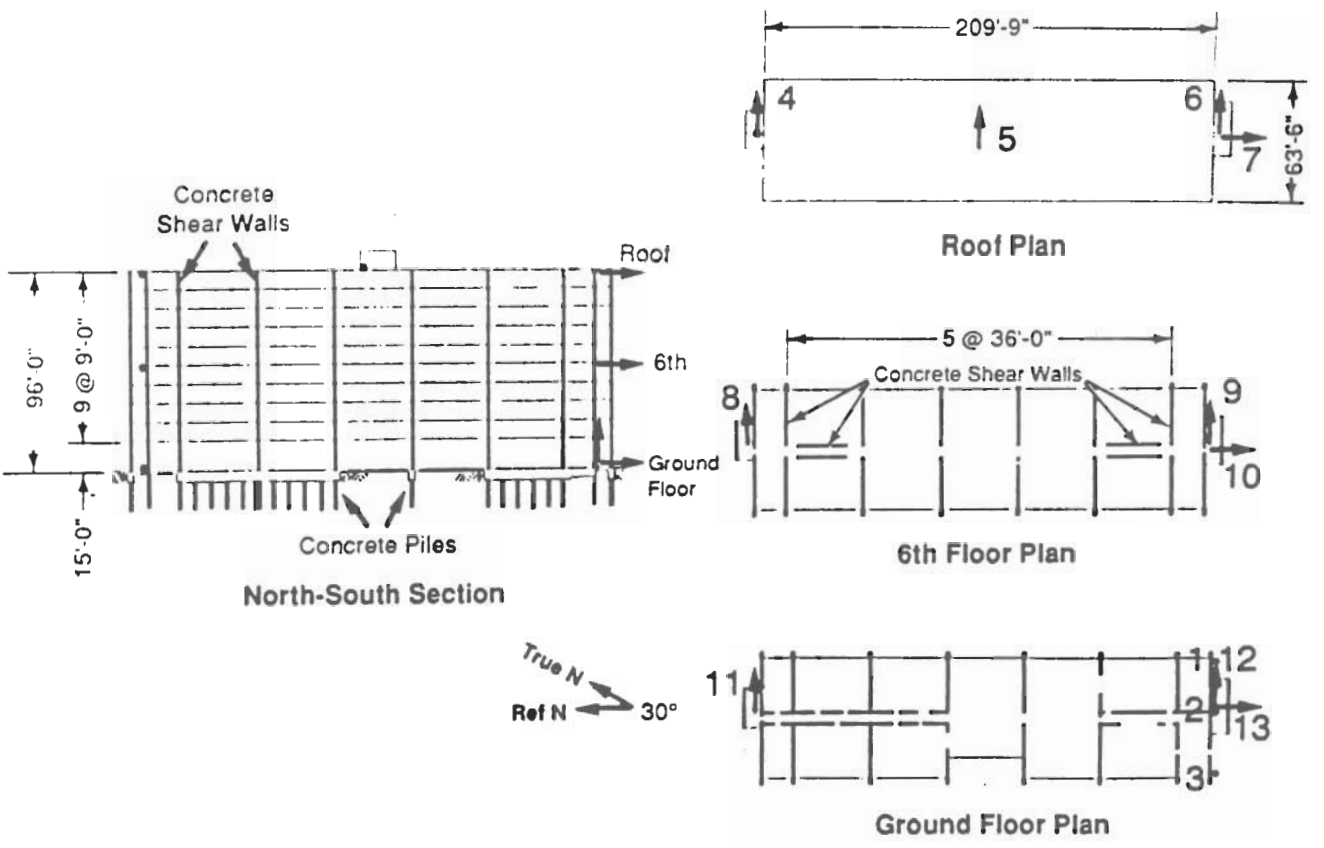


Figure 3. Building #2 - 10 Story Residential Building, San Jose

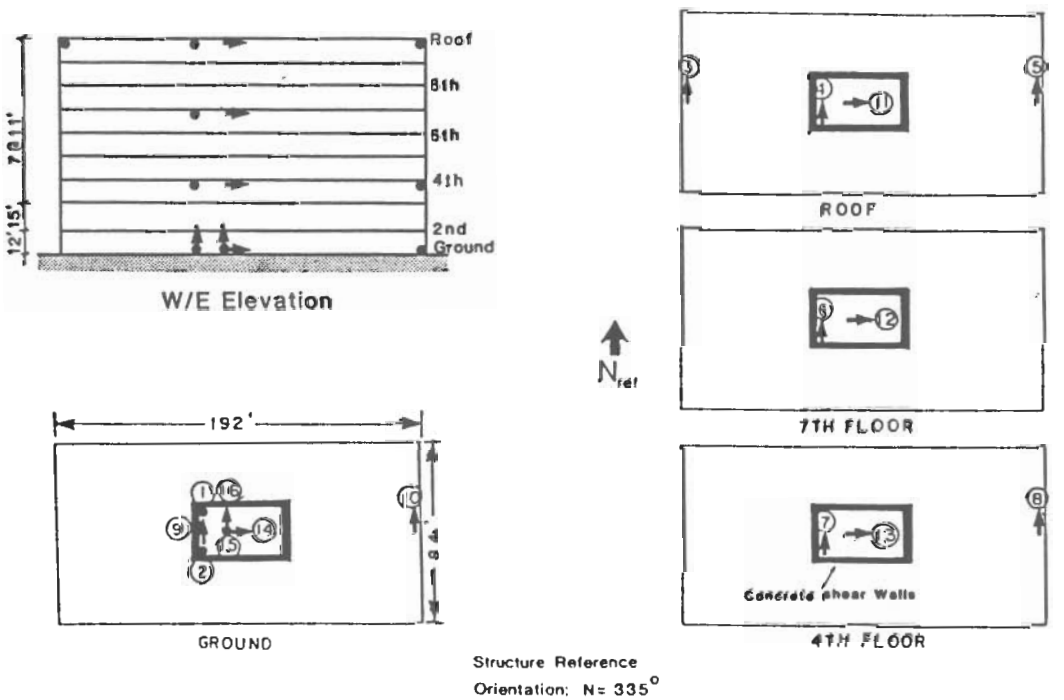


Figure 4. Building #3 - 9 Story Government Office Building, San Bruno

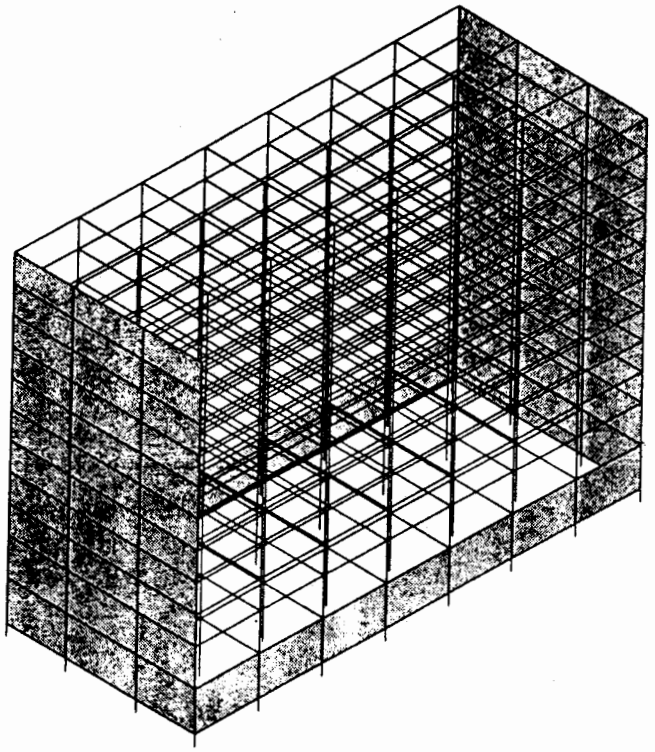

**ETABS COMPUTER MODEL**

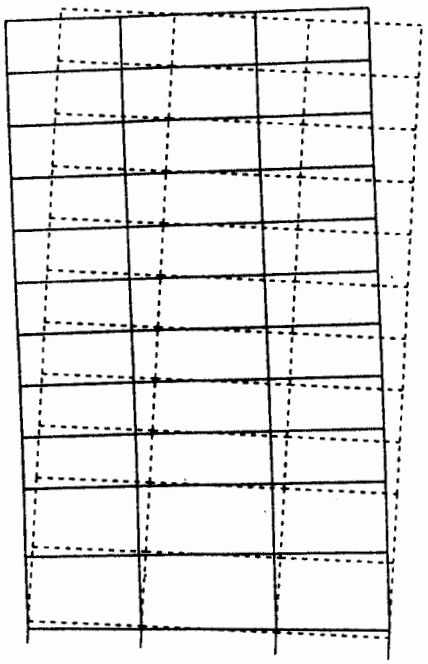

**FIRST MODE SHAPE - TRANSVERSE DIRECTION**

Figure 5. Building #1 - Model and Mode Shape

Figure 6. Building #2 - Model and Mode Shapes

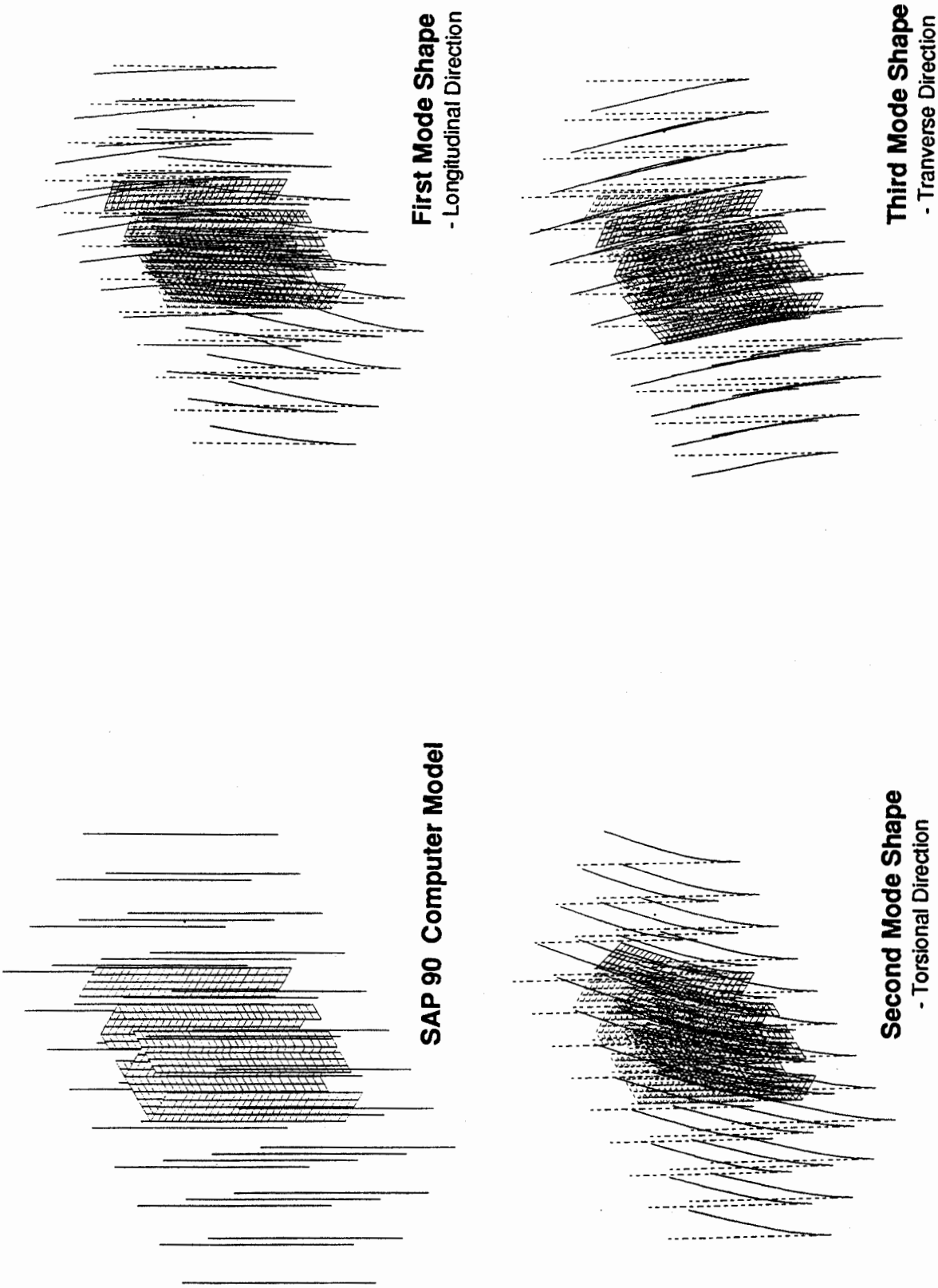


Figure 7. Building #3 - Model and Mode Shapes

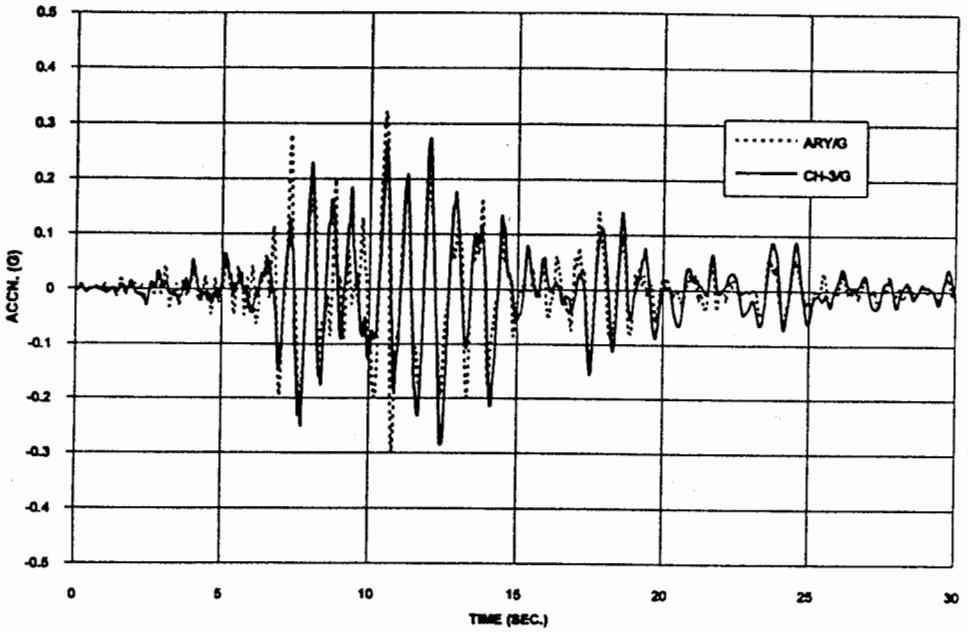


TIME-HISTORY OF RECORDED AND COMPUTED ROOF ACCELERATIONS - TRANSVERSE DIRECTION

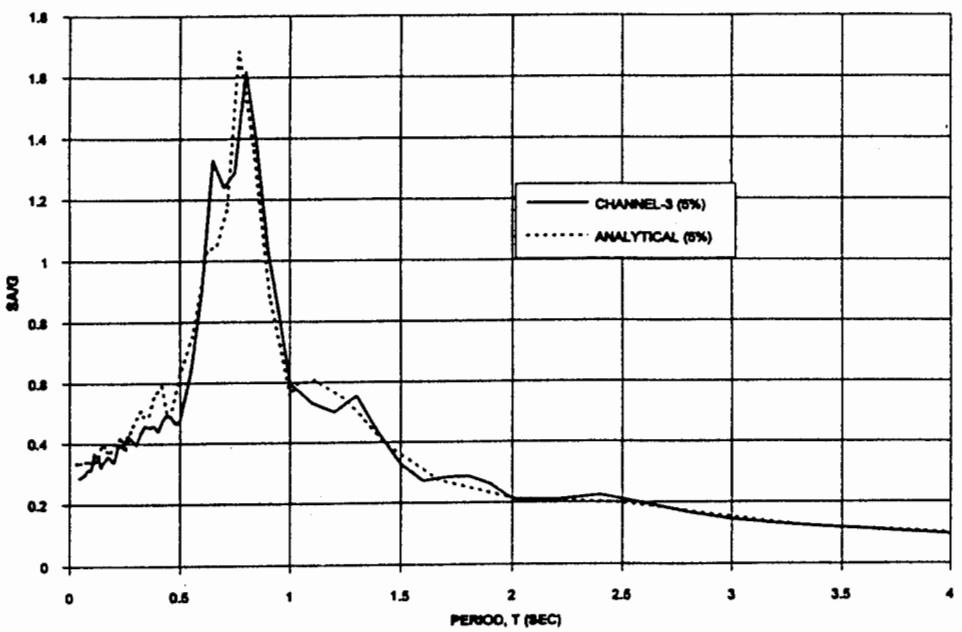


RESPONSE SPECTRA OF RECORDED AND COMPUTED ROOF ACCELERATIONS - TRANSVERSE DIRECTION

Figure 8. Building #1 - Computed and Recorded Roof Motion Response Loma Prieta Earthquake

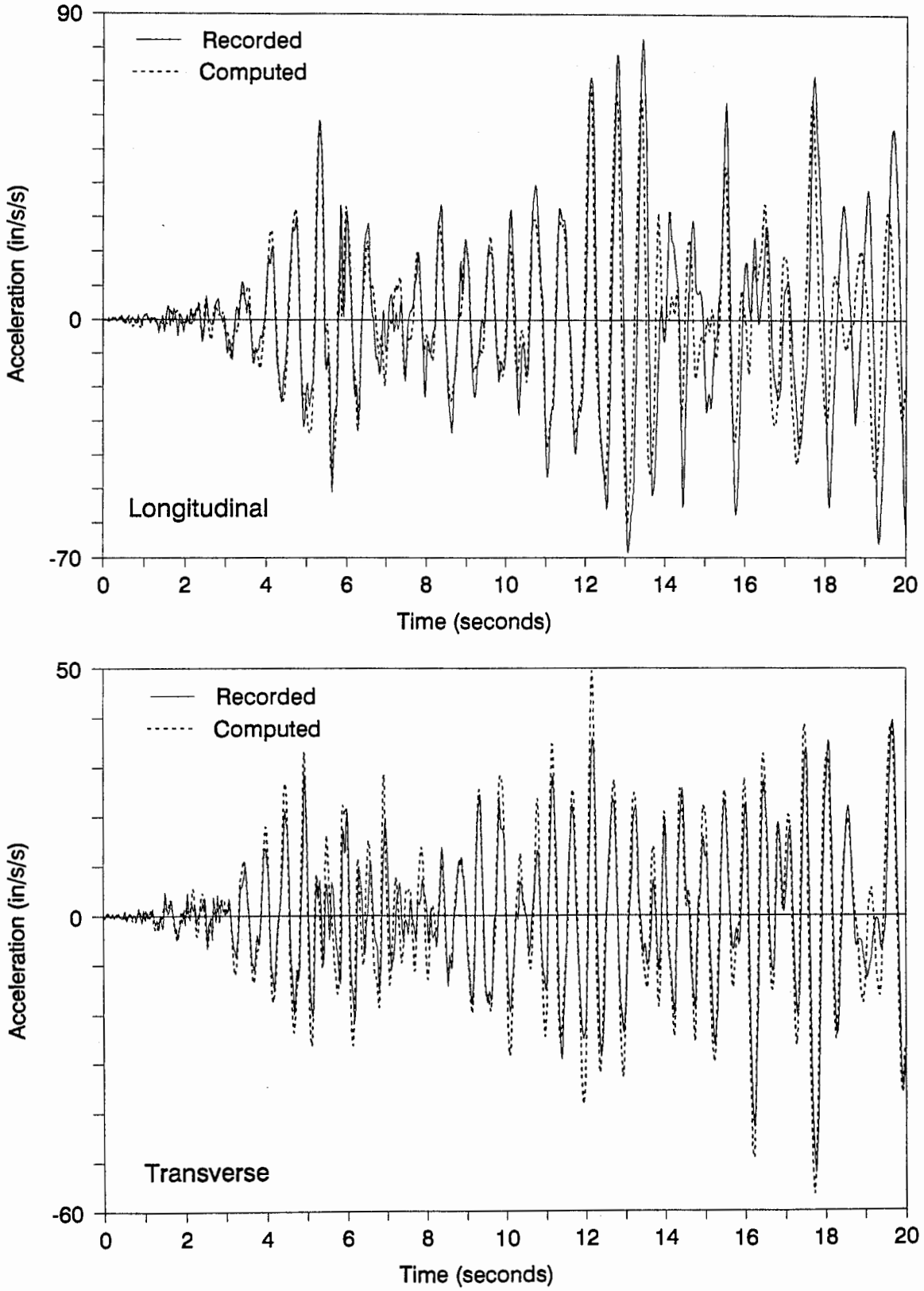


Figure 9. Building #2 - Computed and Recorded Roof Acceleration
Morgan Hill Earthquake